

Electronic Thesis and Dissertation Repository

6-13-2017 12:00 AM

S-Nitrosylation Suppresses Stromal Interaction Molecule-1 Activation and Ameliorates Cardiomyocyte Hypertrophy

Jinhui Zhu, *The University of Western Ontario*

Supervisor: Qingping Feng, *The University of Western Ontario*

Joint Supervisor: Peter Stathopoulos, *The University of Western Ontario*

A thesis submitted in partial fulfillment of the requirements for the Master of Science degree in
Physiology and Pharmacology

© Jinhui Zhu 2017

Follow this and additional works at: <https://ir.lib.uwo.ca/etd>



Part of the [Cellular and Molecular Physiology Commons](#)

Recommended Citation

Zhu, Jinhui, "S-Nitrosylation Suppresses Stromal Interaction Molecule-1 Activation and Ameliorates Cardiomyocyte Hypertrophy" (2017). *Electronic Thesis and Dissertation Repository*. 4591.
<https://ir.lib.uwo.ca/etd/4591>

This Dissertation/Thesis is brought to you for free and open access by Scholarship@Western. It has been accepted for inclusion in Electronic Thesis and Dissertation Repository by an authorized administrator of Scholarship@Western. For more information, please contact wlsadmin@uwo.ca.

Abstract

Stromal interaction molecule 1 (STIM1) is an endo/sarcoplasmic reticulum (ER/SR) calcium (Ca^{2+}) sensor that activates store-operated Ca^{2+} entry (SOCE) following Ca^{2+} depletion. SOCE-induced elevation of cytosolic Ca^{2+} stimulates the calcineurin/nuclear factor of activated T cells (NFAT) pathway, which upregulates pro-hypertrophic gene transcription. Nitric oxide (NO) regulates protein functions by *S*-nitrosylation, but how NO regulates SOCE in inhibiting cardiac hypertrophy is unclear. I hypothesize that NO stabilizes and inhibits STIM1 via *S*-nitrosylation and mitigates cardiomyocyte hypertrophy. STIM1 residues Cys49 and Cys56 were susceptible to *S*-nitrosylation by *S*-nitrosoglutathione (GSNO) and sodium nitroprusside (SNP), resulting in luminal Ca^{2+} sensing domain stabilization, reduced oligomerization, enhanced rigidification, and suppressed hydrophobic exposure upon Ca^{2+} -depletion. Phenotypically, STIM1 siRNA, SOCE channel blocker BTP2, GSNO or ectopic nNOS expression inhibited phenylephrine-induced cardiomyocyte hypertrophy. Collectively, my data show that STIM1 *S*-nitrosylation inhibits SOCE and cardiomyocyte hypertrophy thereby providing new insight into how STIM1 modification contributes to Ca^{2+} signaling in cardiomyocytes.

Keywords

stromal interaction molecule-1, nitric oxide synthase, *S*-nitrosylation, phenylephrine, cardiomyocyte, hypertrophy, store-operated calcium entry, nuclear magnetic resonance spectroscopy, stability, oligomerization

Co-Authorship Statement

Dr. Qingping Feng and Dr. Peter B. Stathopoulos supervised and contributed to the design of all the experiments. Sharon Lu greatly helped with the collection of data associated with the neonatal rat cardiomyocyte experiments.

Acknowledgments

I would like to express my most sincere gratitude towards my supervisors Dr. Qingping Feng and Dr. Peter B. Stathopoulos for their continuous support, understanding and patience. I really appreciate their assistance with not just the design of my experiments but also with my scholarship applications and this Master's thesis. Their expertise and guidance have allowed me to improve my practical laboratory skills, critical thinking skills as well as my ability to effectively write for academic journals and orally communicate to broad audiences. I could not have imagined having a better team of supervisors to mentor me for my Master's study. I would also like to thank my advisory committee members Dr. Wei-Yang Lu and Dr. John DiGuglielmo for their valuable feedback, encouragement and assistance with my research project.

A very special thanks to our lab manager Sharon Lu for her guidance and assistance with all my experiments using neonatal rat cardiomyocytes. The countless weekends and holidays that she sacrificed to help me with my experiment are vital for the successful completion of my project.

I would also like to thank my past and present lab members in Dr. Feng and Dr. Stathopoulos' lab: Yoo Jung Choi, Sam Lee, Jessica Blom, Anish Engineer, Tana Saiyin, Naveed Siddiqui, Steve Chung, Edward Kim and Allen Feng. Their presence and the stimulating discussions we had made my time in the lab an extremely pleasant experience. A huge thanks to our lab volunteer Benjamin Harvey for his assistance with some of the rate limiting steps in my project which has allowed me to spend more time to focus on other areas of my research and efficiently conduct my experiments.

I must also thank my family and friends for the support they have provided me throughout my life and their consoling words that get me through my toughest days. Their encouragement and trust in me have given me the confidence to believe in myself and pursue my dreams.

Table of Contents

Abstract.....	i
Co-Authorship Statement	ii
Acknowledgments	iii
Table of Contents.....	iv
List of Tables	viii
List of Figures.....	ix
Chapter 1 Introduction	1
1.1 Overall goals.....	1
1.2 Calcium.....	2
1.2.1 General functions of Ca ²⁺	2
1.2.2 Ca ²⁺ function in the immune system.....	3
1.2.3 Intracellular Ca ²⁺ compartmentalization.....	3
1.2.4 Ca ²⁺ signalling impairments in the heart	4
1.3 SOCE and CRAC channels	5
1.4 Stromal interaction molecule (STIM) and Orai	9
1.4.1 STIM domain organization.....	9
1.4.2 Orai domain organization	14
1.4.3 STIM1 and Orai1 function.....	15
1.5 Cardiac hypertrophy	17
1.5.1 Physiological and pathological hypertrophy.....	17
1.5.2 Intracellular signalling pathway	18
1.5.3 Role of Ca ²⁺ and SOCE	19
1.6 Nitric oxide synthase	20

1.6.1	iNOS	20
1.6.2	eNOS.....	20
1.6.3	nNOS	21
1.7	<i>S</i> -Nitrosylation.....	22
1.7.1	Mechanism of <i>S</i> -nitrosylation.....	22
1.7.2	Effect of <i>S</i> -nitrosylation on different proteins	22
1.7.3	<i>S</i> -nitrosylation and cardiac function	23
1.8	Summary and Rationale.....	25
1.9	Hypothesis and aims	26
Chapter 2 Methods.....		28
2.1	Generation of STIM1 constructs and mutants	28
2.2	Protein expression and purification	33
2.2.1	pET-28a STIM1 23-213 wildtype and mutants	33
2.2.2	pGEX-4T1 STIM1 24-57	37
2.2.3	pET-28a STIM1 58-201 (EF-SAM).....	41
2.3	<i>S</i> -Nitrosylation of STIM1	44
2.4	Far-UV circular dichroism (CD) spectroscopy.....	44
2.5	Ca ²⁺ binding.....	45
2.6	8-Anilino-naphthalene-1-sulfonic acid (ANS) binding	46
2.7	Dynamic light scattering (DLS).....	47
2.8	Solution nuclear magnetic resonance (NMR) spectroscopy.....	47
2.8.1	STIM1 24-57 backbone assignment and structure	47
2.8.2	Paramagnetic relaxation enhancement (PRE) spectroscopy.....	49
2.9	Urea Denaturation.....	51
2.10	Cardiomyocyte Culture	52

2.10.1	Cardiomyocyte isolation and culture	52
2.10.2	Experimental treatments	52
2.10.3	Cardiomyocyte staining and imaging	52
2.11	Statistical analysis	53
Chapter 3 Results		54
3.1	The α -helicity of STIM1 23-213 is attenuated upon Ca^{2+} depletion.	54
3.2	<i>S</i> -Nitrosylation increases the thermal stability of STIM1 23-213 wildtype protein.	56
3.3	<i>S</i> -Nitrosylation decreases the structural change of STIM1 23-213 upon Ca^{2+} binding.	60
3.4	<i>S</i> -Nitrosylation decreases the level of solvent-exposed hydrophobicity of wildtype STIM1 23-213.	62
3.5	Wildtype STIM1 23-213 undergoes <i>S</i> -nitrosylation mediated de-oligomerization.	65
3.6	<i>S</i> -Nitrosylation of STIM1 24-57 peptide causes residue specific chemical shift changes.	67
3.7	<i>S</i> -Nitrosylation induces thermodynamic stabilization of STIM1 23-213.	72
3.8	STIM1 24-57 peptide transiently interacts with STIM1 58-201 (EF-SAM core) at residues Trp121 and Lys122.	75
3.9	STIM1 23-213 Trp121Glu/Lys122Glu double mutant does not de-oligomerize following GSNO treatment.	79
3.10	STIM1 siRNA and BTP2 blockade of Orai1 channel activity decreased PE-induced hypertrophy	81
3.11	GSNO and adenoviral nNOS inhibits PE-induced hypertrophy	81
Chapter 4 Discussion		86
4.1	Summary	86
4.2	<i>S</i> -Nitrosylation	87
4.3	<i>S</i> -Nitrosylation of luminal STIM1 region increases protein stability	88
4.4	<i>S</i> -Nitrosylation of luminal STIM1 suppresses Ca^{2+} -dependent conformational	

changes and oligomerization.	90
4.5 STIM1 24-57 peptide interacts with STIM1 58-201 (EF-SAM domain) at residues Trp121 and Lys122 to mediate <i>S</i> -nitrosylation-induced stabilization of STIM1.	92
4.6 Inhibition of the SOCE pathway prevents the development of PE-induced cardiomyocyte hypertrophy.	93
4.7 Future directions and limitations	95
4.8 Conclusions.....	96
References.....	100
Curriculum Vitae	120

List of Tables

Table 2.1. Oligonucleotide primers used in the research described in this thesis. (Sigma-Aldrich, St. Louis, MO)	31
Table 2.2. PCR amplification parameters on LifeECO (Bioer).....	32
Table 3.1 Apparent denaturation midpoint (T_m) of STIM1 23-213 wildtype, double and single mutants under conditions with or without Ca^{2+} and/or <i>S</i> -nitrosylation.....	57
Table 3.2 Thermodynamic stability parameters for STIM1 23-213 wildtype and Cys49Ser/Cys56Ser double mutant protein under Ca^{2+} -loaded and -depleted conditions.	73
Table 4.1. Summary of the effect of <i>S</i> -nitrosylation on various properties associated with STIM1 activation.	97

List of Figures

Figure 1.1. Schematic diagram of agonist-induced cardiomyocyte hypertrophy mediated by SOCE.....	8
Figure 1.2. Domain architecture and primary sequence alignment of STIM protein.....	12
Figure 1.3. Depiction of the mechanism through which cysteine residues are <i>S</i> -nitrosylated.....	24
Figure 2.1. Coomassie Blue R-250 staining of STIM1 23-213 on a 15 % (w/v) SDS-PAGE gel.....	35
Figure 2.2. Size exclusion chromatography elution profile of STIM1 23-213.....	36
Figure 2.3. Size exclusion chromatography elution profile of STIM1 24-57 containing the Tyr insert.....	39
Figure 2.4. Transformed mass spectrum of STIM1 24-57 peptide.....	40
Figure 2.5. Anion exchange chromatography elution profile of wildtype EF-SAM protein.....	43
Figure 2.6. ¹ H- ¹⁵ N-Heteronuclear single quantum coherence (HSQC) spectra of STIM1 24-57.....	50
Figure 3.1. Far-UV CD spectra of wildtype STIM1 23-213.....	55
Figure 3.2. <i>S</i> -nitrosylation induced thermal stabilization of STIM1 23-213.....	58
Figure 3.3. <i>S</i> -nitrosylation did not induce thermal stabilization of STIM1 23-213 Cys mutants.....	59
Figure 3.4. Ca ²⁺ binding to STIM1 23-213 wildtype protein with and without NO donors.....	61

Figure 3.5. Extrinsic fluorescence of ANS in the presence of STIM1 23-213.....	64
Figure 3.6. Dynamic light scattering (DLS) analysis of STIM1 23-213.....	66
Figure 3.7. Solution NMR assessment of structural changes caused by <i>S</i> -nitrosylation of STIM1 24-57.....	69
Figure 3.8. NMR chemical shift perturbation (CSP) of STIM1 24-57 before and after <i>S</i> -nitrosylation.....	70
Figure 3.9. Model-free order parameter (S^2) predicted from the random coil index (RCI).....	71
Figure 3.10. <i>S</i> -Nitrosylation-induced thermodynamic stabilization of STIM1 23-213...74	74
Figure 3.11. ^1H - ^{15}N -HSQC spectrum of STIM1 58-201 (EF-SAM) mixed with nitroxide spin-labelled STIM1 24-57.....	76
Figure 3.12. Transient binding between STIM1 24-57 and STIM1 58-201 (EF-SAM)...77	77
Figure 3.13. Structure of the EF-SAM domain under Ca^{2+} loaded condition (2K60.pdb).....	78
Figure 3.14. Dynamic light scattering (DLS) of STIM1 23-213 Trp121Glu/Lys122Glu double mutant protein.....	80
Figure 3.15. Effect of STIM1 siRNA and BTP2 on cardiomyocyte size.....	83
Figure 3.16. Effect of GSNO treatment on cardiomyocyte size.....	84
Figure 3.17. Effect of ectopic Adenoviral nNOS expression on cardiomyocyte size.....	85
Figure 4.1. Proposed model of <i>S</i> -nitrosylation mediated suppression of STIM1 activity and cardiomyocyte hypertrophy.....	99

List of Abbreviations

AEC	anion exchange chromatography
ANS	8-anilino-naphthalene-1-sulfonic acid
APC	antigen-presenting cell
AV	atrioventricular
BTP2	3,5-bis(trifluoromethyl) pyrazole derivative
Ca ²⁺	calcium
CaM	calmodulin
CaN	calcineurin
CC	coiled-coil
CD	circular dichroism
cEF	canonical EF-hand
CRAC	Ca ²⁺ release activated Ca ²⁺
CSP	chemical shift perturbation
Cys	cysteine
DLS	dynamic light scattering
DTT	dithiothreitol
EDTA	ethylenediaminetetraacetic acid
eNOS	endothelial nitric oxide synthase
ER	endoplasmic reticulum
GFP	green fluorescent protein
GPCR	G-protein-coupled receptor
G _s	G-stimulatory alpha subunit
GSNO	S-nitrosoglutathione
HCM	hypertrophic cardiomyopathy
HSQC	heteronuclear single quantum coherence
iNOS	inducible nitric oxide synthase
IP ₃	inositol 1,4,5-trisphosphate
IP ₃ R	inositol 1,4,5-trisphosphate receptor
IPTG	isopropyl β-D-1-thiogalactopyranoside
K ⁺	potassium

K _d	equilibrium dissociation constant
LB	Luria-Bertani broth
LV	left ventricular
MI	myocardial infarction
nEF	non-canonical EF-hand
NFAT	nuclear factor of activated T-cells
Ni-NTA	nickel-nitrilotriacetic acid
NMR	nuclear magnetic resonance
nNOS	neuronal nitric oxide synthase
NO	nitric oxide
NOS	nitric oxide synthase
PE	phenylephrine
PLC	phospholipase C
PM	plasma membrane
RCI	random coil index
SAM	sterile alpha motif
SEC	size-exclusion chromatography
SERCA	sarco/endoplasmic reticulum Ca ²⁺ -ATPase
siRNA	small inhibitory RNA
SNP	sodium nitroprusside
SOCE	store-operated Ca ²⁺ entry
SR	sarcoplasmic reticulum
STIM	stromal interaction molecule
T _m	apparent midpoint of temperature denaturation
WT	wild type

Chapter 1 Introduction

1.1 Overall goals

Calcium (Ca^{2+}) ions are universal signaling entities regulating numerous processes including programmed cell death, homeostasis, gene transcription as well as muscle contraction (Berridge et al., 2003; Mukherjee and Brooks, 2014; Orrenius et al., 2015). Store-operated Ca^{2+} entry (SOCE) is a Ca^{2+} signaling mechanism where extracellular Ca^{2+} entry is mobilized by the initial release of intracellular Ca^{2+} store (Putney, 1986). Specifically, upon sarcoplasmic reticulum (SR) Ca^{2+} depletion, the luminal Ca^{2+} sensor stromal interaction molecule-1 (STIM1) becomes activated, oligomerizes, translocates to SR-plasma membrane (PM) junctions and interacts with Orai1 on the sarcolemma (Liou et al., 2005; Roos et al., 2005; Stathopoulos et al., 2006; Zhang et al., 2005; Zhou et al., 2010a); thus, facilitating the formation of Ca^{2+} release-activated Ca^{2+} (CRAC) channels by the recruited Orai1 (Feske et al., 2006; Prakriya et al., 2006; Vig et al., 2006a; Vig et al., 2006b; Zhou et al., 2010b) and enabling Ca^{2+} to move down its concentration gradient into the cardiomyocyte (Voelkers et al., 2010). The sustained elevation in cytosolic Ca^{2+} concentration activates the calcineurin-NFAT pathway which upregulates the expression of pro-hypertrophic genes causing cardiomyocyte hypertrophy (Hogan et al., 2003; Musaro et al., 1999).

Nitric oxide (NO) is a chemical compound produced in the body by a group of proteins called nitric oxide synthases (NOS). In particular, neuronal NOS (nNOS) is found on the SR membrane in cardiomyocytes and has been shown to regulate Ca^{2+} handling proteins through the addition of NO groups onto reduced Cys residues to form S-nitrosocysteines in a process known as S-nitrosylation (Burger et al., 2009; Gonzalez et al., 2007). A host of over 1,000 proteins are found to be targets for S-nitrosylation in the heart alone (Haldar and Stamler, 2013). However, the effects of S-nitrosylation on STIM1 which is also anchored on the SR membrane and the downstream consequences of nNOS mediated STIM1 S-nitrosylation on cardiomyocyte hypertrophy are unknown. Therefore, the goals of this study are to examine the effects of S-nitrosylation on structure and Ca^{2+} sensing

function of STIM1 and to determine how nNOS-mediated STIM1 *S*-nitrosylation is involved in regulating phenylephrine (PE)-induced cardiomyocyte hypertrophy.

1.2 Calcium

1.2.1 General functions of Ca^{2+}

Ca^{2+} ions are essential in mediating the proper functioning of countless processes. Interestingly, Ca^{2+} promotes the formation of a new life where cytosolic Ca^{2+} elevation facilitates metabolic activity of the fertilized egg and initiates embryonic development (Santella et al., 2004). Alternations to Ca^{2+} signaling can also lead to apoptosis by working in concert with various cell death inducers like members of the Bcl-2 protein family (Pinton et al., 2008). Many vital functions of Ca^{2+} ions are mediated through the action of Ca^{2+} binding proteins. One of the well-known proteins that rely on its interaction with Ca^{2+} is calmodulin (CaM), which is ubiquitously expressed in eukaryotes and regulates downstream proteins based on its Ca^{2+} binding status (Kaleka et al., 2012). It has also been shown that Ca^{2+} acts as a main signaling molecule that regulates the force of muscle contraction, rate of muscle relaxation as well as muscle plasticity, and mutations to Ca^{2+} handling proteins can lead to detrimental pathological conditions like malignant hyperthermia (due to severe muscle contractions) and muscular dystrophies (Berchtold et al., 2000; Mickelson and Louis, 1996; Straub and Campbell, 1997). The positively charged Ca^{2+} can mask negative charges of carboxyl groups in proteins like 15-lipoxygenase, an essential cytosolic enzyme involved in hematopoietic cell differentiation, which allows these proteins to undergo membrane translocation while avoiding disruption of the lipid bilayer (Brinckmann et al., 1998). Another function of Ca^{2+} involves the regulation of neurotransmitter release, where voltage-gated Ca^{2+} channels mediate the transient local increase in cytosolic Ca^{2+} levels, synaptotagmin activation and ultimately the exocytosis of neurotransmitter vesicles from the presynaptic terminal (Südhof, 2012). Moreover, modulation of Ca^{2+} levels is a current approach for cancer treatment since it is involved throughout the course of cancer development from proliferation to invasion and metastasis (Stewart et al., 2015).

1.2.2 Ca²⁺ function in the immune system

Ca²⁺ ions play a crucial role as a second messenger in the immune system. For instance, rapid increase in cytosolic Ca²⁺ traveling through gap junctions to the wounded epidermis is necessary for attracting immune cells to the site of injury and triggering the inflammatory response (Razzell et al., 2013). In the long term, sustained Ca²⁺ elevation in the T cell can occur as a result of an immunological synapse (IS) following the association between a T lymphocyte and an antigen-presenting cell (APC). T cells have a lower level of Ca²⁺ stores compared to other non-excitable cells due to the smaller intracellular space available while accommodating the central nucleus (van der Loo et al., 1981) and the leaky ER membrane (Le Gall et al., 2004). The rise in cytosolic Ca²⁺ concentration is mediated by the phospholipase C (PLC) and inositol 1,4,5-trisphosphate (IP₃) signaling pathway, which triggers the release of the small Ca²⁺ stores. These cytosolic Ca²⁺ ions can initiate the opening of PM Ca²⁺ channels that allows more Ca²⁺ ions to enter and play important roles in T-cell regulation. The activation of a Ca²⁺ dependent protease, calpain, has been found to mediate T-cell immobilization; thus, allowing T cells to change its membrane shape to better associate with APCs. Ultimately, Ca²⁺-dependent upregulation of specific genes is necessary, following antigen detection by surface receptors, for initiating T-lymphocyte and B-lymphocyte activation as a part of the secondary immune response (Randriamampita and Trautmann, 2004). It is important to note that these aforementioned examples are just a few of the essential pathways and processes regulated by Ca²⁺ and by no means constitute an exhaustive list.

1.2.3 Intracellular Ca²⁺ compartmentalization

In order to closely regulate these processes mentioned above, Ca²⁺ is compartmentalized with a high extracellular concentration (~1 mM) and a low cytosolic concentration (~ 0.0001 mM) under basal conditions (Hunton et al., 2002). Moreover, Ca²⁺ is stored in many intracellular organelles such as the endo/sarcoplasmic reticulum (ER/SR), mitochondria and Golgi apparatus (Alonso et al., 2006; Ashby and Tepikin, 2001; Collins et al., 2013). Under resting conditions, Ca²⁺ concentrations in the cytosol and mitochondria are similarly low (~ 0.0001 mM). However, the mitochondria can act as a temporary storage for Ca²⁺ in the form of the Ca²⁺ phosphate complex in order to prevent

cellular Ca^{2+} overload and apoptosis mediated by protease and PLC activation (Nicholls, 2005; Pinton et al., 2008). Therefore, a much higher mitochondrial Ca^{2+} concentration (~ 0.05 mM) is found following cell activation and elevation of local cytosolic Ca^{2+} levels (Alonso et al., 2006). After mitochondrial Ca^{2+} uptake, the Ca^{2+} is quickly dissipated by $\text{Na}^+/\text{Ca}^{2+}$ exchangers (Boyman et al., 2013). The Golgi apparatus has been shown to accumulate Ca^{2+} (~ 0.3 mM) in resting HeLa cells which can be rapidly released upon histamine-induced IP_3 production (Pinton et al., 1998). On the other hand, the largest intracellular organellar Ca^{2+} store is the ER/SR, containing a high Ca^{2+} concentration (~ 0.4 - 0.7 mM) that can be released into the cytosol when needed in response to certain electrical or chemical signals (Collins et al., 2013).

The virtually inexhaustible extracellular source of Ca^{2+} is essential for both excitation-mediated cytosolic Ca^{2+} elevation as well as ER/SR Ca^{2+} store repletion (Hofer and Brown, 2003). Typically, the release of intracellular Ca^{2+} from stores also causes extracellular Ca^{2+} entry that together augment the cytosolic Ca^{2+} levels, after receiving specific voltage dependent and independent signals, in order to quickly initiate the activation of Ca^{2+} dependent pathways (Putney, 1986). The movement of extracellular Ca^{2+} into the cell replenishes the depleted stores, as important Ca^{2+} -dependent processes take place in the ER including protein folding and chaperone function (Araki and Nagata, 2011; Braakman and Hebert, 2013).

1.2.4 Ca^{2+} signalling impairments in the heart

Studies have indicated that impairments to normal Ca^{2+} signalling can lead to serious pathological conditions. For instance, it was found that abnormal Ca^{2+} handling and reduced ryanodine receptor (RyR) inactivation leads to cardiac arrhythmia (Chang et al., 2014). RyR2 mutations (Trp3587Ala/Leu3591Asp/Phe3603Ala) in the CaM binding domain in mice lead to pathological cardiac hypertrophy, reduced left ventricular contractility and fatality shortly after birth (Arnaiz-Cot et al., 2013). On the other hand, CaM mutations (Asn54Ile and Asn98Ser) are associated to patients with ventricular tachycardia and sudden cardiac arrest (Nyegaard et al., 2012). Moreover, heart failure is associated with increased SR Ca^{2+} store depletion through the leaky RyR2 as well as decreased SERCA2a expression and activity (Lipskaia et al., 2010). The reduction in SR

Ca^{2+} concentration is responsible for the decreased contractility characteristic of heart failure (Park and Oh, 2013). Additionally, Ca^{2+} leaked from the SR can trigger fatal cardiac arrhythmias (Yano et al., 2005). Higher resting intracellular Ca^{2+} may be responsible for contracture or impairment of relaxation function of the heart, ultimately leading to diastolic heart failure (Periasamy and Janssen, 2008). The ability for Ca^{2+} to control so many physiological processes demonstrates how essential it is to understand the functional mechanisms of proteins involved in Ca^{2+} regulation and the pathways that control Ca^{2+} signalling. A critical pathway that links both extracellular Ca^{2+} entry and stored Ca^{2+} release from the ER/SR is SOCE (Roberts-Thomson et al., 2010).

1.3 SOCE and CRAC channels

SOCE is a conserved Ca^{2+} signaling mechanism from lower eukaryotes like the fruit fly to higher vertebrates including mouse and human (Cai, 2007; Molnar et al., 2012; Redondo et al., 2006; Yeromin et al., 2004). The SOCE model was first proposed as a mechanism where extracellular Ca^{2+} entry is mobilized by the initial release of intracellular Ca^{2+} store and triggered by agonist binding to surface membrane receptors (Putney, 1986). The essential components involved in SOCE including the ER/SR Ca^{2+} sensor and PM Ca^{2+} channel subunits were identified later to be STIM (Liou et al., 2005; Roos et al., 2005; Zhang et al., 2005) and Orai (Feske et al., 2006; Prakriya et al., 2006; Vig et al., 2006a; Vig et al., 2006b) proteins, respectively. Transient receptor potential (TRP) channels were considered as the main mediators of SOCE (Mignen et al., 2008) and CRAC signalling before STIM and Orai proteins were recognized (Dráber and Dráberová, 2005; Parekh and Penner, 1997; Parekh and Putney, 2005; Varga-Szabo et al., 2009). TRP channels were found to form cation channels and mediate Ca^{2+} influx (Freichel et al., 2012), but these Ca^{2+} entry pathways are not CRAC channels which are exclusively constituted by Orai proteins (Feske et al., 2006; Prakriya et al., 2006). SOCE is a Ca^{2+} mobilization event that can be initiated following the activation of many different PM receptors, including receptor tyrosine kinases (RTK), T-cell receptors (TCR) and G-protein-coupled receptors (GPCR), which all cause IP_3 production and Ca^{2+} store depletion (Cantrell, 2002; Salazar et al., 2007; Schlessinger, 2000; Werry et al., 2003).

The importance of Ca^{2+} signalling in the heart was first recognized over 130 years ago where it was shown that the heart could not beat without the presence of Ca^{2+} ions in the circulating fluid (Ringer, 1883). In cardiomyocytes, SOCE coexists with voltage-gated Ca^{2+} entry that is mediated by L-type Ca^{2+} channels (LTCC) on the sarcolemma and RyRs on the SR following membrane depolarization (Collins et al., 2013; Tojyo et al., 2014). Although there are three isoforms of RyR, RyR1 is highly expressed in the skeletal muscle (Zorzato et al., 1990), RyR3 is found in the brain (Hakamata et al., 1992), whereas RyR2 is in cardiac muscles and regulates excitation-contraction coupling by controlling SR Ca^{2+} store release (Taur and Frishman, 2005). Interestingly, cardiac RyR2 was found to be susceptible to phosphorylation on serine residues and this post-translational modification seems to effect the progression of various cardiovascular diseases (Dobrev and Wehrens, 2014). RyR2 mutations are linked to various heart conditions where Arg4496Cys is associated with impaired contractile function of atrial and ventricular myocardium (Ferrantini et al., 2016), whereas Asn4104Lys, Arg4496Cys and Asn4895Asp are linked to ventricular tachycardia and sudden death (Jiang et al., 2004). The initiation of the excitation-contraction coupling process begins with membrane depolarization-mediated activation of LTCCs, followed by the local intracellular Ca^{2+} elevation mediated activation of junctional SR RyR2s, which ultimately enables the accumulation of a high intracellular Ca^{2+} concentration globally which induces heart muscle contractions (Hund et al., 2008). This process is termed Ca^{2+} induced Ca^{2+} release since the local Ca^{2+} elevation stimulates further SR Ca^{2+} release from RyR2 channels.

SOCE is facilitated by the activation of CRAC channels, which is crucial for Ca^{2+} signalling in response to oxidative stress (Mungai et al., 2011) (Figure 1.1). An initial stimulation, such as the binding of a ligand to its receptor, may lead to the production of secondary messengers and downstream events that cause the release of Ca^{2+} from intracellular stores like the ER/SR. For example, upon activation of specific GPCRs by agonists such as phenylephrine (PE), endothelin 1 (ET-1) and angiotensin II (ANG II), phosphatidyl inositol 4,5-bisphosphate (PIP_2) is converted into IP_3 via the action of PLC. The specific mechanisms of GPCR activation are discussed in more detail below. IP_3 can act as a second messenger that diffuses from the sarcolemma to the ER/SR, where it

binds to IP₃ receptors (IP₃R) anchored on the ER/SR membrane (Wang et al., 2005). IP₃Rs form transmembrane (TM) channels that can adopt an open conformation following the binding of IP₃ and allow the release of Ca²⁺ from the ER/SR into the cytoplasm (Yoshida and Imai, 1997). However, the ER/SR Ca²⁺ store is limited. Therefore, to maintain sustained Ca²⁺ elevation in the cytosol, extracellular Ca²⁺ entry through the sarcolemma is required. The SR Ca²⁺ depletion triggers the assembly and activation of Orai1 CRAC channels in the SOCE pathway, allowing Ca²⁺ influx from the extracellular space and replenishing the ER/SR through the action of SR/ER Ca²⁺-ATPase (SERCA) (Parekh and Putney, 2005). The sustained elevation of cytosolic Ca²⁺ causes the activation of the calcineurin-nuclear factor of activated T cells (NFAT) pathway. The details of this cardiomyocyte hypertrophy-inducing pathway are described in section 1.4.

Overall, the LTCC and RyR2 mediated Ca²⁺ induced Ca²⁺ release is responsible for the fast and high amplitude Ca²⁺ oscillation during heart contractions (Taur and Frishman, 2005), whereas STIM1 and Orai1 mediated SOCE signalling enables longer and lower level Ca²⁺ increases for transcriptional regulation via the calcineurin-NFAT pathway (Hogan et al., 2003).

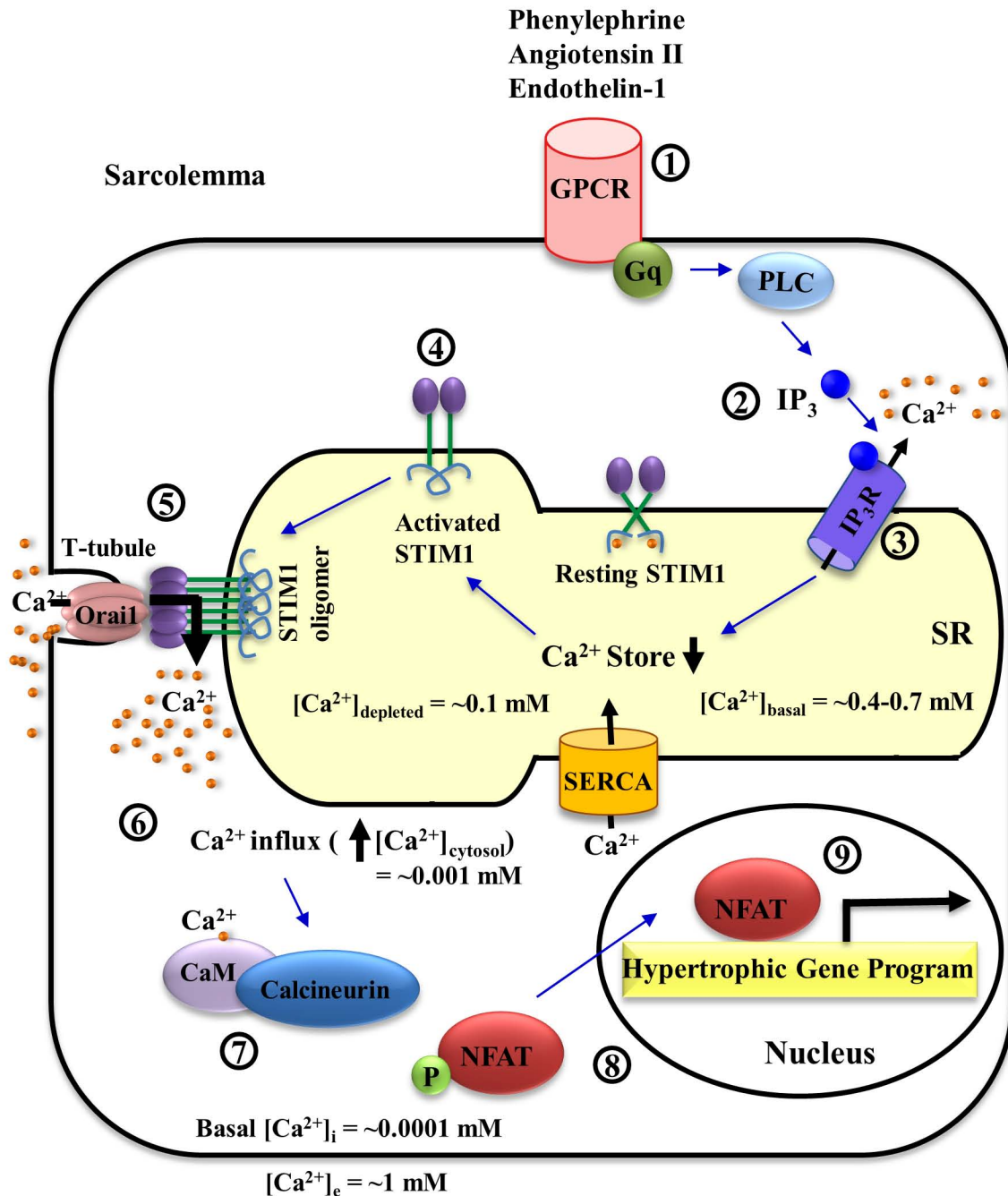


Figure 1.1. Schematic diagram of agonist-induced cardiomyocyte hypertrophy mediated by SOCE. 1. GPCR activation. 2. IP_3 production by PLC. 3. SR Ca^{2+} store depletion via IP_3R . 4. STIM1 activation following Ca^{2+} dissociation from luminal domain. 5. STIM1 mediated Orai1 activation and CRAC channel formation. 6. Ca^{2+} influx via CRAC channels. 7. Activation of the calcineurin-NFAT pathway. 8. NFAT translocation into the nucleus. 9. NFAT-mediated elevation of hypertrophic gene expression.

1.4 Stromal interaction molecule (STIM) and Orai

As previously described, the process of SOCE via CRAC channels is vital for Ca^{2+} signalling in both excitable and non-excitable cells. Two proteins that are essential for the activation, formation and regulation of CRAC channels are STIM and Orai, both of which are found in cardiomyocytes (Voelkers et al., 2010). STIM proteins function as ER/SR Ca^{2+} sensors and CRAC channel activators (Liou et al., 2005; Zhang et al., 2005), whereas Orai proteins are the structural components that form the CRAC channels and mediate Ca^{2+} entry into the cytosol (Feske et al., 2006; Voelkers et al., 2010; Zhang et al., 2011). Interestingly, coexpression of STIM1 and Orai1 in human embryonic kidney (HEK)-293 and rat basophilic leukemia cells has been found to induce enormous Ca^{2+} entry rates which are 103-fold higher compared to vector control cells, whereas expression of Orai1 alone has been shown to attenuate SOCE in the same cell types (Soboloff et al., 2006). In addition, STIM1 or Orai1 knockout mice generally die in utero or shortly after birth from respiratory and immunological complications (Cahalan, 2009; Vig et al., 2008). Several heritable STIM1 and Orai1 mutations have been identified in patients suffering from debilitating immunodeficiency diseases (Feske, 2009). These findings emphasize the importance of STIM and Orai proteins in mediating physiological SOCE functioning and CRAC currents in health and disease.

1.4.1 STIM domain organization

STIM proteins are essential Ca^{2+} sensors and SOCE activators that can be found in most eukaryotic tissues critical for maintaining normal human physiology as well as mediating pathophysiological changes (Ambily et al., 2014; Cui et al., 2017; Darbellay et al., 2010; Wang et al., 2016; Zhou et al., 2014). There are two main human homologues that are highly similar in both protein sequence and domain architecture, STIM1 (685 residues) and STIM2 (746 residues for isoform 2) (Hooper et al., 2013). Human STIM1 is a type I TM protein consisting of several luminal and cytosolic domains working in concert to regulate the activation of CRAC channels in the SOCE pathway (Figure 1.2A). On the other hand, the homologous STIM2 functions as the main regulator of basal Ca^{2+}

homeostasis (Brandman et al., 2007). Although the activity of STIM2 also depends on stored Ca^{2+} levels, it becomes activated even when the stores are near full, likely due to the weaker Ca^{2+} binding affinity of STIM2 (Gruszczynska-Biegala et al., 2011; Stathopoulos et al., 2013; Zheng et al., 2008; Zheng et al., 2011).

In the luminal region of STIM1 downstream of its signal peptide, there are two conserved cysteine residues (Cys49 and Cys56), the canonical EF-hand (residues 63-96) and non-canonical EF-hand (residues 97-128) domains, as well as a sterile α motif (SAM) (residues 132-200) which are essential for mediating the Ca^{2+} sensing function of STIMs, enabling its downstream activation under Ca^{2+} depletion (Figure 1.2B). Initially, results from sequence analysis were only able to reveal a single canonical EF-hand; however, the three dimensional (3D) structure of STIM1 exposed the presence of a non-canonical EF-hand followed by a SAM domain that is connected via a linker region. The non-canonical EF-hand forms hydrogen (H)-bonds with the canonical EF-hand and forms a pocket for interactions with the SAM domain in the presence of Ca^{2+} . When the canonical EF-hand loses Ca^{2+} , the protein undergoes a partial unfolding destabilization, coupled with oligomerization which is the initiation event for SOCE activation (Stathopoulos et al., 2006; Stathopoulos et al., 2009; Stathopoulos et al., 2008).

Live cell fluorescence resonance energy transfer (FRET) and total internal reflective fluorescence (TIRF) experiments showed that ER luminal Ca^{2+} depletion leads to the oligomerization and translocation of STIM1 as illustrated by the formation of distinct STIM1 punctate aggregates at ER-PM junctions (Liou et al., 2007; Mercer et al., 2006; Spassova et al., 2006; Stathopoulos et al., 2013). Moreover, when the luminal EF-SAM region of STIM1 was replaced by the rapamycin-binding protein, FK506-binding protein (FKBP12), the addition of rapamycin itself was sufficient to induce oligomerization of this resultant chimeric protein and initiate its translocation to the ER-PM junctions, leading to activation of CRAC channels even with replete ER Ca^{2+} stores (Luik et al., 2008). However, when the SAM domain was deleted, agonist stimulation was unable to induce STIM1 puncta accumulation near the junction (Baba et al., 2006). Collectively, these data show that oligomerization is required for translocation of STIM1 to ER-PM junctions and activation of Orail channels.

After the single-pass TM domain, the three coiled-coil (CC) regions, CC1 (residues 238-343), CC2 (residues 363-389) and CC3 (residues 399-423) are critical for facilitating the interaction between STIM and Orai proteins. The CC regions also contribute to stable STIM1 oligomerization upon ER Ca^{2+} depletion which was illustrated through the inability of STIM1 mutants lacking cytosolic region to relocalize and form puncta (Covington et al., 2010). The CC regions can also be grouped into three overlapping functional fragments including the Orai1 activating small fragment, OASF (residues 233-450), CRAC activating domain, CAD (residues 342-448) as well as STIM1-Orai1 activating region, SOAR (residues 344-443), all of which are able to induce Orai1 activation and CRAC channel formation (Muik et al., 2009; Park et al., 2009; Yuan et al., 2009). Importantly, CAD (i.e. CC2-CC3) is the minimal coupling and activating Orai1 region.

There are also several distinct regions downstream of the three CC domains near the C-terminus, an acidic inhibitory domain (ID) (residues 470-491) that is necessary for rapid Orai1 inactivation in the presence of ER luminal Ca^{2+} (Derler et al., 2009; Lee et al., 2009; Mullins et al., 2009), a proline-serine (PS) rich region (residues 600-629) where several Ser residues undergo phosphorylation, as well as a polybasic lysine (Lys) rich region (residues 671-685) which associates with PM phospholipids; deletion of the polybasic C-terminus disrupts puncta formation (Barr et al., 2009). Ultimately, the EF-SAM, TM domain, CCs, PS and K regions of STIM are well conserved from lower to higher order species and play vital roles in the proper functioning of the STIM protein (Stathopoulos et al., 2013) (Figure 1.2B).

Figure 1.2. Domain architecture and primary sequence alignment of STIM protein.

A. *Homo sapiens* STIM1 domain architecture. Following the signal peptide, SP (yellow), there are two cysteine residues in the non-conserved N-terminal region, Cys49 and Cys56 shown as red circles below their relative positions. The canonical EF-hand, cEF (light green), non-canonical EF-hand, nEF (bright green) and sterile alpha motif, SAM (cyan) domains are immediately downstream of these two cysteines on the luminal side. A single-pass transmembrane domain, TM domain (dark green) separates the three putative coiled-coil segments, CC1 (blue), CC2 (purple) and CC3 (violet) that are on the cytosolic side from the luminal domains. There are also an inhibitory domain, ID (magenta), a serine/proline-rich region, PS (pink), and a lysine rich region, K (red) near the STIM C-terminal region. **B.** Multiple sequence alignment of luminal STIM regions. Primary sequences of STIM from human to lower-order organisms are aligned, including *Homo sapiens* STIM1, H.STIM1 (NCBI accession NP_003147.2), *Homo sapiens* STIM2, H.STIM2 (NCBI accession NP_065911.3), *Rattus norvegicus* STIM1, R.STIM1 (NCBI accession NP_001101966.2), *Gallus gallus* STIM1, G.STIM1 (NCBI accession XP_420749.5), *Drosophila melanogaster* STIM, D.STIM (NCBI accession NP_523357.2) as well as *Caenorhabditis elegans* STIM, C.STIM (NCBI accession CCD73857.1). Fully conserved (*), highly conserved (:), partially conserved (.), basic (magenta), acidic (blue), polar uncharged (green) and hydrophobic (red) residues are all indicated as shown. Alignment is performed using Clustal Omega on the default settings (Sievers et al., 2011). Conserved domains are highlighted using colours matching the domain architecture in A. The conserved Cys49 and Cys56 positions are coloured red.

1.4.2 Orai domain organization

Orai proteins contain four TM components and predominantly localize at the PM (Cai, 2007; Feske, 2007). They were first identified as the CRAC channel pore forming proteins in 2006 (Feske et al., 2006; Prakriya et al., 2006; Yeromin et al., 2006) and were found to mediate SOCE across different species. A *Drosophila melanogaster* Orai (132-341) quadruple mutant (Cys224Ser/Cys283Thr/Pro276Arg/ Pro277Arg) crystal structure has been solved, where the TM regions are over 70 percent conserved compared to human Orai1 (Hou et al., 2012). The *D. melanogaster* crystal has a six-fold symmetry that supports the formation of a hexameric quaternary structure. Both hexameric and tetrameric models have been proposed for assembled and activated human Orai1 (Demuro et al., 2011; Maruyama et al., 2009; Mignen et al., 2008; Penna et al., 2008; Thompson and Shuttleworth, 2013). Within the TM1 domain in the channel pore region near the extracellular space, residue Glu178 from *D. melanogaster* Orai crystal and Glu106 from human Orai1 are necessary for the protein to specifically bind Ca^{2+} and selectively allow ions to enter the cell. Moreover, the development of a form of heritable severe combined immunodeficiency (SCID) is caused by intracellular TM1 residue Arg91Trp mutation in *H. Sapiens* (Lys163Trp in *D. melanogaster*). The crystal structure revealed that this disease-associated mutation introduces a bulky hydrophobic Trp residue to the exposed TM1 pore surface of Orai1 which interferes with Orai1 CRAC channel activity and Ca^{2+} entry (Hou et al., 2012).

Both the N- and C-termini of Orai are protruding in the cytosol and play important roles in interacting with the cytosolic regions of STIM1, which are necessary for Orai activation and CRAC channel formation (Frischauf et al., 2009; Muik et al., 2008; Muik et al., 2012; Park et al., 2009; Stathopoulos et al., 2013; Yuan et al., 2009; Zheng et al., 2013; Zhou et al., 2010a). At resting state, Orai1 C-terminal domain extending from the TM4 region associates in pairs to form a stable antiparallel structure which interacts with the STIM1 CC region at ER-PM junctions (Stathopoulos et al., 2013). The antiparallel orientation of the C-terminal helices within these dimers elucidated in the *D. melanogaster* Orai crystal structure shows structural compatibility with the NMR structure of the human CC1-CC2 STIM1 region in complex with the human Orai1 C-

terminal peptides suggesting a mechanism for coupling between STIM1 and Orai1 (Stathopoulos et al., 2013).

The three human homologues, Orai1, Orai2 and Orai3, contain highly conserved TM regions and linker regions as well as conserved acidic and basic residues necessary for channel function including Ca^{2+} ion permeability and selectivity (Stathopoulos et al., 2013). All three forms of human Orai protein can be activated by STIM following exogenous expression and can assemble into CRAC channels with different biophysical characteristics based on the combination of STIM and Orai in specific cells (DeHaven et al., 2007; Frischauf et al., 2009; Lis et al., 2007). However, Orai1 is the only homologue that constitutes the endogenous homomeric CRAC channel. Structural elucidation of the Orai1 protein via electron microscopy indicates that it has an extended teardrop-shape and a 10 nm cytoplasmic region which mediates its association directly with STIM1 (Maruyama et al., 2009).

1.4.3 STIM1 and Orai1 function

SOCE activation via CRAC channels is a multi-step process involving many molecular players, notably STIM1 and Orai1. As previously mentioned, STIM1 is an ER/SR Ca^{2+} sensor that binds to, assembles and gates CRAC channels (Zhao et al., 2015). Studies have indicated that the EF-SAM domains of STIM1 are essential for detecting changes in luminal Ca^{2+} concentrations (Stathopoulos et al., 2006) while regions of the long putative CC1 and short CC2 and CC3 domains directly interact with and activate Orai1-composed CRAC channels (Stathopoulos et al., 2013).

When Ca^{2+} concentration in the ER/SR lumen is high, Ca^{2+} binds to the EF-SAM region of STIM1 and keeps it in an inactive state. Following Ca^{2+} release from the ER/SR through particular channels like the IP_3R , low luminal Ca^{2+} levels results in the loss of bound Ca^{2+} to the EF-SAM domain and triggers the destabilization and oligomerization of the EF-SAM domain. This process initiates structural changes on the cytosolic side of STIM1 which leads to the conformational extension and oligomerization of the CC region. These structural changes then result in the translocation of STIM1 to the ER/SR-PM junctions and the recruitment of Orai subunits to the same sites that form the CRAC

channel complex (Stathopoulos et al., 2013). This interaction between STIM1 and Orai1 ultimately induces the opening of CRAC channels made up of Orai1 molecules selective for Ca^{2+} ions and produces the inward current caused by Ca^{2+} entry down its concentration gradient into the cytosol (Stathopoulos et al., 2008).

Active CRAC channels constituted of Orai1 subunits can be inactivated by the CRAC modulatory domain within STIM1 and CaM in a process termed Ca^{2+} dependent inactivation (CDI) (Derler et al., 2009; Mullins et al., 2009; Roos et al., 2005). STIM1 residues 470-491 downstream of the CC3 domain containing 7 acidic residues were found to be vital for STIM1 to rapidly exert its role in the CDI process (Mullins et al., 2009). Interestingly, CaM has been found by various studies to interact with the polybasic region of both STIM1 (667-685) and STIM2 (730-746) C-terminal regions with μM affinity in a Ca^{2+} dependent manner (i.e. $\sim 1 \mu\text{M}$ with Ca^{2+} and $\sim 100 \mu\text{M}$ without Ca^{2+}) and prevent STIM protein from translocating to ER-PM junctions (Bauer et al., 2008; Calloway et al., 2011; Korzeniowski et al., 2009; Walsh et al., 2009; Yuan et al., 2009).

A key step in the initiation of SOCE is the destabilization and activation of STIM1 in response to depleted ER/SR Ca^{2+} stores (Stathopoulos et al., 2006). Thus, an in depth study of modifications that influence STIM1 stability will reveal important new insights on the regulation of SOCE. Previous studies have found that the coiled-coil (CC) regions of STIM1 alone are capable of assembling Orai1 into CRAC channels by forming a multimeric structure and binding to the cytoplasmic surface of Orai1 (Kawasaki et al., 2009; Stathopoulos et al., 2013). However, several aspects concerning the regulation of the STIM1 N-terminal region and its allosteric effect on the STIM1 CC regions and on the activation of Orai1 still need to be elucidated. The short, non-conserved N-terminal regions of STIM1 and STIM2, containing two modifiable cysteine residues, have been shown to modulate the stability of the Ca^{2+} -sensing EF-SAM core and thereby the activation of SOCE (Stathopoulos et al., 2009; Zhou et al., 2009); thus, it is prudent to study the effect of specific modifications of residues in this region on the overall function of STIM. Moreover, since many studies have detected STIM1 in cardiomyocytes and SOCE is known to play a central role in cardiac hypertrophy, investigations on the

precise molecular mechanisms of SOCE regulation will reveal important insights into the underlying pathophysiological signals contributing to heart dysfunction (Hulot et al., 2011; Hunton et al., 2002; Luo et al., 2012; Zhu-Mauldin et al., 2012).

1.5 Cardiac hypertrophy

The human heart is a vital organ in the circulatory system that works continuously through one's lifespan of likely over 80 years. While pumping blood throughout the circulatory system, the heart is often exposed to a myriad of electrical and chemical stimuli that could be physiological or pathophysiological and needs to react promptly to meet these demands in an appropriate manner. Transient stress can cause the heart to respond with reversible hyperfunction and return back to basal conditions once the stressor is no longer present. However, when stress on the heart becomes persistently high, often due to high blood pressure, valve dysfunction or myocardial infarction (MI), the heart increases its ventricular wall thickness in order to maintain the necessary level of cardiac output. This chronic compensatory hyperfunction of the heart can cause progressive cardiac dilation and dysfunction that ultimately lead to the development of severe disease conditions including pathological cardiac hypertrophy and heart failure (Tardiff, 2006).

1.5.1 Physiological and pathological hypertrophy

Cardiac hypertrophy is characterized by an enlargement of the heart muscle due to an increase in cardiomyocyte size. This resultant phenotype is developed because adult cardiomyocytes have lost the ability to replicate themselves and can only grow by increasing their cell size (Soonpaa et al., 1996). Not all forms of cardiac hypertrophy are disease related. For instance, physiological hypertrophy can develop in athletes, which results in normal if not enhanced cardiac function (Pluim et al., 2000). A trained athlete's heart has distinct morphological differences, including a higher ventricular wall thickness, elevated left ventricular volume and heart weight, due to the increased cardiac output, pressure and volume overload experienced during intense exercise regimens (Fagard, 1997; Pluim et al., 2000; Spirito et al., 1994). On the other hand, pathological cardiac hypertrophy can stem from conditions such as MI, high blood pressure and

particular genetic mutations of sarcomere proteins (Levy et al., 1988; Seidman and Seidman, 2001). For patients with pathological cardiac hypertrophy, otherwise known as hypertrophic cardiomyopathy, monitoring left ventricular wall thickness using echocardiography can indicate the extent of disease progression. The increased maximal ventricular wall thickness directly correlates with poorer treatment prognosis and an elevated risk for sudden death even in the absence of symptoms (Spirito et al., 2000). Moreover, pathological cardiac hypertrophy is accompanied by an increase in pro-inflammatory cytokines, impaired cell signaling as well as the development of cardiac fibrosis (Shimizu and Minamino, 2016). There are many intracellular mechanisms that contribute to the development of physiological and pathological cardiac hypertrophy. Studies have found an increase in fatty acid and glucose oxidation during exercise in humans (Gertz et al., 1988), whereas cells from pathologically hypertrophied hearts have lower fatty acid oxidation and elevated glucose metabolism (Allard et al., 1994; Christie and Rodgers, 1994; Davila-Roman et al., 2002). The initial onset of increased glucose metabolism is likely a compensatory mechanism aimed at protecting the heart by producing more ATP (van Bilsen et al., 2009). However, as the disease progresses, the development of insulin resistance effectively cripples the ability of the hypertrophied heart to produce the necessary ATP and contributes to the development of other comorbidities (Kolwicz and Tian, 2011; Neubauer, 2007; Paternostro et al., 1999).

1.5.2 Intracellular signalling pathway

Many receptors and pathways under investigation are associated with the development of pathological cardiac hypertrophy. For instance, it has long been revealed that GPCRs are vital in mediating cell signaling, regulating protein expression and interacting with other receptors in cells from the cardiovascular system (Salazar et al., 2007; Tang and Insel, 2004). Typically, this pathway is initiated when a ligand binds to the GPCR (see below), causing this PM protein to change in conformation and couple with heterotrimeric guanine-nucleotide regulatory proteins (G proteins) containing α , β and γ subunits, which then dissociate and activate downstream effectors. The $G\alpha$ subunit includes $G\alpha_s$ which is stimulatory and becomes activated upon β -adrenergic receptor (AR) stimulation, $G\alpha_i$ that is inhibitory following ligand binding to a muscarinic receptor, and $G\alpha_q$ which is

stimulated as a result of α_1 -AR activation. The downstream effector for $G\alpha_s$ and $G\alpha_i$ is adenylyl cyclase, whereas PLC acts as the effector for $G\alpha_q$ and produces secondary messengers IP_3 and diacylglycerol (DAG) following activation (Luttrell, 2006).

Studies have shown that in cardiomyocytes, the GPCRs associated with $G\alpha_q$ activation, including the previously mentioned α_1 -AR, ANG II and ET-1 receptors, can all mediate the development of cardiac hypertrophy via the calcineurin-NFAT pathway and often work in concert with the mitogen-activated protein kinase (MAPK) pathway (Knowlton et al., 1993; Sugden, 1999). Interestingly, transgenic mice overexpressing $G\alpha_q$ exhibit cardiomyocyte hypertrophy, heart weight elevation, myocardial contractility impairment, fractional shortening attenuation, biventricular failure and higher mortality (D'Angelo et al., 1997), while cardiac specific overexpression of ANG II receptor leads to the development of an abnormally slow heart rate and death a few weeks after birth (Hein et al., 1997). On the other hand, inhibition of $G\alpha_q$ signaling by overexpression of a $G\alpha_q$ inhibitory peptide results in substantial attenuation of cardiac hypertrophy and MAPK activation following transverse aortic constriction-induced pressure overload (Akhter et al., 1998; Esposito et al., 2001).

Transgenic overexpression of $G\alpha_s$ protein in the heart has also been found to mediate the development of cardiomyocyte hypertrophy, myocardial fibrosis and apoptotic cell death leading to heart failure in mice (Gaudin et al., 1995; Iwase et al., 1996). The protein kinase B (Akt) and mammalian target of rapamycin (mTOR) signaling pathway is also shown to be involved in pathological hypertrophy, in which mTOR overexpression mitigates the inflammatory reaction in cardiomyocytes and prevents the cardiac dysfunction that typically occurs after pressure overload (Song et al., 2010).

1.5.3 Role of Ca^{2+} and SOCE

Following PE-mediated activation of its corresponding GPCR [α_1 (α_1)-AR] which is associated with the heterotrimeric protein $G\alpha_q$, the production of IP_3 by PLC triggers the activation of IP_3R on the ER/SR membrane and the Ca^{2+} -depletion mediated activation of the SOCE pathway. Sustained increases in intracellular Ca^{2+} levels mediated by SOCE results in the activation of calcineurin, a Ca^{2+} and CaM-dependent protein phosphatase,

which cleaves a phosphate group off NFAT. The dephosphorylated transcription factor NFAT then translocates into the nucleus to upregulate the transcription of pro-hypertrophic genes (Hogan et al., 2003; Musaro et al., 1999).

1.6 Nitric oxide synthase

NO is a chemical compound ubiquitously produced in the body by a group of proteins called NOS and has been shown to play an important role in regulating contractility, excitation-contraction coupling as well as hypertrophic signalling in cardiomyocytes (Kelly et al., 1996). There are three isoforms of NOS, namely, nNOS, inducible NOS (iNOS) and endothelial NOS (eNOS) that differ in both structure and function. nNOS and eNOS are typically expressed constitutively and are Ca^{2+} dependent, whereas iNOS is only highly expressed after inflammatory cytokine induction and is not sensitive to Ca^{2+} level changes (Stuehr, 1997). The three NOS homologues play vital roles in various eukaryotic tissues.

1.6.1 iNOS

The expression of iNOS can be induced by particular cytokines, bacterial lipopolysaccharides and other agonists in almost any cell type (Forstermann et al., 1994). The synthesis of NO by iNOS in macrophages is the major contributor mediating its cytotoxic effect on downstream pathogens (Nathan and Hibbs, 1991). The large amount of NO produced by macrophages can exert its effect by directly causing DNA fragmentation in the target bacterial or fungal cells (Wink et al., 1991). Moreover, iNOS expression contributes to the development of heart failure post-MI in mice (Feng et al., 2001), which is supported by studies that show improved cardiac function post-MI following inhibition of iNOS activity (Liu et al., 2005; Sun et al., 2009).

1.6.2 eNOS

eNOS is the predominant NOS isoform found in endothelial cells and the pulsatile production of NO by eNOS in response to particular stimuli, such as the Ca^{2+} -dependent binding of calmodulin, leads to vascular smooth muscle dilation and enhanced microcirculation (Sandoo et al., 2010). eNOS is an important regulator of blood pressure

and its deficiency results in elevations of blood pressure (Barouch et al., 2003). In cardiomyocytes, eNOS is found in the sarcolemma and facilitates β_2 -AR signalling by *S*-nitrosylating G protein receptor kinase 2, β -arrestin2 and dynamin; thus enabling an increase in contractility and cardiac output (Haldar and Stamler, 2013). eNOS was identified as a necessary mediator of ginseng-induced cardioprotection during ischemia and reperfusion (I/R). It was revealed that eNOS knockout (eNOS^{-/-}) mice did not experience reduced myocardial infarction even with the ginseng treatment (Wu et al., 2011). eNOS also plays a role in atrioventricular (AV) valve development via the process of endothelial to mesenchymal transition (EMT). eNOS^{-/-} results in incomplete formation of the cardiac AV valve (Liu et al., 2013) as well as the development of atrial septal defects (ASD) and ventricular septal defects (VSD) (Feng et al., 2002). eNOS deficiency can also result in a congenital heart defect called hypoplastic coronary artery disease that is caused by the incomplete development of coronary arteries and linked with poor treatment outcomes as well as high mortality rates (Liu et al., 2014).

1.6.3 nNOS

nNOS is predominantly found in the central and peripheral neurons and has been demonstrated to play an important role in long term potentiation, learning and memory formation (Zhou and Zhu, 2009). In cardiomyocytes, nNOS is found in the SR membrane (Xu et al., 1999). nNOS regulates Ca²⁺ handling proteins such as cardiac RyRs and L-type Ca²⁺ channels through *S*-nitrosylation, to name a few (Burger et al., 2009; Gonzalez et al., 2007). Stimulation of integrin from neonatal rat cardiomyocytes was found to induce the development of a hypertrophic phenotype in a NO-dependent manner (Umar et al., 2009). Studies have indicated that nNOS is present in the SR and mitochondria of cardiomyocytes and can modulate cellular Ca²⁺ concentration and transport by inhibition of cardiac SR Ca²⁺-ATPase activity (Kanai et al., 2001; Xu et al., 1999). Additionally, nNOS has been found to function as an essential regulator of basal myocardial contractility and Ca²⁺ handling in left ventricular (LV) cardiomyocytes (Sears et al., 2003). Mice with nNOS^{-/-} have higher cardiac oxidative stress (Kar et al., 2014) as well as increased ventricular arrhythmia and mortality after MI by left coronary artery ligation (Burger et al., 2009). Moreover, nNOS^{-/-} and eNOS^{-/-} mice have elevated mortality rates,

cardiac hypertrophy, progressive interstitial fibrosis and hypertension (Barouch et al., 2003). nNOS overexpression in transgenic mice attenuates cardiac deterioration following chronic pressure-overload induced heart failure by modulating Ca^{2+} cycling (Loyer et al., 2008). On the other hand, the effect of nNOS overexpression in PE-induced cardiomyocyte hypertrophy has not been well characterized.

1.7 S-Nitrosylation

Protein post-translational modifications such as phosphorylation and ubiquitination have long been recognized as critical processes for ensuring proper signal transduction and cell functions. It was only in the past 20 years that accumulating evidence has been discovered emphasizing the vital regulatory role of *S*-nitrosylation working in concert with many other post-translational mechanisms which includes the aforementioned phosphorylation and ubiquitination, as well as acetylation, palmitoylation, sumoylation and redox modifications, to name a few (Hess and Stamler, 2012).

1.7.1 Mechanism of S-nitrosylation

S-Nitrosylation is a readily reversible cysteine (Cys) modification that can occur under the presence of an NO donor and an electron acceptor. Specifically, *S*-nitrosylation involves the addition of NO groups onto reduced Cys residues to form *S*-nitrosocysteines (Figure 1.3) which affects the structure and function of the *S*-nitrosoproteins (Gould et al., 2013). More than 1,000 proteins are found to be *S*-nitrosylated in the heart alone; a list which will likely expand with the emergence of better detection methods (Haldar and Stamler, 2013; Hess and Stamler, 2012).

1.7.2 Effect of S-nitrosylation on different proteins

Selective *S*-nitrosylation of specific Cys residues was found to effect protein stability, activation, structure, localization and function (Gould et al., 2013). *S*-nitrosylation of glyceraldehyde-3-phosphate dehydrogenase (GAPDH) at Cys247 has been shown to inhibit its ability to appropriately function as a chaperone protein, thus leading to the ubiquitination and degradation of ribosomal protein L13a (Jia et al., 2012). Dysregulation of particular enzymes involved with *S*-nitrosylation or denitrosylation often results in

serious pathological conditions. For instance, GSNO reductase (GSNOR) is a metabolic enzyme that selectively reduces the *S*-nitrosothiol group from GSNO and cellular proteins using NADH as an electron donor. The activity of GSNOR is tightly regulated in order to maintain physiological homeostasis and resist damage from nitrosative stress. Since NO is physiologically produced from L-arginine via the action of NOS enzymes, many pathological conditions stem from the dysregulation of arginine metabolic pathways and lack of NO production, including allergic asthmas and pulmonary hypertension (Maarsingh et al., 2006; Morris et al., 2008).

1.7.3 *S*-nitrosylation and cardiac function

S-nitrosylation may elevate or inhibit protein functions depending on the specific protein it targets. For example, a recent study has shown that GSNOR overexpression in mice inhibits isoproterenol-induced left ventricular hypertrophy, reduces interstitial fibrosis and increases myocardial Ca²⁺ sensitivity by preventing *S*-nitrosylation of several Ca²⁺ handling proteins, such as cardiac troponin C, phospholamban and RyR (Irie et al., 2015). On the other hand, GSNOR knockout (GSNOR^{-/-}) mice have excess SNO formation which results in blood pressure dysregulation, elevated tissue injury and increased mortality rate following endotoxic shock (Liu et al., 2004). Interestingly, *S*-nitrosylation has also been found to activate or suppress protein function depending on the specific Cys residue being modified. *S*-nitrosylation of Ca²⁺/CaM-dependent protein kinase II at Cys290 after Ca²⁺/CaM treatment leads to autonomous activation, whereas *S*-nitrosylation of Cys273 prior to Ca²⁺/CaM treatment inhibits kinase activation and reduces the effect exerted by Ca²⁺/CaM afterwards (Erickson et al., 2015). *S*-nitrosylation also regulates the function of many ion channels that are involved in excitation-contraction coupling in cardiomyocytes (Bers, 2002). For example, *S*-nitrosylation by exogenous SNP treatment or ionomycin-induced endogenous NOS activation leads to the persistent activation of voltage-gated Na⁺ channels and a sustained residual Na⁺ current (Ahern et al., 2000). Moreover, *S*-nitrosylation of cardiac L-type Ca²⁺ channels using *S*-nitrosoacetyl-penicillamine (SNAP), *S*-nitrosocysteine (SNC) or GSNO attenuates whole-cell patch recording currents (Hu et al., 1997). The distinct impact of *S*-nitrosylation on a variety of proteins and its effect on cardiac physiology make it essential to investigate.

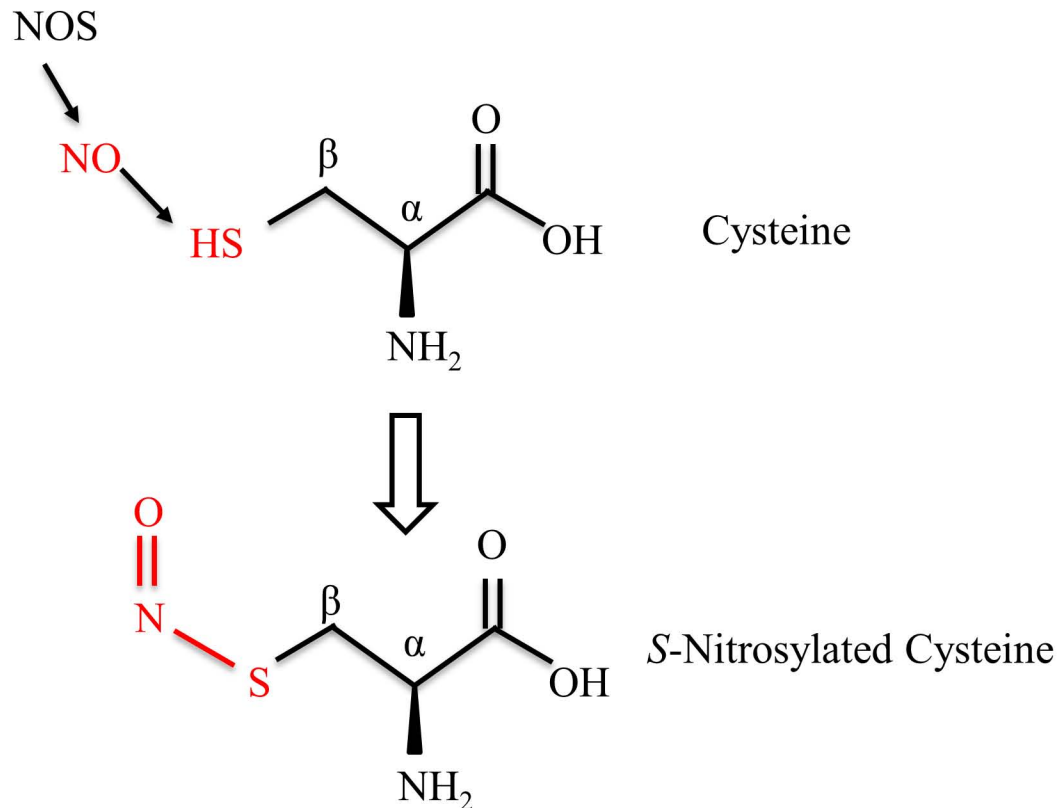


Figure 1.3. Depiction of the mechanism through which cysteine residues are *S*-nitrosylated. NO molecules produced by specific NOS isoforms, such as nNOS, eNOS and iNOS, can react with the SH side chain on the cysteine residue's beta carbon and form *S*-nitrosocysteines under oxidative conditions. The inherent chemical instability associated with this covalent bond enables this cysteine modification to be readily reversible. The atoms directly modified via *S*-nitrosylation are highlighted in red.

1.8 Summary and Rationale

SOCE is a major contributor to Ca^{2+} signalling and regulation. However, SOCE-mediated intracellular Ca^{2+} elevation cannot occur without the activation of STIM1, which is linked to its luminal domain Ca^{2+} sensitivity and stability. Although studies have revealed that SOCE is vital in Ca^{2+} regulation within non-excitable cells (Molnar et al., 2012; Redondo et al., 2006; Tojyo et al., 2014), the extent of its contribution to Ca^{2+} homeostasis in cardiomyocytes is less well-studied. Moreover, precisely how NO may regulate the ER/SR Ca^{2+} sensor STIM1 and its influence on SOCE is still unknown. The non-conserved N-terminal ends of STIMs are recognized to contribute to the differential activation of STIM proteins (Stathopoulos et al., 2009; Zhou et al., 2009), which is why I postulate that the two partially conserved N-terminal Cys residues of STIM1 could have important functional and mechanistic roles (Figure 1.2B). Interestingly, recent studies suggest that STIM1 Cys49 and Cys56 undergo *S*-glutathionylation following oxidative stress where Cys56 *S*-glutathionylated STIM1 becomes constitutively active and activates SOCE regardless of luminal Ca^{2+} concentration (Hawkins et al., 2010). Due to their susceptibility of oxidative stress, these Cys residues are also candidate sites for *S*-nitrosylation. Previous studies have shown that *S*-nitrosylation can play an inhibitory role on proteins including the fast and slow Na^+ channels (Renganathan et al., 2002) as well as NMDA receptors (Takahashi et al., 2007). Moreover, *S*-nitrosylation of tripartite motif-containing protein 72 (TRIM72) was found to stabilize this protein, allow for membrane repair and augment cardiomyocyte survival (Kohr et al., 2014). Importantly, the lack of *S*-nitrosylation resulting from nNOS and eNOS deficiency has been shown to cause cardiac hypertrophy (Barouch et al., 2003; Barouch et al., 2002). Thus, modification of Cys49 and Cys56 residues in STIM1 via NO treatment would also be expected to inhibit STIM1 activation by promoting its stabilization.

I propose that the stability and function of STIM1 may be regulated by *S*-nitrosylation of its luminal domain at Cys residues 49 and 56. Thus, the aim of my study is to reveal the effect of NO on STIM1 structure and stability *in vitro* and the downstream effects of STIM1 *S*-nitrosylation on cardiomyocyte hypertrophy. Understanding the mechanisms by which STIM1 *S*-nitrosylation contributes to Ca^{2+} signaling will enhance our

comprehension of the SOCE pathway in health and disease. Specifically, identifying the role of *S*-nitrosylated STIM1 in PE-induced cardiac hypertrophy will contribute to our understanding of the pathogenic progression of cardiovascular disease and open exciting avenues to novel treatments.

1.9 Hypothesis and aims

Hypothesis:

NO directly stabilizes and inhibits STIM1 by *S*-nitrosylation of the Cys49 and Cys56 thiol residues, thereby suppressing the Ca²⁺ sensitivity of STIM1. Furthermore, *S*-nitrosylation of STIM1 mitigates PE-induced neonatal rat cardiomyocyte hypertrophy by suppressing SOCE activation.

Aim 1: To elucidate the effect of *S*-nitrosylation on the stability, oligomerization, structure and Ca²⁺ sensing function of STIM1 *in vitro*.

The luminal Ca²⁺ sensing region, STIM1 23-213, was cloned into a pET-28a vector, expressed in BL-21 *E. coli* and purified using nickel-nitrilotriacetic acid agarose (Ni-NTA) beads in order to study this luminal STIM1 domain in an *in vitro* environment. The purified STIM1 23-213 protein contains two thiol residues available for modification, Cys49 and Cys56, which was treated with excess concentration of NO donors, GSNO and sodium nitroprusside (SNP) to monitor the susceptibility and effect of *S*-nitrosylation. Moreover, a structurally unresolved region at high resolution, STIM1 24-57, located upstream of the EF-SAM domain and containing the Cys49 and Cys56 residues was subcloned into a pGEX-4T1 vector, expressed and purified before being *S*-nitrosylated to reveal the structural changes to this peptide associated with the modification.

Aim 2: To examine how STIM1 *S*-nitrosylation is involved in mediating cardiomyocyte hypertrophy.

Cardiomyocytes were isolated from 1-2 day old neonatal Sprague-Dawley rats and incubated for 24 h on gelatin coated plates prior to treatment using PE to induce hypertrophy. Various other reagents were also added to the cultured cardiomyocytes following the PE treatment, including Orai1 inhibitor BTP2, STIM1 siRNA, NO donor GSNO and ectopic expression of adenoviral nNOS, to investigate the phenotypic effect of CRAC channel inhibition and NO on PE-induced cardiomyocyte hypertrophy. The cells were then immunostained using a cardiac specific marker, α -actinin, and their surface areas were measured after fluorescence microscopy imaging as an indicator of hypertrophy.

Chapter 2 Methods

2.1 Generation of STIM1 constructs and mutants

The luminal region (residues 23-213) of *Homo sapiens* STIM1 (NCBI accession NP_003147.2) containing the Ca²⁺ sensing EF-SAM domain (residues 58-201) together with the region containing the two Cys residues (Cys49 and Cys56) available for S-nitrosylation (residues 23-57), was cloned into a pET-28a vector that has been used previously for expressing the EF-SAM domain (residues 58-201) of STIM1 (Stathopoulos et al., 2006).

H. sapiens STIM1 residues 24-57 (NCBI accession NP_003147) was first subcloned from pCMV6 STIM1 residues 1-685 template into pET-28a vector using NheI and XhoI restriction sites. The DNA encoding the STIM1 24-57 peptide was then subcloned into the pGEX-4TI (GE Healthcare) vector using BamHI and EcoRI restriction sites. Specifically, in order to obtain a STIM1 24-57 insert, a 150 μ L PCR solution mixture was first created using 112.5 μ L dH₂O, 30 μ L 5 \times high fidelity (HF) Buffer, 0.75 μ L 90 ng μ L⁻¹ pCMV6 STIM1 template, 1.5 μ L of each forward and reverse primer (Table 2.1), 3 μ L 10 mM dNTPs and 0.75 Phusion DNA polymerase (Thermo Fisher Scientific). The 150 μ L PCR solution was then divided into two PCR tubes with 75 μ L in each and amplified as described in Table 2.2. The final PCR product was electrophoresed at 125 V for 50 min on a 1.5% (w/v) agarose gel using a running buffer (TAE) that contains 0.5 \times Tris, acetic acid and ethylene diamine tetra acetic acid (EDTA). In order to estimate the size of the PCR product (130 bp expected), 4 μ L DNA ladder (GeneRuler 1kb Plus, ThermoFisher) was run on a separate lane. The agarose gel was stained by submerging it in 0.5 μ g mL⁻¹ ethidium bromide dissolved in water and shaking for 30 min at room temperature. The STIM1 24-57 insert was visualized on the agarose gel under UV light (302 nm), excised and transferred into an eppendorf tube. The DNA was extracted from the gel using GeneFlow Gel/PCR kit according to the manufacturer's protocol.

Sticky end overhangs were created by double digestion with BamHI and EcoRI on both the STIM1 insert and pGEX-4TI vector. Digestion mixtures were prepared with 35 μ L of STIM1 insert, 4 μ L Cut Smart Buffer and 0.5 μ L of each restriction enzyme in one microcentrifuge tube, and 11 μ L pGEX-4TI vector, 2 μ L Cut Smart Buffer, 1 μ L of each

restriction enzyme and 5 μL dH_2O in the microcentrifuge tube. The digestion mixtures were incubated overnight at 37 $^\circ\text{C}$. The digested DNA samples were separated on an agarose gel, stained and observed under UV light as described above. The final BamHI and EcoRI-digested STIM1 24-57 insert (102 bp after digestion) and pGEX-4TI vector (4960 bp after digestion) were extracted from the agarose gel as described above.

Ligation of the digested insert into the digested pGEX-4TI vector was done by combining 4.5 μL dH_2O , 2.5 μL pGEX-4TI vector, 10 μL STIM1 24-57 insert and 2 μL T4 DNA ligation buffer, heating the mixture at 42 $^\circ\text{C}$ for 2-3 min, chilling it on ice for 1 min and adding 1 μL T4 DNA ligase. This ligation mixture was then placed in a water bath at 16 $^\circ\text{C}$ for 16 hours. The ligation product was transformed through heat shock into DH5 α *E. coli* and selectively grown on ampicillin agar plates (100 $\mu\text{g mL}^{-1}$). Several bacterial colonies were screened for the correct pGEX-4TI STIM1 24-57 vector by scraping each colony with a pipette tip and placing it into an eppendorf tube that contains 20 μL of dH_2O . Afterwards, 5 μL of this colony-solubilized water was added into 10 μL 2 \times Taq Frogga Mix, 0.5 μL pGEX forward primer, 0.5 μL pGEX reverse primer (Table 2.1) and 4 μL dH_2O , and the entire mixture was subjected to PCR for 25 cycles (Table 2.2). The PCR screen product was electrophoresed on 1.5% (w/v) agarose gel at 125 V for 50 min, stained with ethidium bromide and colonies which showed the expected band size (~ 5000 bp) were grown in 5 mL Luria-Bertani broth (LB) containing 100 $\mu\text{g mL}^{-1}$ of ampicillin overnight. The next day pGEX-4TI plasmids containing the STIM1 24-57 insert were isolated from the liquid culture using the Presto Mini Plasmid kit (Geneaid) according to the manufacturer guidelines.

A tyrosine (Tyr) residue was subsequently introduced by site-directed mutagenesis immediately N-terminal to residue 24 to simplify protein detection via Coomassie staining and facilitate UV at 280nm measurements for protein concentration determination. Specifically, 0.5 μL of the forward and reverse primers (Table 2.1) were each added to 14.15 μL dH_2O , 4 μL 5 \times HF buffer, 0.4 μL DMSO, 0.25 μL undiluted pGEX-4TI STIM1 24-57 template DNA, 0.5 μL dNTPs and 0.2 μL Phusion DNA polymerase (Thermo Fisher Scientific). The two PCR solutions containing either the forward or reverse primer were first subjected to 10 PCR cycles under the parameters

listed (Table 2.2); the resultant PCR products were immediately mixed together and the final mixture was subjected to 25 more amplification cycles. The amplification product was run alongside the same amount of input template DNA on a 1.5% (w/v) agarose gel at 125 V for 50 min. A higher relative intensity of the PCR product under UV light (302 nm) compared to the input template was used as an indication of amplification success. Subsequently, 0.75 μ L (15 units) of DpnI restriction enzyme (New England BioLabs, Inc.) was added to the remaining 25 μ L of amplification product and incubated for 2 h 30 min at 37 °C to digest the methylated template DNA. The digestion product was transformed into DH5 α *E. coli* and plated on an ampicillin LB plate. The next day, colonies were grown in an overnight liquid culture and plasmids were isolated from the liquid culture ~16 h later using the Presto Mini Plasmid kit (Geneaid).

In order to elucidate the importance of residues Trp121 and Lys122 in the luminal region of STIM1, a double mutated construct pET-28a STIM1 23-213 Trp121Glu/Lys122Glu was generated via the same mutagenic process as described above, using the primers and amplification parameters in Tables 2.1 and 2.2.

All the subcloned and mutated constructs were made using High-Fidelity PCR polymerase (Thermo Scientific, Inc.). All primers were synthesized by Sigma-Aldrich and synthesized using the 0.025 μ mol scale and cartridge purification (Table 2.1). The isolated pET-28a STIM1 23-213 and pGEX-4TI STIM1 24-57 plasmids were sequenced at Robart's DNA Sequencing facility (Robarts Research Institute, Western University) using the T7 reverse terminator primer and pGEX forward primer respectively (Table 2.1).

Table 2.1. Oligonucleotide primers used in the research described in this thesis. (Sigma-Aldrich, St. Louis, MO)

Primer	Sequence
pET-28a	5'-GGCCAGGCTAGCAGCCATAGTCACAGTGAGAAG-3'
STIM1 24-57^a	3'-GTTTCTCCTCGAGTTAGTGACACAGGGGCTTGTCAATTC-5'
pGEX-4TI	5'-GGCCAGGGATCCAGCCATAGTCACAGTGAGAAG-3'
STIM1 24-57^a	3'-GTTTCTCGAATTCTTAGTGACACAGGGGCTTGTCAATTC-5'
pGEX-4TI	5'-CTGGTTCGCGTGGATCCTATAGCCATAGTCACAGTGAGAAG-3'
STIM1 24-57	
Y-insert^b	3'-CTTCTCACTGTGACTATGGCTATAGGATCCACGCGGAACCAG-5'
pET-28a	5'-CATCAGCGTGGAGGACCTGGAGGAGGCATGGAAGTCATCAG-3'
STIM1 23-213	
Trp121Glu/ Lys122Glu^c	3'-CTGATGACTTCCATGCCTCCTCCAGGTCCTCCACGCTGATG-5'
T7 terminator^d	5'-GCTAGTTATTGCTCAGCGG-3'
pGEX forward^{d,e}	5'- GGGCTGGCAAGCCACGTTTGGTG-3'
pGEX reverse^e	3'- CCGGGAGCTGCATGTGTCAGAGG-5'

^aSubcloning primers for STIM1 24-57

^bMutagenesis primer for pGEX-4TI STIM1 24-57

^cMutagenesis primer for pET-28a STIM1 23-213

^dSequencing primer

^eScreening primers for pGEX-4TI STIM1 24-57

Table 2.2. PCR amplification parameters on LifeECO (Bioer).

	pGEX-4TI STIM1 24-57 screening		pGEX-4TI STIM1 24-57 subcloning		pGEX-4TI STIM1 24-57 Y-insert mutagenesis		pET-28a STIM1 23-213 Trp121Glu/ Lys122Glu mutagenesis	
	25 Cycles		35 Cycles		10 Cycles + 25 Cycles		10 Cycles + 25 Cycles	
	Temp (°C)	Time (sec)	Temp (°C)	Time (sec)	Temp (°C)	Time (sec)	Temp (°C)	Time (sec)
Initial Denaturation	98	30	98	30	98	35	98	35
# Cycles								
Denatura- tion	98	10	98	10	98	10	98	10
Annealing	54	30	54	30	53	30	54	30
Extension	72	30	72	30	72	180	72	180
Final Extension	72	30	72	30	72	330	72	330
Storage	4	∞	4	∞	4	∞	4	∞

2.2 Protein expression and purification

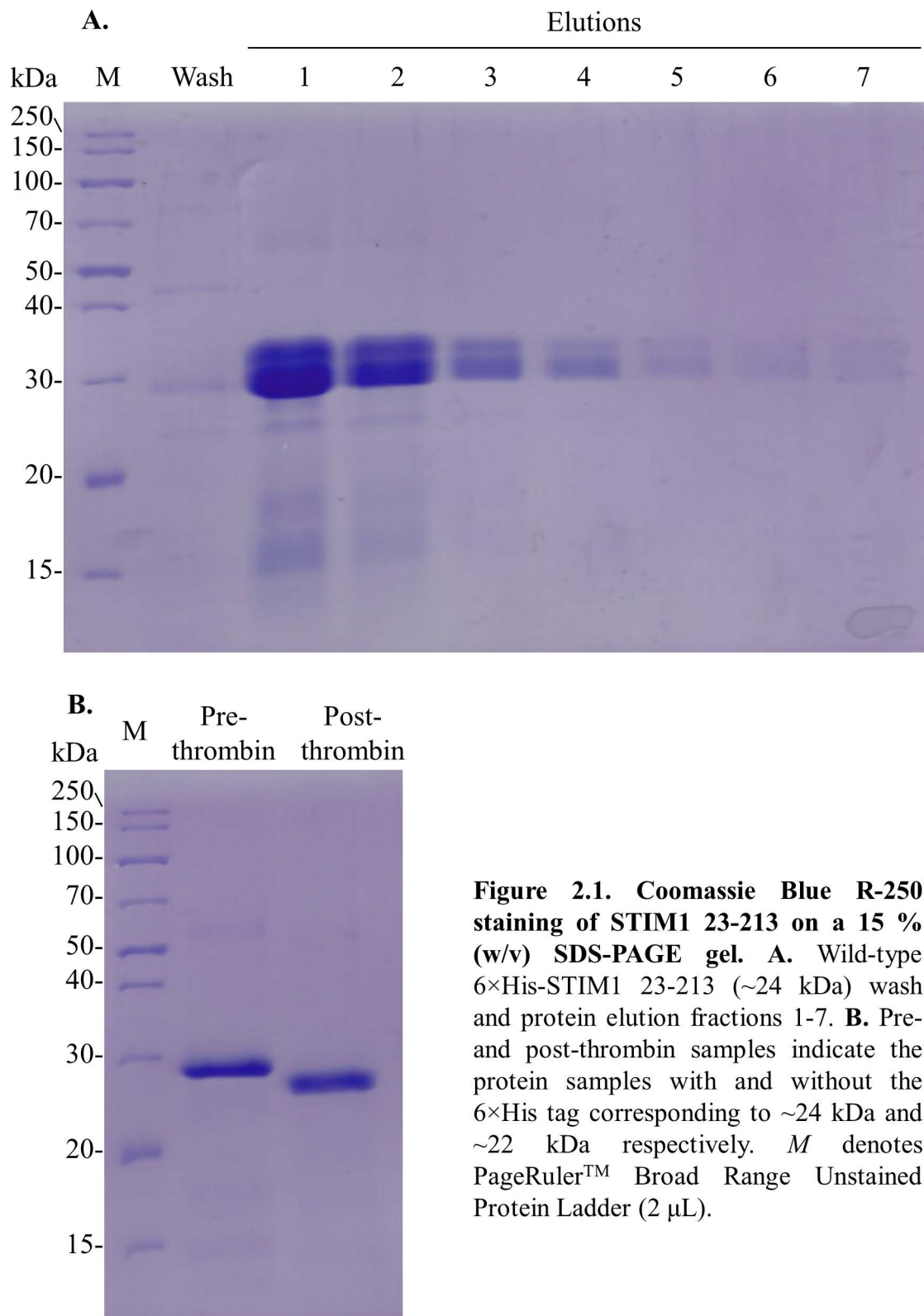
2.2.1 pET-28a STIM1 23-213 wildtype and mutants

Transformants of pET-28a STIM1 23-213 were selected by using kanamycin LB agar plates where incorporation of the gene construct into BL21(DE3) *E. coli* is necessary for those bacteria cells to form viable colonies. Individual colonies were picked for 65 mL starter liquid cultures in a 500 mL flask. This 65 mL of starter culture was used for 6 × 1 L LB expression containing 60 µg mL⁻¹ kanamycin using 6 × 4 L flasks. The cultures were grown at 37 °C with 190 rpm constant shaking. The cultures were grown until the optical density at 600 nm (OD₆₀₀) was in the ~0.6-0.8 range, at which point, 200 µM of isopropyl β-D-1-thiogalactopyranoside (IPTG) was added to induce protein expression. Upon IPTG addition, the temperature was dropped to 25 °C. After ~4 h of growth at 25 °C and 190 rpm, the bacterial cells were collected using a JA10 rotor in a J2-21M Induction drive centrifuge (Beckman, Inc.) with the parameters set to 9,300 ×g, 4 °C for 30 min. The pelleted cells were stored at -80 °C until purification. The 200 µM IPTG concentration, 25 °C expression temperature and 4 h growth period were determined by varying these parameters in an incrementing fashion until the optimal conditions that produced the most proteins with least degradation were found.

The STIM1 23-213 protein was purified by first manually homogenizing 7-8 mL of wet bacterial cell pellet collected from 2 L of LB culture in 40 mL of 6 M guanidine hydrochloride, 20 mM Tris-HCl (pH 8) and 5 mM β-mercaptoethanol (BME) with a motorized 10 mL transfer pipette. The homogenized mixture was rotated in a hybridization oven at room temperature for 90 min to release the protein from inclusion bodies, and then centrifuged using a JA20 rotor in a J2-21M Induction drive centrifuge at 12,100 ×g, 8 °C for 40 min to obtain the protein supernatant and remove insoluble debris. The clarified lysate containing the solubilized protein was incubated subsequently with 450 µL of 50% (v/v) nickel-nitrilotriacetic acid (Ni-NTA) agarose bead slurry (HisPur, ThermoFisher Scientific) in the hybridization oven and rotated for another 90 min at room temperature to bind the hexahistidine (6×His)-tag of the protein to the beads. The STIM1 23-213 protein bound to the beads was then retained in a gravity flow protein

purification column, washed three times with 10 mL of 6 M Urea, 20 mM Tris-HCl (pH 8) and 5 mM BME, eluted seven times with 2 mL of 6 M Urea, 20 mM Tris-HCl (pH 8), 5 mM BME and 300 mM imidazole following 2 min incubation between each elution. After the presence of the protein in the elution fractions was confirmed on a Coomassie stained SDS-PAGE gel (Figure 2.1A), the elutions that contain the protein of interest were pooled together into a 3,500 Da molecular weight cutoff dialysis membrane (BioDesign Inc.) and placed into the 1 L refolding buffer [20 mM Tris-HCl (pH 8), 300 mM NaCl, 1 mM dithiothreitol (DTT) and 5 mM CaCl₂]. A magnetic stir bar was used to ensure homogeneous exchange between the unfolding and folding buffers overnight at 4 °C. Following ~24 h of refolding, ~1 U of thrombin (BioPharm Laboratories, Inc.) per mg of protein was added into the dialysis membrane bag and placed back in the refolding buffer for another ~24 h. The efficiency of thrombin cleavage was elucidated by running a sample of the protein aliquot before and after the addition of thrombin on an SDS-PAGE gel (Figure 2.1B). Size-exclusion chromatography (SEC) was performed to further separate STIM1 23-213 from contaminant proteins expressed in the cell (Figure 2.2). STIM1 23-213 wildtype protein concentration was estimated using a $\epsilon_{280\text{ nm}} = 1.2418\text{ mg mL}^{-1}\text{ cm}^{-1}$ extinction coefficient. Approximately 4 mg of protein was obtained from each 2 L LB culture pellet.

The single mutant STIM1 23-213 Cys49Ser and STIM1 23-213 Cys56Ser as well as the double mutant STIM1 23-213 Cys49Ser/Cys56Ser and STIM1 23-213 Trp121Glu/Lys122Glu proteins were also expressed and purified the same way as the wildtype protein with similar yields, except reducing agents BME and DTT were not added while purifying STIM1 23-213 Cys49Ser/Cys56Ser since there was no possibility of disulfide bond formation. The STIM1 23-213 Cys49Ser, STIM1 23-213 Cys56Ser, STIM1 23-213 Cys49Ser/Cys56Ser and STIM1 23-213 Trp121Glu/Lys122Glu protein concentrations were estimated using $\epsilon_{280\text{ nm}} = 1.2427\text{ mg mL}^{-1}\text{ cm}^{-1}$, $1.2427\text{ mg mL}^{-1}\text{ cm}^{-1}$, $1.2436\text{ mg mL}^{-1}\text{ cm}^{-1}$ and $0.9909\text{ mg mL}^{-1}\text{ cm}^{-1}$ extinction coefficients, respectively.



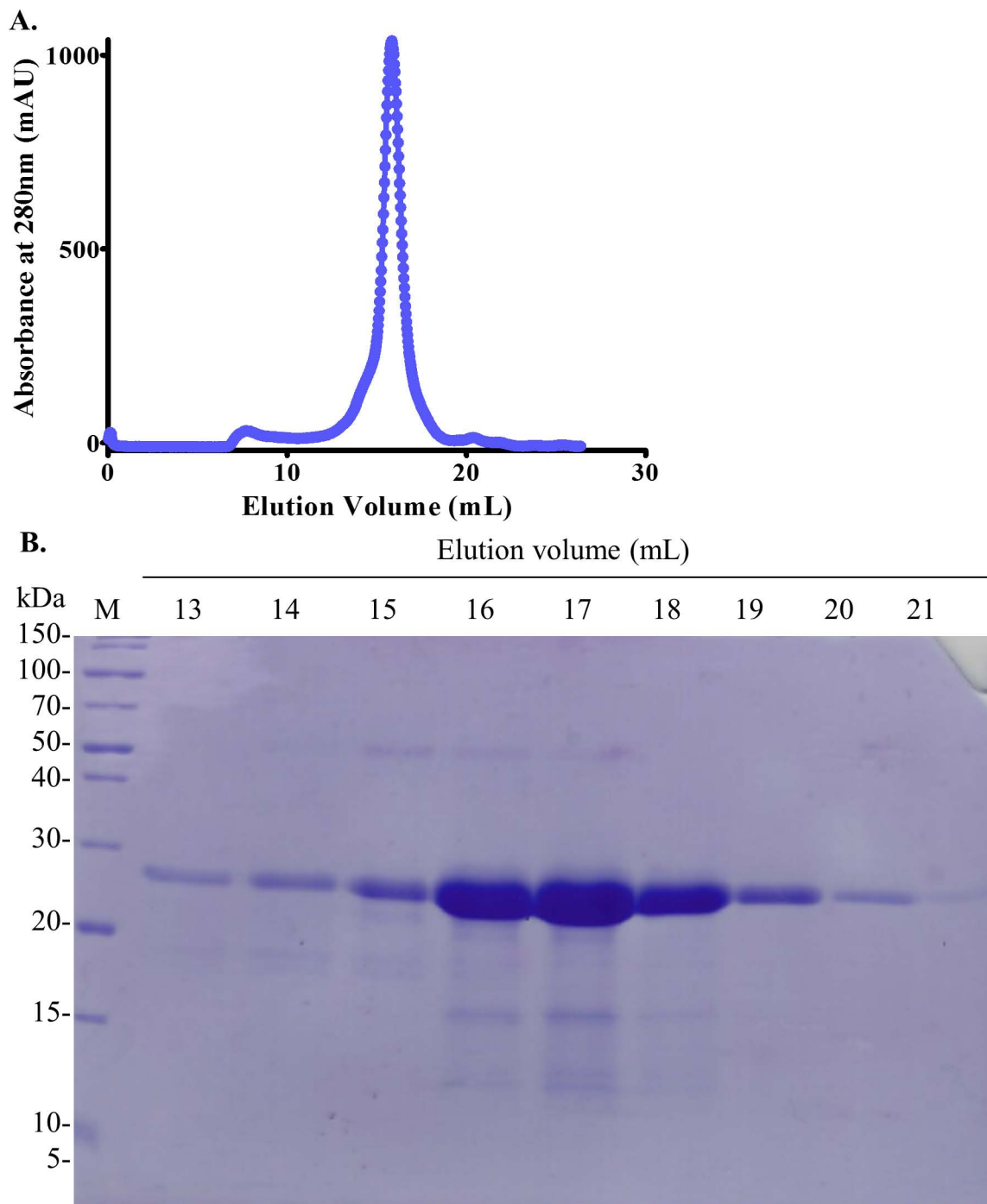


Figure 2.2. Size exclusion chromatography elution profile of STIM1 23-213. Size-exclusion chromatography was performed using Superdex 200 10/300 GL column (GE Healthcare, Inc.). **A.** Elution profile is shown as absorbance at 280 nm (A_{280}) in arbitrary units (mAU) *versus* elution volume. **B.** Coomassie Blue R-250 staining of STIM1 23-213 (~24 kDa) on a 15% (w/v) SDS-PAGE gel of elution volumes ~13-21 mL. *M* denotes PageRuler™ Broad Range Unstained Protein Ladder (2 μ L).

2.2.2 pGEX-4TI STIM1 24-57

The pGEX-4TI STIM1 24-57 construct containing the Tyr insert mutation immediately upstream of residue 24 was transformed by heat shock into BL21(DE3) *E. coli* cells as described above for the pET-28a STIM1 23-213, except 100 $\mu\text{g mL}^{-1}$ ampicillin was used as the selection marker. Colonies were picked and expressed in 30 mL LB in a 250 mL Erlenmeyer flask containing 100 $\mu\text{g mL}^{-1}$ ampicillin at 37 °C and 190 rpm overnight. The next day, 10 mL of this starter culture was added to 1 L of LB contained in a 4 L Erlenmeyer flask and supplemented with ampicillin at 100 $\mu\text{g mL}^{-1}$. The culture was grown at 37 °C and 190 rpm until the OD_{600} reached $\sim 0.6-0.8$. Subsequently, 300 μM IPTG was added and the expression temperature was dropped to 30 °C. The cells were cultured for ~ 4 h before being collected as described above.

The wet cell pellets were purified essentially as described in the manufacturer's glutathione-S-transferase (GST) Sepharose protocol (Genescript). Specifically, the 5 mL cell pellet obtained from a 2 L LB expression was resuspended in 45 mL wash buffer containing 1 \times PBS and 1 mM DTT. The bacterial mixture was then sonicated on ice at 40 % power using the Fisher Sonic Dismembrator Model 150 for 10 min in 3 sec on and 3 sec off cycles. After the addition of 0.2% (v/v) triton x-100, the resultant mixture was rotated in the cold room for 90 min to release the STIM1 24-57 peptide into solution and centrifuged at 12,100 $\times g$, 8 °C for 40 min using a JA20 rotor in a J2-21M Induction drive to separate the insoluble cell debris. Approximately 1 mL of 50 % (v/v) GST beads in 10 % ethanol was added to 30 mL of wash buffer that contains 1 \times PBS and 1 mM DTT and the excess liquid was poured off following centrifugation at 2000 $\times g$ for 5 min. The washed GST beads were then added to the protein clarified lysate and rotated in the cold room for another 90 min. The STIM1 24-57 peptide bound to the GST beads was retained using a gravity flow purification column and washed with 3 \times 10 mL wash buffer that contains 1 \times PBS and 1 mM DTT. Sixteen mL of protein folding buffer containing 20 mM TRIS, 150 mM NaCl, 1 mM DTT (pH 7.5) and thrombin (~ 5 units mg^{-1} of total protein) were added to the peptide bound GST beads. After rocking in the cold room overnight, the STIM1 24-57 peptide was liberated from the GST bound to the resin by thrombin and eluted from the column. More peptide was collected by washing the GST

beads with 3×1 mL protein folding buffer with the components described above. The pre-thrombin solution, elution and three washes were run on a gel to verify the presence of the peptide in the elution and typically in the first wash. The samples containing the STIM1 24-57 peptide were then pooled and further purified by SEC (Figure 2.3). STIM1 24-57 peptide concentration was estimated using a $\epsilon_{280 \text{ nm}} = 0.3296 \text{ mg mL}^{-1} \text{ cm}^{-1}$ extinction coefficient. Approximately 5 mg of protein was obtained from each 2 L LB culture pellet. Due to the aberrant migration of the protein on SDS-PAGE gel (Figure 2.3), a sample of the purified protein was analyzed by electrospray ionization mass spectrometry to confirm the identity of the purified protein. The theoretical monomeric mass of the STIM1 24-57 construct was calculated to be 3,719.92 Da; the mass spectrometry measured mass was 3,720.09 Da, confirming the identity of the purified peptide as STIM1 24-57 (Figure 2.4).

For NMR experiments, the STIM1 24-57 peptide was uniformly ^{15}N -labelled or double ^{15}N and ^{13}C -labelled using M9 medium containing 42 mM Na_2HPO_4 , 22 mM KH_2PO_4 and 8.6 mM NaCl (pH 7.4) as well as additives that were filtered through a 0.2 μm syringe filter (Millipore). The additives included 0.2 % (w/v) D-glucose or D-glucose- ^{13}C , 100 μM CaCl_2 , 50 μM thiamine, 1 mM MgSO_4 , 1 $\mu\text{g mL}^{-1}$ biotin and 1 mg mL^{-1} ^{15}N - NH_4Cl . First, a 30 mL starter liquid culture was grown in LB overnight for ~ 16 h at 37 $^\circ\text{C}$ and 190 rpm. The bacterial liquid culture was centrifuged at $2,400 \times g$ for 15 min, decanted to remove the LB medium, resuspended in 10 mL of M9 medium and transferred into the 1L M9 expression medium containing all the aforementioned additives. The rest of the expression protocol including growth temperature, time, IPTG concentration, collection and purification were the same as the non-labelled sample described above with similar yields.

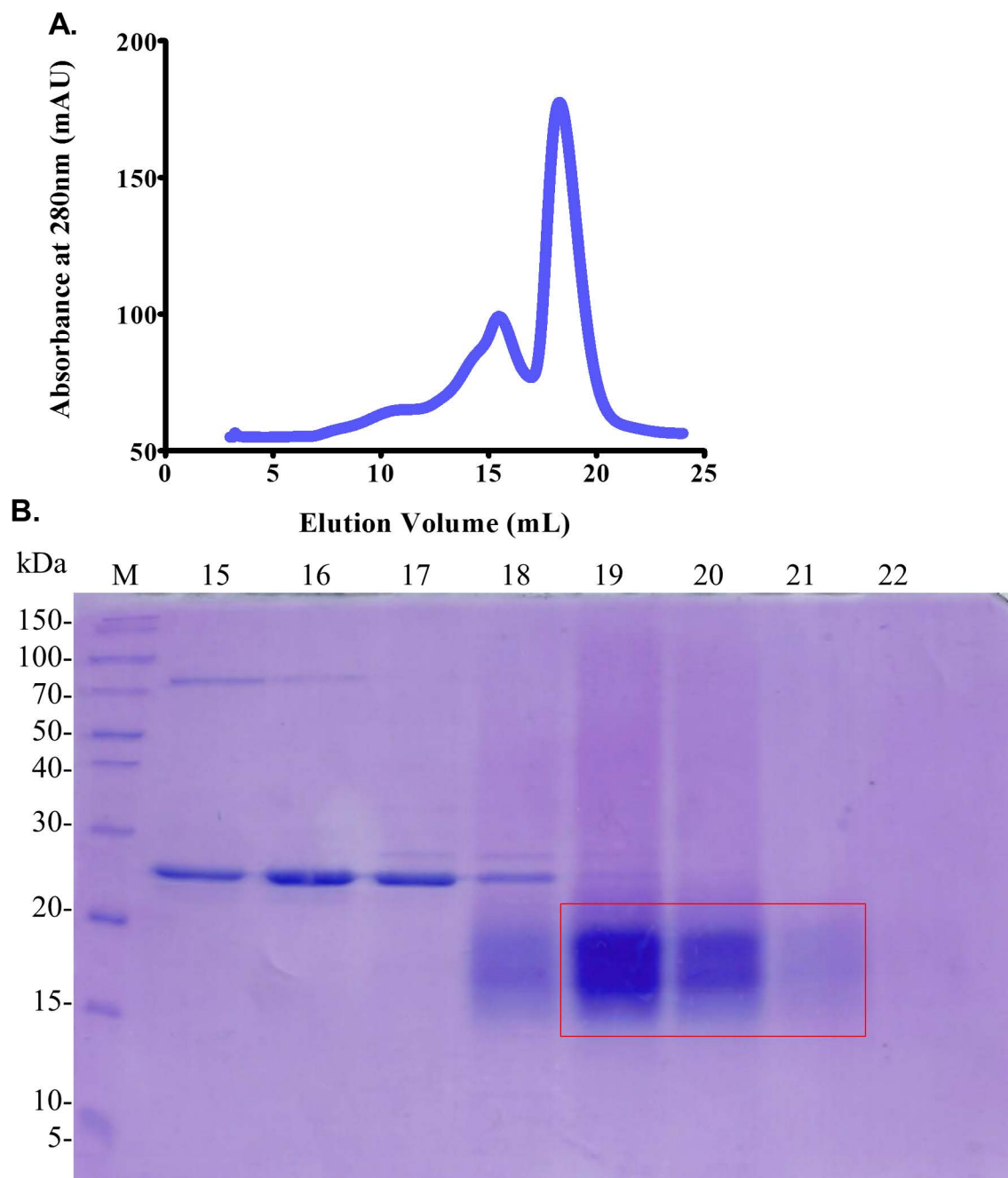


Figure 2.3. Size exclusion chromatography elution profile of STIM1 24-57 containing the Tyr insert. Size-exclusion chromatography was performed using Superdex 200 10/300 GL column. **A.** Elution profile shown as absorbance at 280 nm (A_{280}) in arbitrary units (mAU) *versus* elution volume. **B.** Coomassie Blue R-250 staining of STIM1 24-57 (3.8 kDa) on a 15 % (w/v) SDS-PAGE gel of elution volumes ~15-22 mL. The elutions containing the STIM1 24-57 peptide with the Tyr insert are enclosed in the red box. *M* denotes PageRuler™ Broad Range Unstained Protein Ladder (2 μ L).

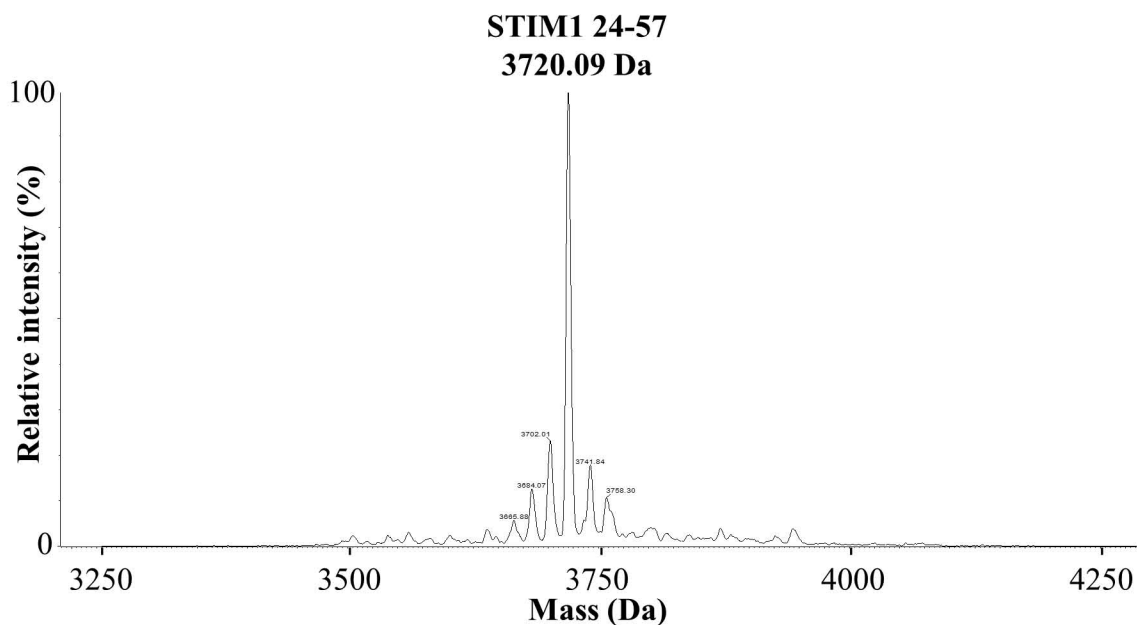


Figure 2.4. Transformed mass spectrum of STIM1 24-57 peptide. The peptide was prepared using a Zeba spin Desalting column (ThermoFisher, Inc.). Electrospray ionization mass spectrometry was performed by UWO Biology Mass Spectrometry Laboratory at Siebens-Drake Research Institute on a Quattro Micro mass spectrometer (Waters) equipped with a Z-spray source and run in positive ion mode with an Agilent 1100 HPLC used for flow injection. The mass of the major component was found to be 3720.09 Da, which is within the 0.5 Da mass error from the theoretical mass of STIM1 24-57 (3719.92 Da) based on its primary sequence and expected isotopic abundance.

2.2.3 pET-28a STIM1 58-201 (EF-SAM)

pET-28a STIM1 58-201 (EF-SAM) was expressed in BL21(DE3) *E. coli* using LB that contains 60 $\mu\text{g mL}^{-1}$ kanamycin at 37 °C and 190 rpm. A similar overnight starter culture approach was applied here, as described for STIM1 23-213. After OD_{600} reached ~ 0.6 - 0.8 , 200 μM IPTG was added and the temperature was dropped to 22 °C with constant shaking at 190 rpm for an additional ~ 16 h. The cells were collected as described above and the pellets were stored at -80 °C until purification. Purification was performed using Ni-NTA agarose beads as described for STIM1 23-213 with the following modifications. The STIM1 58-201 (EF-SAM) protein bound to the beads was retained in a gravity flow column, washed three times with 10 mL of wash buffer that contains 6 M Urea and 20 mM Tris-HCl (pH 8) as well as eluted seven times with 2 mL of elution buffer that contains 6 M Urea, 20 mM Tris-HCl (pH 8) and 300 mM imidazole following 2 min incubation between elutions. The 5 mM BME was not present in the wash and elution buffers because there are no Cys residues that need to be reduced in the EF-SAM protein segment. The elutions that contain the protein of interest were pooled together into a 3,500 Da molecular weight cutoff dialysis membrane (BioDesign Inc.) and placed into the 1 L refolding buffer with 20 mM Tris-HCl (pH 8), 150 mM NaCl and 5 mM CaCl_2 . After ~ 24 h of refolding at 4 °C aided by the use of a magnetic stir bar, ~ 1 U of thrombin (BioPharm Laboratories, Inc.) per mg of protein was added into the dialysis membrane and placed back into the refolding buffer for an additional ~ 24 h to cleave off the 6 \times His tag. After thrombin digestion, anion-exchange chromatography (AEC) was performed as an additional purification step. A 1 mL DEAE FF column (GE Healthcare) was used for AEC, and this column was first equilibrated with a no salt buffer containing only 20 mM Tris-HCl (pH 8) and 5 mM CaCl_2 . Proteins were then slowly bound onto the column at a rate of 1 mL min^{-1} after being diluted with the no salt buffer to a final ~ 15 mM NaCl concentration and filtered through a 0.45 μm syringe filter. During the 30 mL elution stage, the salt concentration in the column was gradually increased from 0 to 600 mM NaCl at 1 mL min^{-1} using a high salt buffer that contains 1 mM NaCl, 20 mM Tris-HCl (pH 8) and 5 mM CaCl_2 . A representative Coomassie-blue stained gel of elutions is shown in Figure 2.5. The elutions containing the protein of interest were pooled and dialyzed into the specific experimental buffer that typically contains 20 mM Tris-HCl

(pH 8), 50 mM NaCl and 5 mM CaCl₂. EF-SAM protein concentration was estimated using a $\epsilon_{280\text{ nm}} = 1.6062\text{ mg mL}^{-1}\text{ cm}^{-1}$ extinction coefficient. Approximately 0.5 mg of protein was obtained from each 2 L LB culture pellet.

¹⁵N-labelled STIM1 58-201 (EF-SAM) protein expression was done via the same process as the ¹⁵N-labelled STIM1 24-57 peptide except using the expression parameters described above for EF-SAM (~16 h expression at 22 °C). Protein purification was done through the same process as the non-labelled EF-SAM protein with similar yields.

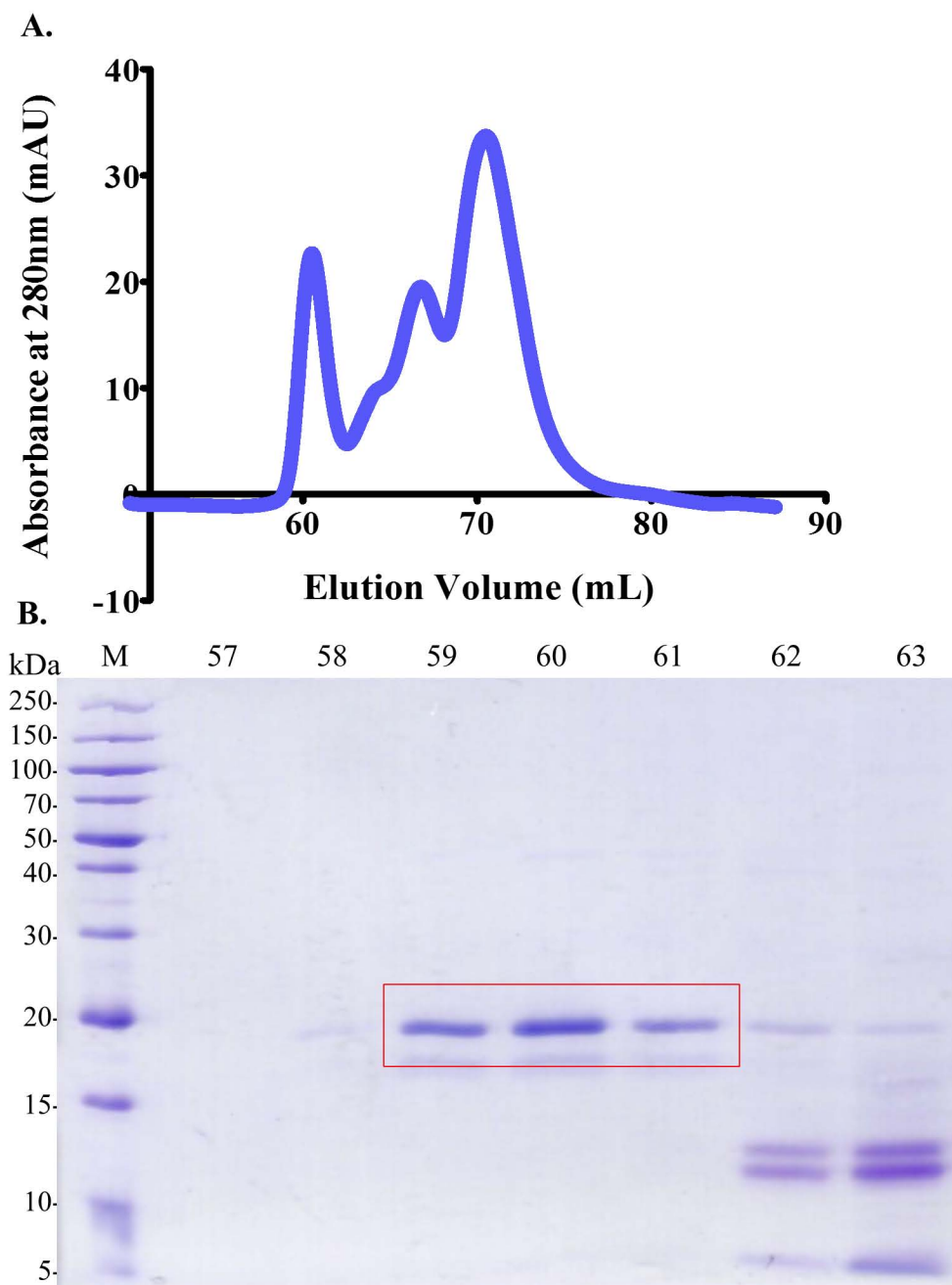


Figure 2.5. Anion exchange chromatography elution profile of wildtype EF-SAM protein. Anion exchange chromatography was performed using a HiTrap DEAE Fast Flow 1 ml column (GE Healthcare, Inc.). **A.** Elution profile is shown as absorbance at 280 nm in arbitrary units (mAU) *versus* elution volume. **B.** Coomassie Blue R-250 staining of EF-SAM (17.4 kDa) on a 15 % (w/v) SDS-PAGE gel of elution volumes 57-63 mL. The elutions containing the EF-SAM protein are enclosed in the red box. *M* denotes PageRuler™ Broad Range Unstained Protein Ladder (2 μ L).

2.3 *S*-Nitrosylation of STIM1

The proteins of interest (*i.e.* STIM1 23-213 wildtype, single mutants Cys49Ser and Cys56Ser, double mutants Cys49Ser/Cys56Ser and Trp121Glu/Lys122Glu, STIM1 24-57 with Tyr insert) were exchanged into a buffer containing excess NO donors (1 mM GSNO or 2 mM SNP) by ultrafiltration. Essentially, a 20×20×20-fold buffer exchange was done at 2,500 ×g, 4 °C, using centrifugal concentrators (Vivaspin 20) with 10,000 or 3,000 MWCO (Sartorius, Inc.) for STIM1 23-213 and STIM1 24-57, respectively.

The ~500 mM stock GSNO was synthesized by dissolving 1.54 g of reduced glutathione in 5.9 mL of 570 mM HCl. This acidic glutathione solution was stirred vigorously while 1 mL of 5 M NaNO₂ was added, and this mixture was stirred for an additional 5 min in the dark. The final GSNO stock solution was adjusted to pH 6 using 1 M NaOH and brought to a final volume of 10 mL using dH₂O. The concentration of GSNO was measured using a spectrophotometer set to 335 nm wavelength and an extinction coefficient of 0.92 mM⁻¹ cm⁻¹ (Broniowska et al., 2013). The 500×, 750× and 1000× diluted GSNO samples were used for concentration measurements to accurately assess the GSNO stock concentration. The ~500 mM stock GSNO was stored in 1 mL aliquots at -80 °C. Different *S*-nitrosylation buffer components were used depending on the specifics of the experiment conducted, details of which will be described below.

2.4 Far-UV circular dichroism (CD) spectroscopy

The STIM1 23-213 wildtype, single and double mutant protein samples were transferred into the selective buffers using a centrifugal concentrator (Vivaspin 20 with 10,000 MWCO; Sartorius, Inc.) essentially through a 20×20×20-fold buffer exchange. The control buffer contained 1 mM DTT, 10 mM TRIS-HCl and 5 mM CaCl₂ (pH 7.4) while the experimental buffer contained 1 mM GSNO or 2 mM SNP, 10 mM TRIS-HCl and 5 mM CaCl₂ (pH 7.4). To prepare the protein samples for experiments under the Ca²⁺-depleted condition, 50 mM EDTA was added the day prior to the buffer exchange process and the sample was incubated for ~ 16 h at 4 °C. The exchange was subsequently performed in the absence of Ca²⁺, as described above. UV absorbance at 280 nm (A₂₈₀) was used to estimate protein concentration and 275 μL of 0.5 mg/mL protein was used in

each experiment. Far-UV CD spectra and thermal melt analyses were performed to characterize the protein secondary structure and thermal stability, respectively. Data were acquired on a Jasco J-815 CD Spectrometer (Jasco Inc.) with a Jasco PTC-423S temperature controller. Spectra were acquired at 20 °C from 240 nm to 200 nm in 1 nm increments (20 nm min⁻¹) by using a 0.1 cm pathlength quartz cuvette, an 8-s averaging time, an average of 3 accumulations and 1 nm bandwidth. Moreover, the protein spectra were corrected for buffer contributions (10 mM TRIS ± 5 mM CaCl₂, pH = 7.4).

Thermal melts were acquired by monitoring the change in the 225 nm CD signal as a function of temperature in 0.1 cm pathlength quartz cuvettes, an 8-s averaging time, 1 nm bandwidth and a 1 °C min⁻¹ scan rate. The apparent midpoints of temperature denaturation (T_m) were extracted from the thermal melts using Boltzmann sigmoidal fits in GraphPad, where the Boltzmann sigmoid equation used was:

$$Y = \frac{Min + (Max - Min)}{1 + 10^{[(\log T_m - X) \cdot slope]}}$$

where Y = change in CD signal,

Min = minimum CD signal (folded baseline),

Max = maximum CD signal (unfolded baseline),

T_m = temperature of denaturation,

and X = temperature.

2.5 Ca²⁺ binding

It has been previously demonstrated that EF-SAM Ca²⁺ binding affinity estimates using intrinsic fluorescence changes are similar to direct binding estimates using ⁴⁵Ca²⁺ assays (Stathopoulos et al., 2006). After overnight incubation in 50 mM EDTA, wildtype STIM1 23-213 protein was exchanged into a buffer containing 20 mM TRIS, 150 mM NaCl, and 1 mM DTT or 1 mM GSNO (pH 7.4) via the same ultrafiltration process described above. Fluorescence readings at 37 °C were obtained on a Cary Eclipse

spectrofluorimeter (Varian/Agilent, Inc) using 600 μL of 0.1 mg mL^{-1} protein in 600 μL quartz cuvettes. The intrinsic protein fluorescence emission spectra were measured from 300 nm to 450 nm using an excitation wavelength of 280 nm. The excitation and emission slit widths were 5 nm and 10 nm, respectively, and the photomultiplier (PMT) detector was set at 600 V. The equilibrium dissociation constant (K_d) was estimated from the change in intrinsic fluorescence using a one site-binding model which takes into account protein concentration:

$$P + Ca \xrightleftharpoons{K_d} PCa, PCa = \frac{1}{2} [K_d + P_{tot} + Ca - \sqrt{(K_d + P_{tot} + Ca)^2 - 4P_{tot} \cdot Ca}]$$

where K_d = equilibrium dissociation constant,

P = free protein concentration,

Ca = total Ca^{2+} concentration,

PCa = Ca^{2+} bound protein concentration,

and P_{tot} = total protein concentration.

2.6 8-Anilidonaphthalene-1-sulfonic acid (ANS) binding

The relative levels of solvent-exposed hydrophobicity were assessed via extrinsic fluorescence of ANS on a Cary Eclipse spectrofluorimeter (Varian/Agilent, Inc). Wildtype and double mutant Cys49Ser/Cys56Ser STIM1 23-213 protein samples were *S*-nitrosylated as described above via ultrafiltration. The control and experimental buffers contained 20 mM TRIS, 150 mM NaCl with and without Ca^{2+} as well as 1 mM DTT or 1 mM GSNO (pH 7.4). UV absorbance at 280 nm (A_{280}) was used to estimate protein concentration and 600 μL of 0.143 mg mL^{-1} protein was loaded in 600 μL quartz cuvettes for each experiment. The extrinsic ANS-induced fluorescence (excitation wavelength, λ_{ex} = 372 nm) was measured from 400 nm to 600 nm at 37 $^{\circ}\text{C}$ using an excitation wavelength of 372 nm. Excitation and emission slit widths were set at 10 nm and 20 nm, respectively, while the PMT detector was set at 700 V.

2.7 Dynamic light scattering (DLS)

Wildtype and double mutant Cys49Ser/Cys56Ser and Trp121Glu/Tyr122Glu STIM1 23-213 proteins were exchanged into their experimental buffers via ultrafiltration as described above. The control and experimental buffers contained 20 mM TRIS, 150 mM NaCl, and 1 mM DTT or 1 mM GSNO (pH 7.4). A final concentration of 0.46 mg mL⁻¹ was obtained and proteins were centrifuged at 12,000 ×g before a 5 µL aliquot was loaded into a dust-free quartz MicroCuvette (JC501) for light scattering measurements on a DynaPro Nanostar (Wyatt Technology). The control and experimental buffers that were originally used for ultrafiltration were first loaded into the quartz cuvette and a reading was taken after 5 min equilibration to ensure that the cuvette was dust-free. Experiments were conducted at 37 °C, where the cuvette containing the protein of interest was allowed to equilibrate for 5 min before 10 consecutive acquisitions were recorded per sample with each acquisition averaged for 5 seconds. The regularization for polydisperse solutions using the accompanying instrumental software was performed with the low and high cut-offs for the hydrodynamic size set to 1.5 nm and 150 nm respectively.

2.8 Solution nuclear magnetic resonance (NMR) spectroscopy

2.8.1 STIM1 24-57 backbone assignment and structure

Solution NMR spectroscopy experiments were performed using a 600 MHz Inova NMR spectrometer (Varian/Agilent, Inc.) equipped with a cryogenic, triple HCN resonance probe. A set of pilot experiments were first conducted to determine the optimal temperature and salt concentration for the STIM1 24-57 peptide. Approximately 200 µM of ¹⁵N single-labelled STIM1 24-57 peptide was exchanged into a buffer containing 150 mM or 300 mM NaCl, 20 mM TRIS, 1 mM DTT (pH 7.5) via ultrafiltration. Afterwards, ¹H-¹⁵N heteronuclear single quantum coherence (HSQC) experiments (Farrow et al., 1994; Kay et al., 1992) were conducted at varying temperatures and NaCl concentrations. Since most of the crosspeaks became visible under lower NaCl concentration and temperature conditions, the optimal experimental condition was chosen to be 50 mM NaCl at 15 °C. Wilmad 5 mm frequency matched NMR tubes were used for all the

experiments. Moreover, 60 μM 4,4-dimethyl-4-silapentane-1-sulfonic acid (DSS) and 10 % D_2O (v/v) were added to each NMR sample.

To determine the backbone chemical shift assignments and associated secondary structure of the STIM1 24-57 peptide, 600 μL experimental sample was prepared by mixing ~ 200 μM of ^{15}N , ^{13}C double-labelled STIM1 24-57 peptide in a buffer that contains 20 mM TRIS, 50 mM NaCl and 2 mM GSNO or 2 mM DTT (pH = 7.4) with 60 μM 4,4-dimethyl-4-silapentane-1-sulfonic acid (DSS) and 10 % D_2O (v/v). Sequential backbone assignments were made using ^1H - ^{15}N HSQC, HNCACB and HNCO experiments (Grzesiek and Bax, 1993; Wang et al., 1994). The parameters for HNCACB were 5000 Hz ^1H sweep width, 9600 Hz ^{13}C sweep width, 1700 Hz ^{15}N sweep width, 48 transients, 44 increments in the ^{13}C dimension and 24 increments in the ^{15}N dimension. The parameters for HNCO were 5000 Hz ^1H sweep width, 3770 Hz ^{13}C sweep width, 1700 Hz ^{15}N sweep width, 20 transients, 20 increments in the ^{13}C dimension and 24 increments in the ^{15}N dimension.

The two- and three-dimensional spectra were processed, and resonance assignments were made using NMRPipe and XEASY, respectively (Bartels et al., 1995; Delaglio et al., 1995). The efficiency and structural changes associated with *S*-nitrosylation were assessed based on the chemical shift perturbations calculated from the backbone amides as well as the C_α and C_β carbons. The chemical shift perturbations (CSP) of the STIM1 24-57 peptide were calculated using the following equations:

$$\text{Alpha carbon: } \text{C}_\alpha\text{CSP} = \sqrt{(\Delta\delta\text{C}_\alpha)^2}$$

$$\text{Beta carbon: } \text{C}_\beta\text{CSP} = \sqrt{(\Delta\delta\text{C}_\beta)^2}$$

$$\text{Amide backbone CSP: total H(N) CSP} = \sqrt{(\Delta\delta\text{H})^2 + 0.14 (\Delta\delta\text{N})^2}$$

2.8.2 Paramagnetic relaxation enhancement (PRE) spectroscopy

In order to nitroxide spin label the STIM1 24-57 protein, 0.116 mg of ^{15}N labelled STIM1 24-57 peptide was first dialyzed twice into N-morpholino propanesulfonic acid (MOPS) buffer containing 20 mM MOPS, 50 mM NaCl and 0.1 mM TCEP-HCl (pH 8.3). Subsequently, 4 mM methanethiosulfonate (MTSL) was added to the peptide and this sample was incubated in the dark at room temperature for 2 hours. Finally, the nitroxide spin labelled peptide was dialyzed twice into the NMR buffer containing 20 mM TRIS, 50 mM NaCl and 5 mM CaCl_2 (pH 7.4) to remove the unreacted label and leave the sample in the experimental buffer. An ^1H - ^{15}N -HSQC spectrum was acquired on the 600 MHz Inova NMR spectrometer (Varian/Agilent, Inc.) with a 5000 Hz ^1H sweep width, 1700 Hz ^{15}N sweep width, 16 transients and 64 increments in the ^{15}N dimension. The 600 μL sample contained ~ 50 μM nitroxide spin ^{15}N labelled STIM1 24-57 peptide, 60 μM DSS and 10 % D_2O (v/v). The ^1H - ^{15}N -HSQC exhibited very few peaks due to the peak broadening effect by the spin label. A second HSQC spectrum was obtained using identical parameters following the addition of 15 mM DTT to remove the nitroxide spin label from the Cys residues. The DTT treatment restored a majority of the crosspeaks, thereby validating the spin label methodology (Figure 2.6).

To map the interacting site of the STIM1 24-57 peptide on EF-SAM, ~ 0.25 mg of unlabelled STIM1 24-57 peptide was nitroxide spin-labelled as described above and finally dialyzed into the NMR buffer that contains 20 mM TRIS, 50 mM NaCl and 5 mM CaCl_2 (pH 7.4). ^{15}N single-labelled EF-SAM protein was also dialyzed into the NMR buffer containing 20 mM TRIS, 50 mM NaCl and 5 mM CaCl_2 (pH 7.4) for these experiments. The 107 μM nitroxide spin labelled STIM1 24-57 peptide and 46 μM ^{15}N single-labelled EF-SAM protein samples were mixed together, and an HSQC spectrum monitoring the binding sites of the peptide on EF-SAM as suppressed amide resonances was obtained. A second HSQC spectrum was obtained following the addition of 15 mM DTT which removed the nitroxide spin label from the Cys residues by reduction, in order to ascertain amide reference intensities. The ^1H - ^{15}N -HSQC parameters employed for these PRE experiments were 8000 Hz ^1H sweep width, 1800 Hz ^{15}N sweep width, 32 transients and 64 increments in the ^{15}N dimension.

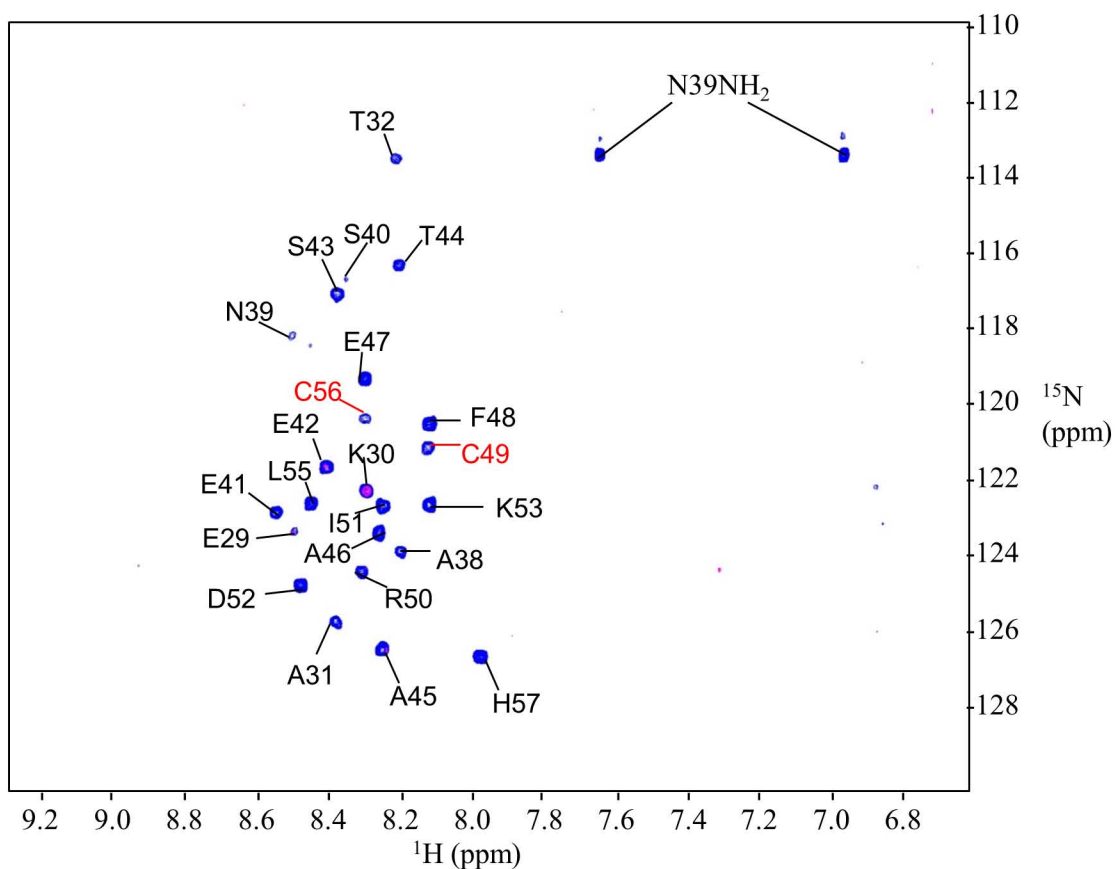


Figure 2.6. ^1H - ^{15}N -Heteronuclear single quantum coherence (HSQC) spectra of **STIM1 24-57**. Approximately 50 μM of nitroxide spin-labelled ^{15}N STIM1 24-57 protein in 20 mM TRIS (pH 7.5), 50 mM NaCl, 5 mM CaCl_2 in the absence (magenta) or presence of 15 mM DTT (blue) was supplemented with 60 μM DSS and 10 % (v/v) D_2O . The ^1H - ^{15}N -HSQC spectra were obtained using the 600 MHz Inova NMR spectrometer (Varian/Agilent, Inc) at 15 $^\circ\text{C}$. In the absence of DTT, the vast majority of peaks are broadened beyond detection; upon DTT-induced reduction of the spin-label most of the crosspeaks become visible, thereby validating my spin-labelling methodology for this region of STIM1.

2.9 Urea Denaturation

Wildtype and double mutant Cys49Ser/Cys56Ser STIM1 23-213 protein samples were exchanged into a buffer containing 5 mM CaCl₂, 150 mM NaCl, 20 mM TRIS (pH 7.4) as well as 1 mM DTT or 1 mM GSNO by ultrafiltration. Samples were prepared with urea concentrations ranging from 0 to 5 M, while protein concentration was kept constant at 5 μM. After incubation in the water bath overnight at 25 °C, intrinsic fluorescence readings were taken for each sample. The excitation wavelength was set at 280 nm which excites the aromatic residues Phe, Tyr and Trp, and fluorescence emission spectra were acquired between 300-450 nm. Chemical denaturation curves were constructed from the change in fluorescence emission intensity at 339 nm or 337 nm versus urea concentration for the Ca²⁺ loaded and Ca²⁺ depleted conditions, respectively. Thermodynamic stability parameters were extracted from the chemical denaturation curves by non-linear regression fitting of the data to a two state, folded to unfolded model. The denaturant dependence of Gibbs free energy (*m*-value) and Gibbs free energy of unfolding in the absence of denaturant (ΔG_{H_2O}) were fit using the linear extrapolation method (Pace, 1986) according to the following equations:

$\Delta G = -RT \ln K = \Delta G_{H_2O} - m \times [\text{urea}]$, where R is the universal gas constant, T is temperature in Kelvin and K is the equilibrium constant of two state unfolding. K is related to the fraction of unfolded (F_U) protein as

$$F_U = \frac{K}{1 + K}$$

, and thus F_U can be solved by rearranging $\Delta G = -RT \ln K$ as

$$F_U = \frac{\exp\left(\frac{-\Delta G}{RT}\right)}{1 + \exp\left(\frac{-\Delta G}{RT}\right)}$$

, where $\Delta G = \Delta G_{H_2O} - m \times [\text{urea}]$

The midpoint of chemical denaturation, C_{mid} , was calculated from

$$\frac{\Delta G_{H_2O}}{m}$$

2.10 Cardiomyocyte Culture

2.10.1 Cardiomyocyte isolation and culture

Neonatal (1-2 day old) Sprague Dawley rat hearts were removed into cool D-hanks balance solution, washed and minced aseptically. The ventricular tissue was transferred into $10 \mu\text{g mL}^{-1}$ Liberase TH (Roche Cat. #05401135001) in D-hanks solution, digested for 3×10 min and collected by centrifugation at $500 \times g$ for 5 min. The collected cells were resuspended to 1 million mL^{-1} in culture medium containing a 2:1 mixture of DMEM and M199 as well as 10% FBS and 1% penicillin streptomycin (PS). After 60 min pre-plate on a 35 nm dish in the CO_2 incubator, the cells were filtered and seeded in 1 % gelatin coated plates.

2.10.2 Experimental treatments

Following 24 h of growth at 37°C , ventricular cardiomyocyte cultures in selective wells were treated with $50 \mu\text{M}$ PE for 2 days to induce the hypertrophic phenotype. For particular wells that need to be treated with 10 nM of control siRNA or 10 nM STIM1 siRNA, the PE treatment was delayed until 24 h after these RNA oligos were incorporated into the cardiomyocytes using the jetPRIME transfection reagent (Polyplus transfection) according to the manufacture's protocol. The adenoviral nNOS and adenoviral GFP treatments ($\text{moi} = 10$) were also administered 24 h prior to PE treatment, while the $5 \mu\text{M}$ BTP2 and $100 \mu\text{M}$ GSNO treatments were applied with PE. The culture medium was exchanged every 24 h and the necessary treatments were supplemented into selective wells.

2.10.3 Cardiomyocyte staining and imaging

The cultured ventricular cardiomyocytes were first washed using PBS, which is followed by a 30 min fixation period using 4 % paraformaldehyde (PFA). After another PBS wash, the cells were permeabilized by the 0.1 % triton x-100 in PBS treatment for 8 min. 1 % BSA in PBS was used to block the permeabilized cells for 1 h. This was followed by an overnight incubation using 1:1000 diluted 1° anti- α actinin antibody produced in mouse (Sigma-Aldrich). The cells were washed again using PBS and incubated with 1:1000

diluted 2° anti-mouse antibody for 1 h. After a short 2-3 min incubation period with 1:1000 diluted Hoechst stain, the cells were washed using PBS and the coverslips were mounted using Dako fluorescence mounting medium onto the slides and stored at 4 °C. Following fluorescence microscopy imaging of ~ 100 cardiomyocytes from ~4 separate cultures per treatment group, AxioVision program was used to outline the cell borders and estimate the cardiomyocyte size.

2.11 Statistical analysis

Statistical analyses were performed using an unpaired t-test when comparing between two independent groups, whereas one-way ANOVA followed by Tukey's post-hoc test was used to compare more than two treatment groups. Tukey's multiple comparison analysis was used as opposed to other methods because of its conservative estimate of the α -value, which decreases the likelihood of obtaining a false positive significance. Other tests such as the Newman-Keuls method are less stringent and can reach statistical significance more easily (McHugh, 2011). Since the effect of S-nitrosylation on STIM1 and its downstream effect on PE-induced cardiomyocyte hypertrophy is fairly uncertain, I used the Tukey's post-hoc test in order to obtain statistics on the differences among all the different groups.

Chapter 3 Results

3.1 The α -helicity of STIM1 23-213 is attenuated upon Ca^{2+} depletion.

The Ca^{2+} -depletion induced loss in STIM1 EF-SAM α -helicity and stability is a hallmark of SOCE initiation. Using far-UV CD spectra obtained from 240 nm to 200 nm, I examined the secondary structure of wildtype STIM1 23-213 protein in buffers containing 10 mM TRIS-HCl (pH 7.4) and 1 mM DTT with or without 5 mM CaCl_2 (Figure 3.1). Spectra were corrected for buffer contributions. As expected, this luminal region of STIM1 encompassing the EF-SAM domain (residues 58-201) together with the region containing the two conserved Cys residues (Cys49 and Cys56) showed a typical α -helical spectrum with two characteristic minima at around 225 nm and 208 nm. Moreover, I observed an attenuation of α -helicity in the protein samples depleted of Ca^{2+} as indicated by the reduction in the intensity of the negative ellipticity at the 208 and 225 nm. The effects of *S*-nitrosylation were not amenable to investigation by acquisition of far-UV-CD spectra because below ~ 210 nm wavelength, the high tension (HT) of the samples rose above 800 V, thereby distorting the spectra and making the reading unreliable.

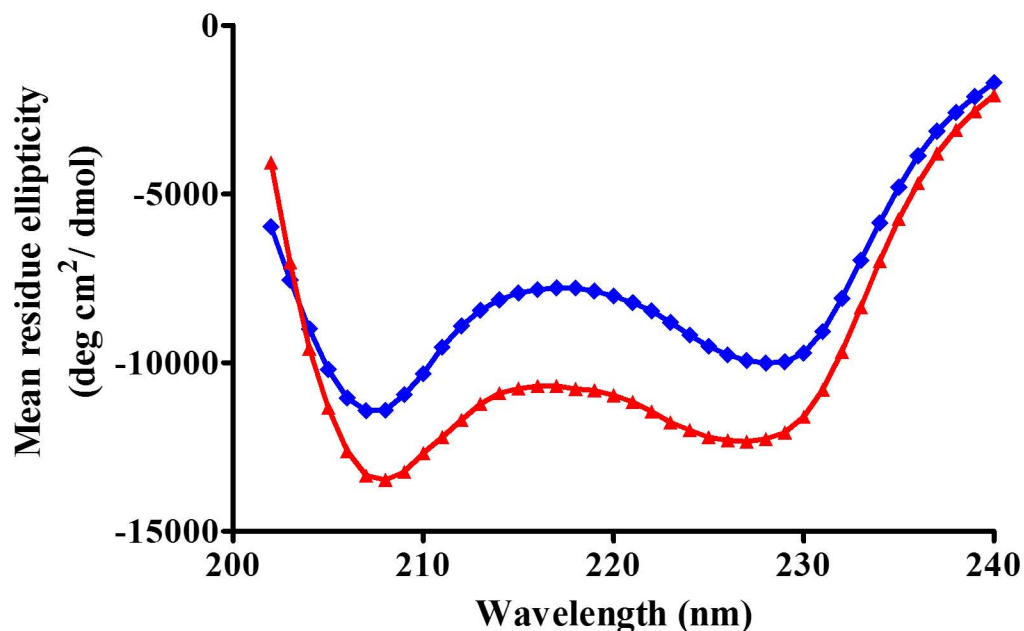


Figure 3.1. Far-UV CD spectra of wildtype STIM1 23-213. Spectra were acquired at 20 °C from 200-240 nm in 0.1 cm pathlength cuvettes using 0.5 mg mL⁻¹ wildtype STIM1 23-213 protein under the Ca²⁺ loaded (red) or Ca²⁺ depleted (blue) conditions. Spectra were corrected for buffer contributions that contains 10 mM TRIS-HCl (pH 7.4), 1 mM DTT with or without 5 mM CaCl₂. The data indicate that Ca²⁺-depleted STIM1 23-213 has less α -helical structure compared to the Ca²⁺-loaded state. The representative spectra shown are from four separate Ca²⁺ loaded and five separate Ca²⁺ depleted experiments.

3.2 *S*-Nitrosylation increases the thermal stability of STIM1 23-213 wildtype protein.

While monitoring changes in secondary structure caused by *S*-nitrosylation by far-UV CD was not possible due to high absorbance of the NO donor containing buffer at wavelengths below ~210 nm, assessing changes in thermal stability due to *S*-nitrosylation was possible since the high tension does not rise above 800 V at 225 nm in the presence of GSNO or SNP over the temperature range monitored. Three treatment groups were present in this experiment: 1 mM DTT as the control, 1 mM GSNO and 2 mM SNP as the NO donors which were introduced by ultrafiltration. The apparent denaturation midpoints (T_m) for each treatment group (Table 3.1) were obtained as an indication of protein stability. A systematic shift to the right was observed for the thermal melt curves of wild type proteins with NO donors GSNO or SNP compared to the control monitored at 225 nm (Figure 3.2A and 3.2C). This approach of using excess NO donors to *S*-nitrosylate proteins *in vitro* has been previously used (Albertos et al., 2015; Ji et al., 1999) due to the labile nature of the modification which is readily reversible upon removal of the NO donor. Boltzmann sigmoidal fits were used to estimate the apparent T_m where a higher apparent T_m is indicative of a more stable protein sample (Table 3.1). The apparent T_m of wildtype STIM1 23-213 in the Ca^{2+} -loaded state was significantly increased by ~ 2 °C in the presence of either excess GSNO or SNP (Figure 3.2A and 3.2B). Remarkably, the increase in apparent T_m was much more pronounced under Ca^{2+} depletion conditions (i.e. $\Delta T_m = \sim +4^\circ C$, * $p < 0.05$), indicating a greater stabilization of luminal STIM1 23-213 by the presence of excess NO donors in the absence of Ca^{2+} (Figure 3.2C and 3.2D) which is the state that initiates STIM1 oligomerization for SOCE activation. Importantly, double mutant STIM1 with both native Cys replaced by Ser (i.e. Cys49Ser/Cys56Ser) (Figure 3.3A and 3.3B) did not undergo stabilization, suggesting a Cys-specific response. Surprisingly, however, single mutant versions of STIM1 23-213 with one of the Cys replaced by Ser (Figure 3.3C-F) did not exhibit stabilization.

Collectively, these data demonstrated that the STIM1 luminal domain stability is enhanced in the presence of excess NO. Furthermore, the increase in stability is

detectable by thermal denaturation when both Cys49 and Cys56 are present. Stabilization of the STIM1 luminal domains would suppress the destabilization-coupled oligomerization event which triggers SOCE activation, suggesting a mechanistic basis for nNOS-mediated SOCE inhibition in cardiomyocytes.

Table 3.1 Apparent denaturation midpoint (T_m) of STIM1 23-213 wildtype, double and single mutants under conditions with or without Ca^{2+} and/or *S*-nitrosylation.

STIM1 23-213	Condition	Apparent T_m (°C) (Mean \pm SEM)
	Ca^{2+} loaded	
Wildtype	Unmodified/+1mM DTT (n = 4)	62.49 \pm 0.49
	S-Nitrosylated/+1mM GSNO (n = 3)	64.26 \pm 0.31*
	S-Nitrosylated/+2mM SNP (n = 3)	64.46 \pm 0.07*
	Ca^{2+} depleted	
Wildtype	Unmodified/+1mM DTT (n = 5)	41.72 \pm 0.57
	S-Nitrosylated/+1mM GSNO (n = 4)	45.08 \pm 0.88*
	S-Nitrosylated/+2mM SNP (n = 4)	45.04 \pm 0.68**
	Ca^{2+} depleted	
Double mutant (Cys49Ser/Cys56Ser)	Unmodified/+1mM DTT (n = 3)	37.89 \pm 0.51
	S-Nitrosylated/+1mM GSNO (n = 6)	37.82 \pm 0.43
	S-Nitrosylated/+2mM SNP (n = 3)	39.12 \pm 0.20
	Ca^{2+} depleted	
Single mutant (Cys49Ser)	Unmodified/+1mM DTT (n = 3)	39.04 \pm 0.13
	S-Nitrosylated/+1mM GSNO (n = 3)	39.05 \pm 0.16
	Ca^{2+} depleted	
Single mutant (Cys56Ser)	Unmodified/+1mM DTT (n = 4)	38.63 \pm 0.19
	S-Nitrosylated/+1mM GSNO (n = 4)	38.02 \pm 0.47

Statistical analysis was performed using one-way ANOVA followed by Tukey's test.

* $p < 0.05$, ** $p < 0.01$ vs. DTT control

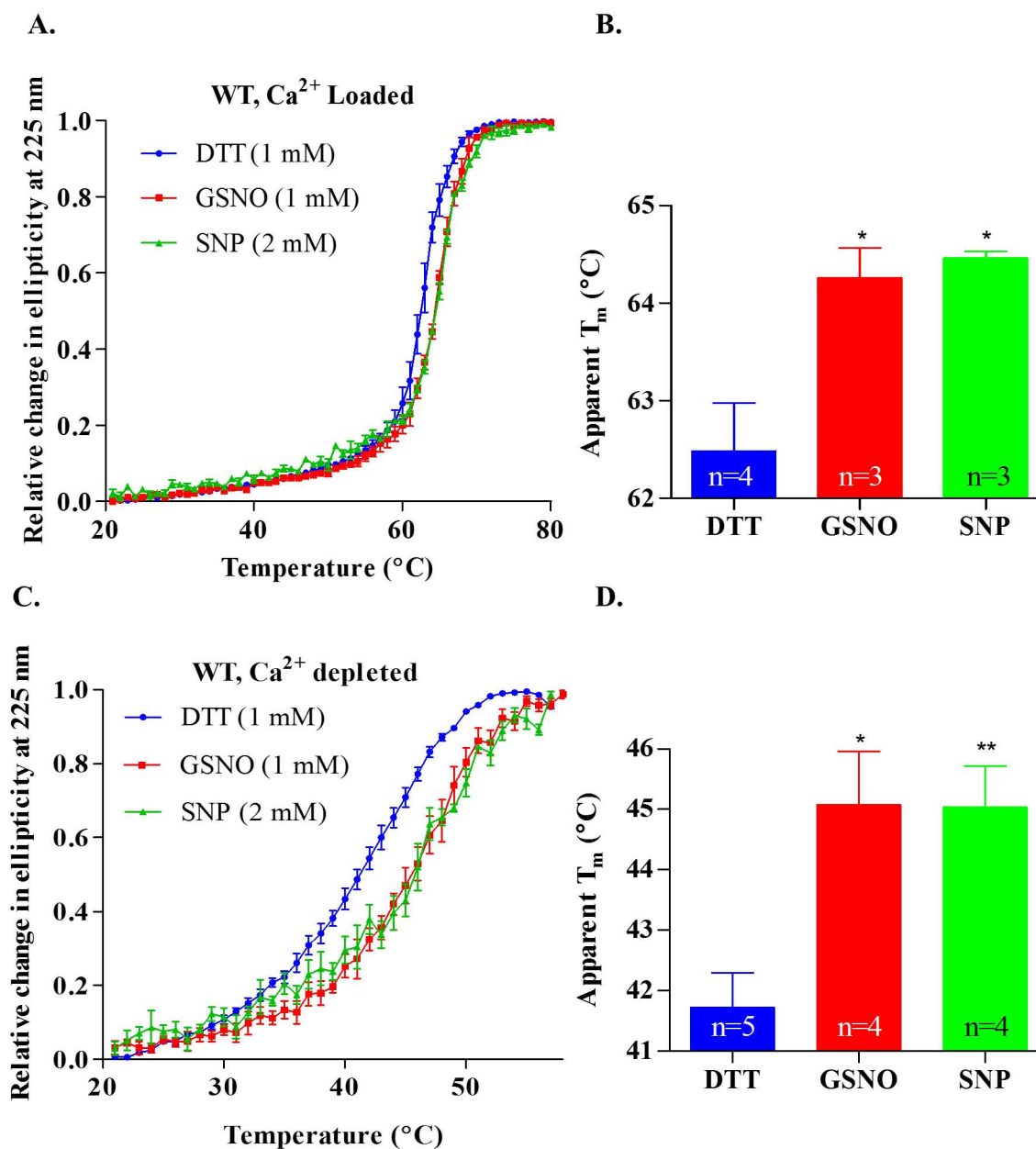


Figure 3.2. S-nitrosylation induced thermal stabilization of WT STIM1 23-213.

Thermal stability observed by changes in far-UV CD signal of unmodified (+1 mM DTT) and S-nitrosylated (+1 mM GSNO or +2 mM SNP) STIM1 23-213 protein (0.5 mg mL⁻¹) with or without 5 mM CaCl₂. **A.** Wild-type, Ca²⁺ loaded; **C.** Wild-type, Ca²⁺ depleted. The data suggest that excess NO donors stabilize STIM1 23-213 in a Cys-specific manner. Statistical analysis was performed using one-way ANOVA followed by Tukey's test for the **B.** Wildtype, Ca²⁺ loaded; **D.** Wildtype, Ca²⁺ depleted protein samples. *p < 0.05, **p < 0.01 vs. DTT control (means ± SEM).

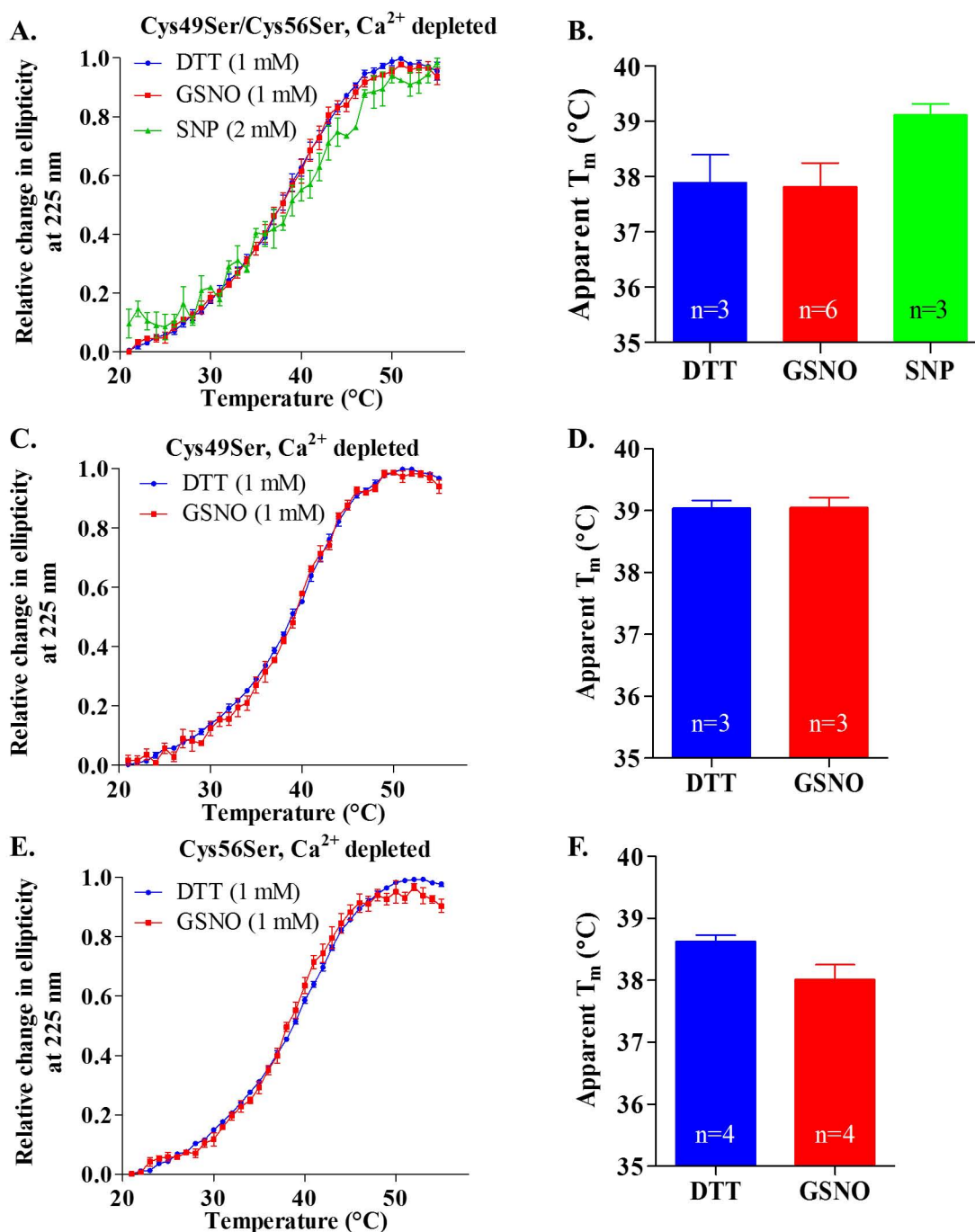


Figure 3.3. *S*-nitrosylation did not induce thermal stabilization of STIM1 23-213 Cys mutants. Thermal stability observed by changes in far-UV CD signal of unmodified (+1 mM DTT) and *S*-nitrosylated (+1 mM GSNO or +2 mM SNP) STIM1 23-213 protein (0.5 mg mL⁻¹) under Ca²⁺ depletion. **A.** Cys49Ser/Cys56Ser double mutant; **C.** Cys49Ser; and **E.** Cys56Ser single mutants. One-way ANOVA followed by Tukey's test was performed for **B.** Cys49Ser/Cys56Ser double mutant. Unpaired t-test was performed for **D.** Cys49Ser; and **F.** Cys56Ser single mutants (means ± SEM).

3.3 *S*-Nitrosylation decreases the structural change of STIM1 23-213 upon Ca²⁺ binding.

Given that Ca²⁺ binding affinity drives the sensitivity of the STIM1 luminal domain to changes in ER/SR Ca²⁺ levels (Stathopoulos et al., 2006), I therefore assessed changes in Ca²⁺ binding in the presence and absence of NO. Ca²⁺ binding was assessed by monitoring changes in intrinsic fluorescence using 0.1 mg mL⁻¹ wildtype STIM1 23-213 protein in a buffer that contains 20 mM TRIS-HCl (pH 7.4), 150 mM NaCl and 1 mM DTT or 1 mM GSNO at 37 °C. In the absence of the NO donor, the structural change approached saturation in the ~mM CaCl₂ concentration range. Fitting the relative change in fluorescence intensity to a one-site binding model which takes into account protein concentration revealed an apparent equilibrium dissociation constant (K_d) for wildtype STIM1 23-213 in 1 mM DTT of 0.2958 ± 0.0364 mM (mean ± SEM, n=3) (Figure 3.4). This Ca²⁺ affinity is in the same range of affinities measured previously for STIM1 EF-SAM using multiple techniques including changes in intrinsic fluorescence (Stathopoulos et al., 2006). The K_d for the sample in 1 mM GSNO appeared to show a tighter Ca²⁺ affinity compared to the sample with DTT, with a K_d of 0.0187 ± 0.0162 mM (mean ± SEM, n=3). However, the structural change associated with binding was much smaller, reflected in the smaller relative change in fluorescence intensity upon addition of apparently saturating amounts of CaCl₂. These Ca²⁺ binding experiments suggest that the affinity the STIM1 luminal domain for Ca²⁺ may be enhanced in the presence of GSNO, but more compellingly demonstrate that the structural change associated with Ca²⁺ binding is suppressed in the presence of the NO donor.

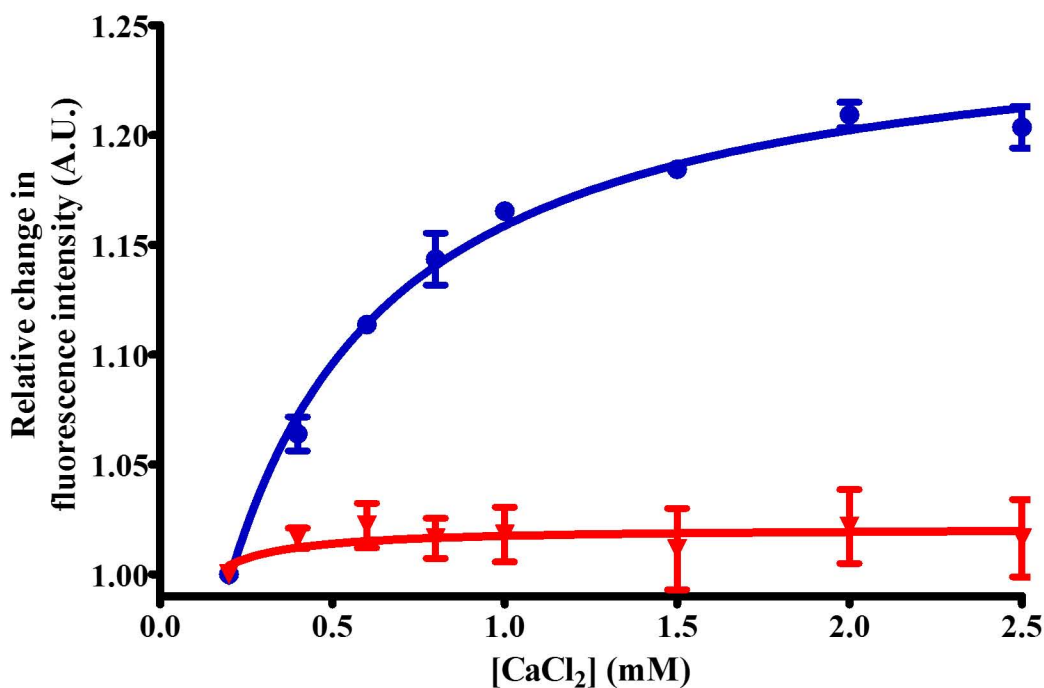


Figure 3.4. Apparent Ca²⁺ binding to STIM1 23-213 wildtype protein with and without NO donors as monitored by Ca²⁺-induced intrinsic fluorescence changes. Representative Ca²⁺ binding curves of 0.1 mg mL⁻¹ STIM1 23-213 wildtype protein in 20 mM TRIS-HCl (pH 7.4), 150 mM NaCl and 1 mM DTT (blue) or 1 mM GSNO (red) are shown. Intrinsic protein fluorescence ($\lambda_{\text{ex}} = 280$) was monitored from 300 nm to 450 nm at 37 °C. Excitation and emission slit widths were 5 nm and 10 nm. The PMT voltage was 600 V. The solid lines through the data represent the non-linear least squares fit of the dissociation constant (K_d) based on a one site binding model which takes into account protein concentration. The fitted K_d values of Ca²⁺ binding to STIM1 23-213 wildtype protein in 1 mM DTT sample and 1 mM GSNO were 0.30 ± 0.04 mM and 0.019 ± 0.016 mM, respectively (means \pm SEM, n=3).

3.4 *S*-Nitrosylation decreases the level of solvent-exposed hydrophobicity of wildtype STIM1 23-213.

The Ca^{2+} -depletion-induced oligomerization of STIM1 EF-SAM has previously been shown to be linked with an increased hydrophobic exposure (Stathopoulos et al., 2006). Thus, I next sought to evaluate the level of hydrophobicity of the STIM1 23-213 luminal domain in the presence and absence of NO donors using an extrinsic fluorescence probe (ANS) which binds to surface exposed hydrophobic patches of proteins (Stryer, 1965). As expected, the extrinsic fluorescence emission of ANS ($\lambda_{\text{ex}} = 372 \text{ nm}$) was higher in the sample containing 0.143 mg mL^{-1} of Ca^{2+} -depleted protein compared to buffer alone (Figure 3.5A). The fluorescence intensity of the buffer, measured from 400 nm to 600 nm, did not change with the addition of 5 mM CaCl_2 . However, the ANS fluorescence of the protein sample markedly decreased when 5 mM CaCl_2 was added, indicating a decrease in exposed hydrophobic residues (Figure 3.5A and 3.5C). The right shift in intensity maximum caused by Ca^{2+} binding is consistent with increased folding and higher stability (Figure 3.5A and 3.5C) (Hawe et al., 2008).

In contrast, when evaluating the Ca^{2+} response of STIM1 23-213 wildtype protein in the presence 1 mM GSNO (Figure 3.5B), the ANS fluorescence change suggested less exposed hydrophobicity in the absence of Ca^{2+} and a smaller conformational change after the addition of 5 mM CaCl_2 due to the persistently well-folded structure of the *S*-nitrosylated protein. Importantly, the STIM1 23-213 Cys49Ser/Cys56Ser double mutant protein not susceptible to *S*-nitrosylation (Figure 3.5C) exhibited the same fluorescence intensity as the wildtype protein (Figure 3.5A); however, even in the presence of excess GSNO, the STIM1 23-213 Cys49Ser/Cys56Ser double mutant protein showed a higher fluorescence intensity (Figure 3.5D) compared to the wildtype protein (Figure 3.5B), indicative of a less compact structure. The slightly lower fluorescence intensity of the GSNO treated double mutant protein sample (Figure 3.5D) compared to the DTT sample (Figure 3.5C) may have been caused by a quenching effect (Flaugh and Lumb, 2001; Tokuriki et al., 2004) exerted by GSNO on ANS fluorescence. This notion is supported by the absence of a substantial blue shift in intensity maximum for the double mutant

protein in GSNO buffer (Figure 3.5D) versus the DTT buffer (Figure 3.5C) (~3 nm and 6 nm for Ca²⁺ depleted and Ca²⁺ loaded samples respectively), which was found for the wildtype protein sample (Figure 3.5A and 3.5B) (~26 nm and 23 nm for Ca²⁺ depleted and Ca²⁺ loaded samples respectively). Collectively, the ANS data demonstrated that STIM1 23-213 undergoes a Ca²⁺-depletion dependent increase in exposed hydrophobic surface area which is suppressed in the presence of GSNO, and this suppression of exposed hydrophobicity is dependent on the presence of Cys49 and Cy56.

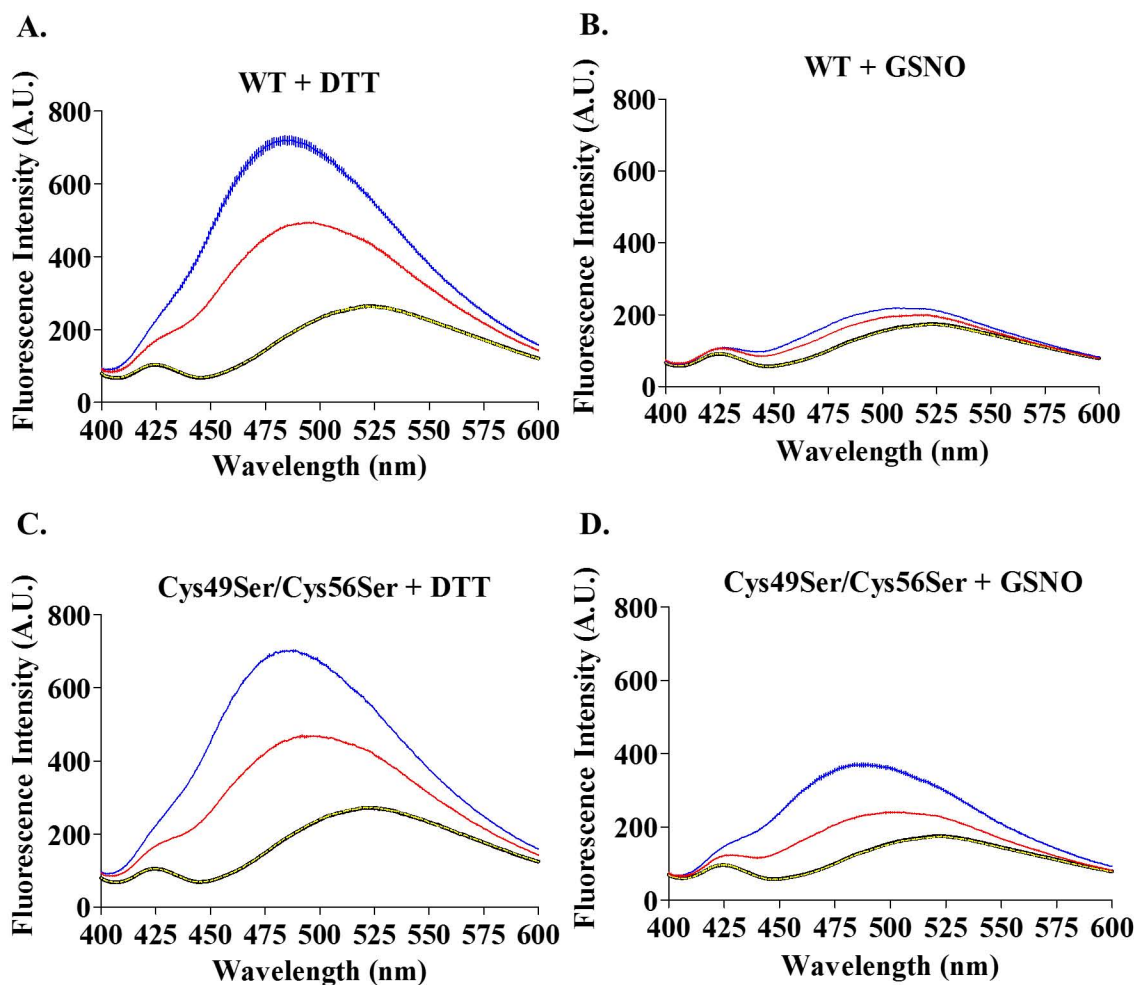


Figure 3.5. Extrinsic fluorescence of ANS in the presence of STIM1 23-213. ANS-induced fluorescence (excitation wavelength (λ_{ex}) = 372 nm) of **A.** STIM1 23-213 wildtype protein in DTT buffer (n=3). **B.** STIM1 23-213 wildtype protein in GSNO buffer (n=3). **C.** STIM1 23-213 double mutant Cys49Ser/Cys56Ser protein in DTT buffer (n=3). **D.** STIM1 23-213 double mutant Cys49Ser/Cys56Ser protein in GSNO buffer (n=3) at 37 °C. Each sample contained 0.143 mg mL⁻¹ protein, 0.05 mM ANS and 0.5 mM EDTA. Excitation and emission slit widths were set to 10 nm and 20 nm, respectively. The PMT was set to 700V. The samples contained buffer alone without CaCl₂ (black) or with 5 mM CaCl₂ (yellow), or protein solubilized in the buffer without CaCl₂ (blue) or with 5 mM CaCl₂ (red). Data are means \pm SEM of n=3 separate experiments.

3.5 Wildtype STIM1 23-213 undergoes *S*-nitrosylation mediated de-oligomerization.

To test whether the effects of *S*-nitrosylation on hydrophobicity and structure correlate with oligomerization propensity, I analyzed Ca²⁺-depleted STIM1 23-213 hydrodynamic size by DLS. Prior to taking any measurements, the protein and buffer samples were centrifuged at 12,000 ×g, 4 °C for 5 min to remove any aggregates or dust present in the samples. The control and experimental buffers contained 20 mM TRIS-HCl (pH 7.4), 150 mM NaCl, and 1 mM DTT or 1 mM GSNO, respectively. The autocorrelation functions were fit to the regularization algorithm to deconvolute the polydisperse distribution of hydrodynamic sizes, and the percent intensity contribution to the light scattering signal versus particle radius was assessed as an indication of protein oligomerization. The shift to the left in the size distribution for the STIM1 23-213 wildtype protein sample which was exchanged into the GSNO buffer compared to the sample in the DTT buffer suggested that this luminal region of STIM1 de-oligomerizes following *S*-nitrosylation since both samples were first Ca²⁺ depleted (see Methods section 2.3) (Figure 3.6A). This is a de-oligomerization event because the protein samples were first stored in a buffer that contains 1 mM DTT, 20 mM TRIS-HCl (pH 8), 300 mM NaCl and 5 mM CaCl₂ and then subjected prior to the exchange into the DTT control buffer or the GSNO buffer that *S*-nitrosylates the sample. While the change in hydrodynamic size distribution appears modest, the difference is quite marked when considering that light scattering intensity scales with particle size to the sixth power (Li et al., 2011). Thus, the hydrodynamic sizes less than 7 nm contribute greater than 95 % of the light scattering signal in the GSNO-treated sample. This DLS data is consistent with the ANS data showing suppressed hydrophobicity and the thermal melt measurements demonstrating enhanced stability for the *S*-nitrosylated Ca²⁺ depleted protein. On the other hand, without the *S*-nitrosylation sites, the STIM1 23-213 Cys49Ser/Cys56Ser double mutant protein did not undergo de-oligomerization after being exchanged into the GSNO experimental buffer (Figure 3.6B). Taken together, the DLS observations demonstrate that GSNO de-oligomerizes luminal STIM1 in a Cys49 and Cys56-dependent manner.

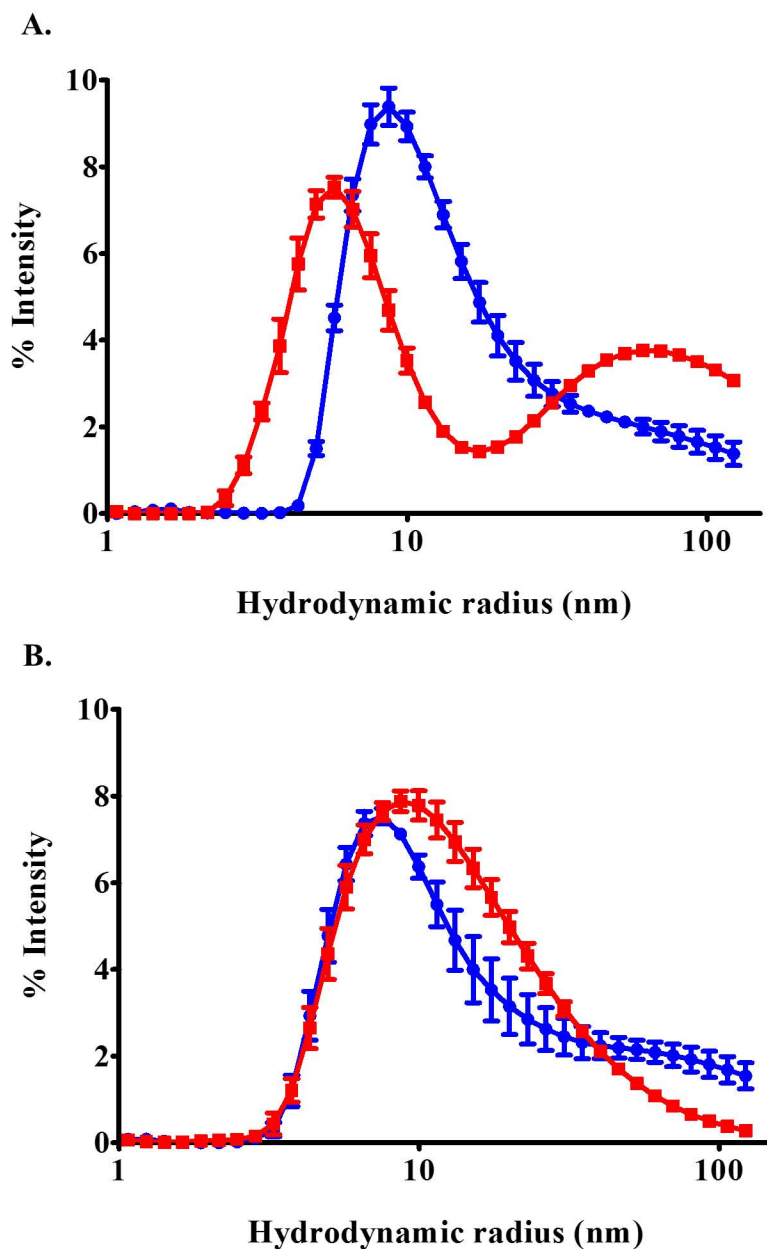


Figure 3.6. Dynamic light scattering (DLS) analysis of STIM1 23-213. The contribution of the deconvoluted particle size distributions to the light scattering intensity of Ca^{2+} depleted **A.** wildtype ($n = 3$) and **B.** Cys49Ser/Cys56Ser double mutant ($n = 3$) STIM1 23-213 (0.46 mg ml^{-1}) in 20 mM TRIS-HCl (pH 7.4), 150 mM NaCl, and 1 mM DTT (blue) or 1 mM GSNO (red). Since light scattering intensity is proportional to radius of particle size to the power of six, the majority (i.e. > 95 % by mass) of solubilized protein is represented by the first peak distribution of sizes. The shift of the wildtype protein sample size distribution after GSNO treatment compared to the control DTT sample suggests protein deligomerization after *S*-nitrosylation.

3.6 *S*-Nitrosylation of STIM1 24-57 peptide causes residue specific chemical shift changes.

Next, I used solution NMR spectroscopy to probe the structural effects of *S*-nitrosylation at higher resolution. The ^1H - ^{15}N HSQC NMR spectrum of ^{13}C , ^{15}N double labelled STIM1 24-57 protein showed the amide H(N) crosspeaks clustered in the ~ 7.5 - 8.5 ppm region (Figure 3.7). The low peak dispersion clustered in the central region of the ^1H - ^{15}N -HSQC was indicative of an unfolded state (Yao et al., 1997). To ascertain precisely which residues were being affected by the NO donor GSNO and evaluate any structural changes associated with the modification(s), a 3D HNCACB spectrum was acquired for sequential backbone assignment. This approach enabled the assignment of $\sim 85\%$ of the $\text{C}\alpha$, $\text{C}\beta$, H, N backbone chemical shifts for the STIM1 24-57 fragment in GSNO buffer.

After the protein was exchanged into a buffer containing 2 mM DTT, another set of ^1H - ^{15}N -HSQC and HNCACB experiments were run. Furthermore, $\sim 84\%$ of the $\text{C}\alpha$, $\text{C}\beta$, H, N backbone chemical shifts were assigned for the peptide in the presence of DTT (Figure 3.7). A comparison of the ^1H - ^{15}N -HSQCs in the presence of excess GSNO or DTT and associated assignments revealed numerous chemical shift perturbations (Figure 3.7). These chemical shift changes suggest residue-specific structural changes associated with the NO modifications. A subsequent chemical shift perturbation (CSP) map revealed that the largest chemical shift changes were clustered near the Cys49 and Cys56 residues (Figure 3.8A and 3.8B), as expected for Cys-specific *S*-nitrosylation.

With the majority of the backbone chemical shifts assigned, the chemical shift index (CSI) of the STIM1 24-57 fragment with and without *S*-nitrosylation of the Cys49 and Cys56 was then calculated to probe for the possible formation of regular secondary structure (Hafsa et al., 2015). The CSI showed that, in isolation, this region of STIM1 does not form regular secondary structure either in the *S*-nitrosylated or in the fully reduced state. Remarkably, an evaluation of the random coil index (RCI) (Berjanskii and Wishart, 2005) revealed strikingly higher order parameters (S^2) for residues clustered near the Cys49 site, suggesting a rigidification of this region of STIM1 upon *S*-nitrosylation (Figure 3.9).

Collectively, these solution NMR data revealed that excess NO donor site-specifically modifies the Cys49 and Cys56 residues, causes a structural change in the non-conserved N-terminal fragment and results in a remarkable rigidification of the residues localized around the Cys49.

A.

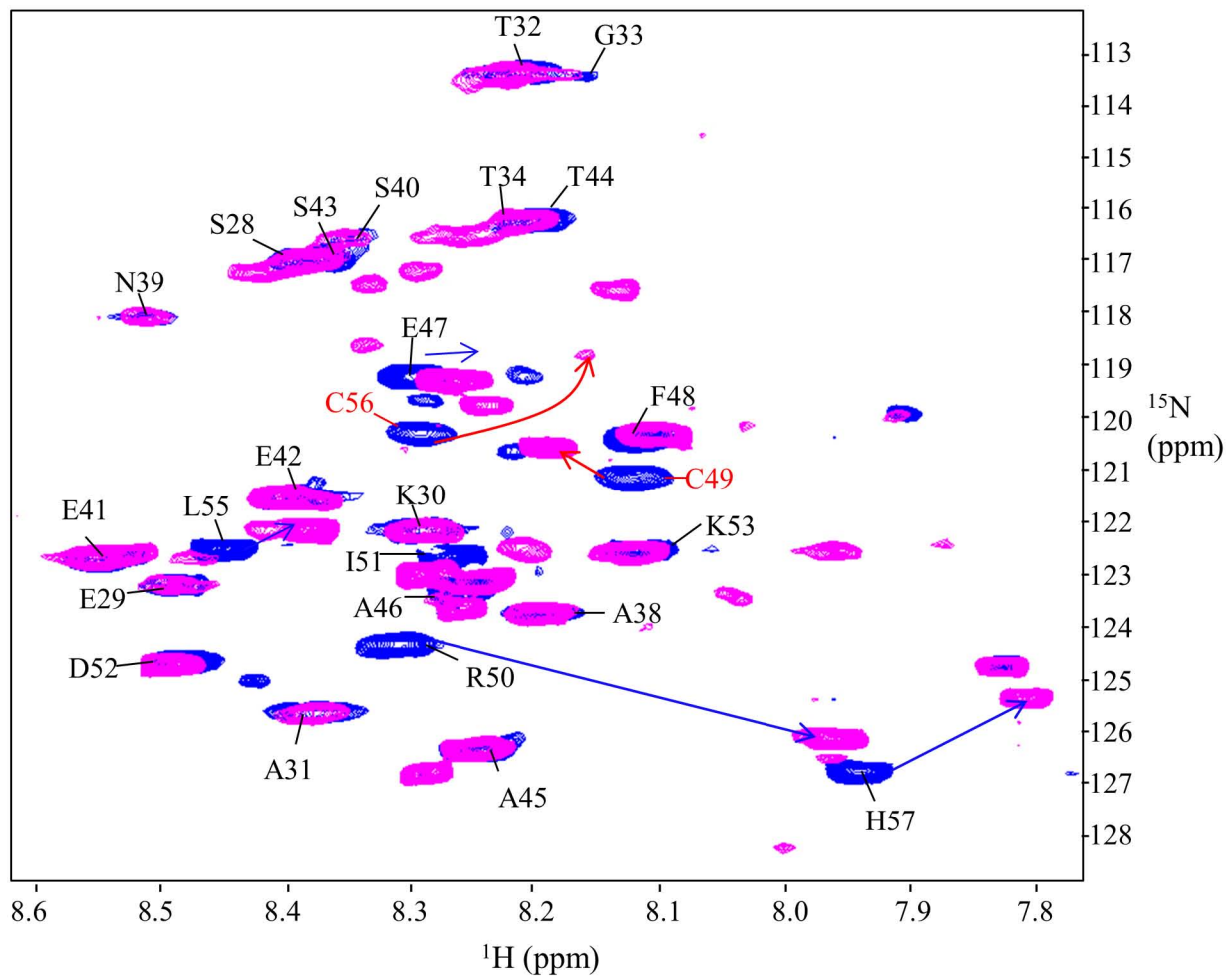


Figure 3.7. Solution NMR assessment of structural changes caused by *S*-nitrosylation of STIM1 24-57. ^1H - ^{15}N -HSQC spectra of $\sim 200 \mu\text{M}$ STIM1 24-57 in 50 mM NaCl, 20 mM TRIS-HCl (pH 7.4) and 2 mM GSNO (magenta) or 2 mM DTT (blue) at 15 $^\circ\text{C}$.

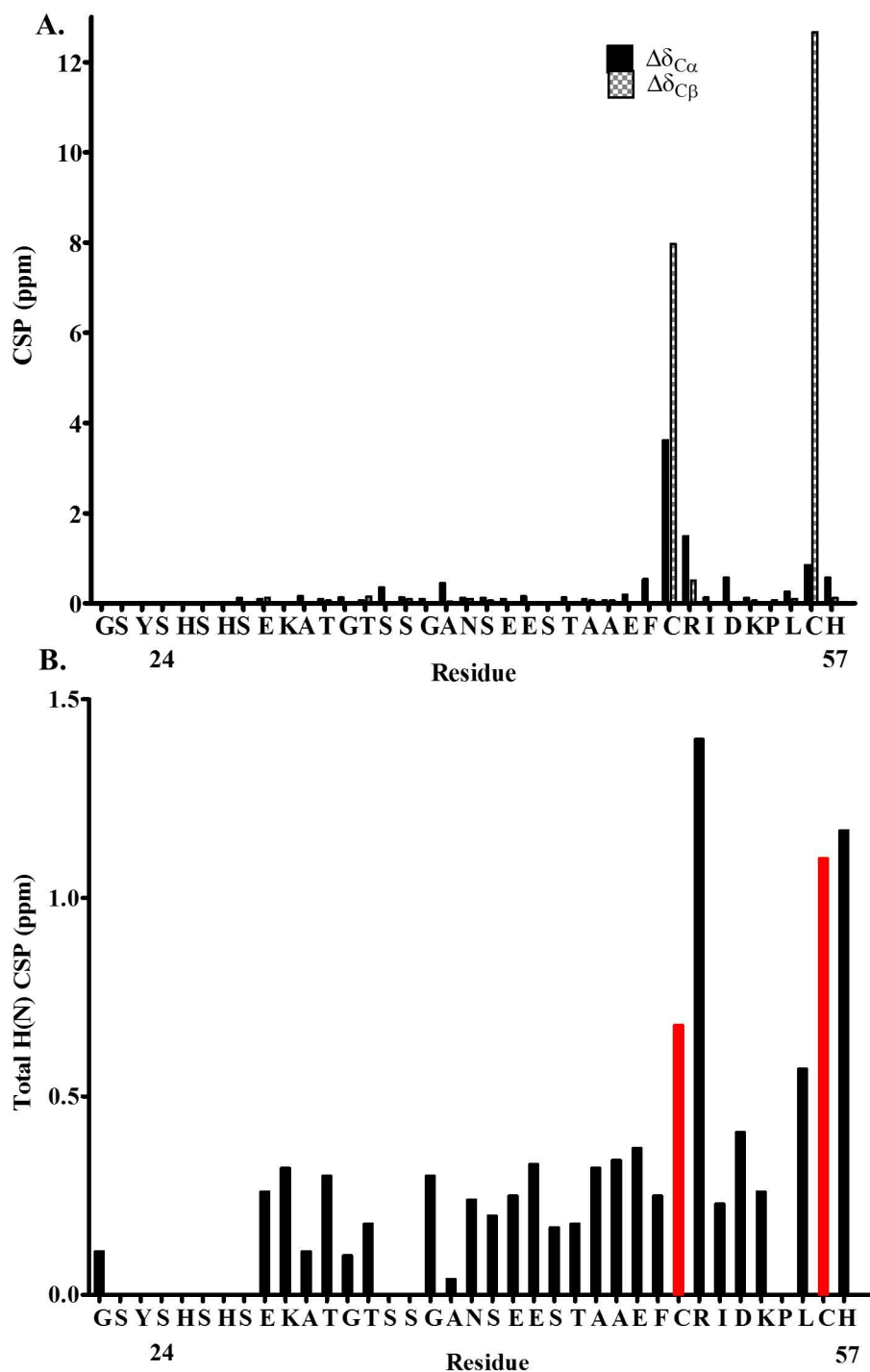


Figure 3.8. NMR chemical shift perturbation (CSP) of STIM1 24-57 before and after *S*-nitrosylation.

A. The alpha carbon CSP was calculated as $(C_{\alpha}CSP = \sqrt{(\Delta\delta_{C\alpha})^2})$ and the beta carbon as $(C_{\beta}CSP = \sqrt{(\Delta\delta_{C\beta})^2})$.

B. Normalized total H(N) CSP calculated as $= \sqrt{(\Delta\delta H)^2 + 0.14 (\Delta\delta N)^2}$.

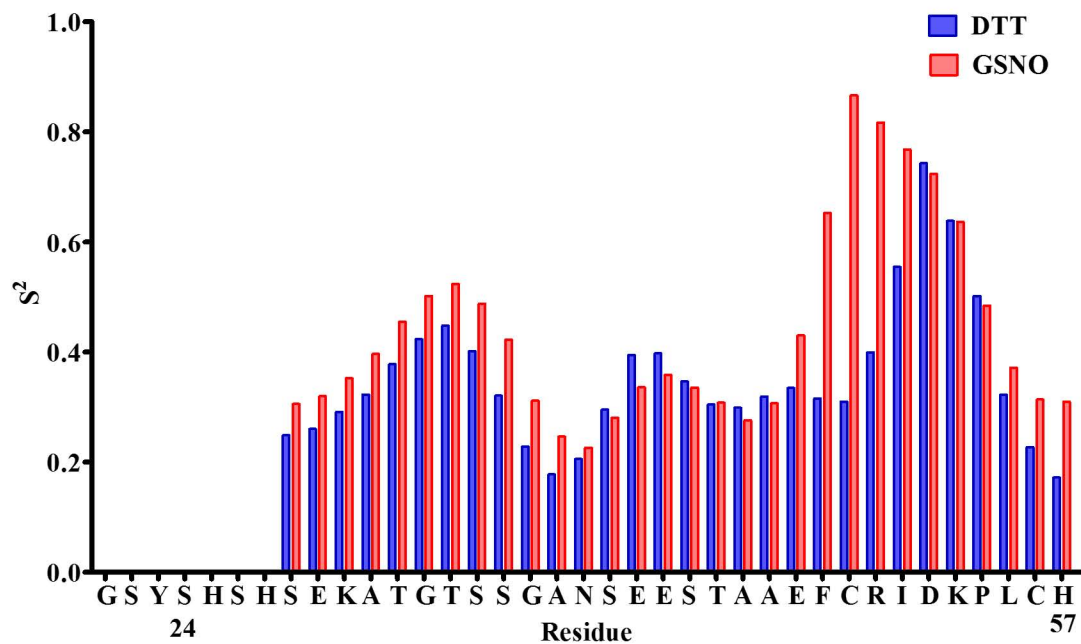


Figure 3.9. Model-free order parameter (S^2) predicted from the random coil index (RCI) (Berjanskii and Wishart, 2005). The higher S^2 near Cys49 suggests a rigidification of this region of STIM1 upon *S*-nitrosylation.

3.7 *S*-Nitrosylation induces thermodynamic stabilization of STIM1 23-213.

To more carefully assess how the rigidification of the 24-57 region affected the entire STIM1 luminal domain stability, I next performed chemical denaturation experiments to thermodynamically quantify the stability changes caused by *S*-nitrosylation. Unlike the thermal denaturation experiments described in section 3.2, the chemical denaturation process was completely reversible and was thus amenable to equilibrium analyses. Urea unfolding was monitored by changes in intrinsic fluorescence ($\lambda_{\text{ex}} = 280$ nm, $\lambda_{\text{em}} = 339$ nm) at 25 °C using 5 μ M STIM1 23-213 wildtype or Cys49Ser/Cys56Ser double mutant protein solubilized in a buffer that contains 20 mM TRIS, 150 mM NaCl and 1 mM DTT or 1 mM GSNO with or without 5 mM CaCl₂. The urea concentrations ranged from 0 to 5 M, while the protein concentration was kept constant at 5 μ M. Chemical denaturation curves (Figure 3.10A-C) were constructed and the thermodynamic stability parameters such as Gibbs free energy of unfolding in water ($\Delta G_{\text{H}_2\text{O}}$) (Figure 3.10G-I), and the cooperativity of unfolding (*m*-value), were extracted via a non-linear regression fitting of the data to a two state, folded to unfolded model. The urea concentration where half of the protein macromolecules have unfolded, C_{mid} (Figure 3.10D-F), was calculated by dividing $\Delta G_{\text{H}_2\text{O}}$ by *m* (Table 3.2). *S*-Nitrosylation of STIM1 23-213 wildtype protein by GSNO under the Ca²⁺ loaded condition indicated increased protein stability, reflected by the significant increases in C_{mid} and $\Delta G_{\text{H}_2\text{O}}$ values (Figure 3.10A, D and G). Under the Ca²⁺-depleted conditions, this increase in protein stability was even more pronounced with GSNO treatment compared to the DTT control sample (Figure 3.10B, E and H). However, for the STIM1 23-213 Cys49Ser/Cys56Ser double mutant protein without the *S*-nitrosylation sites, GSNO treatment did not have an effect on the C_{mid} value (Figure 3.10C and F). In fact, GSNO slightly decreased the $\Delta G_{\text{H}_2\text{O}}$ value of the double mutant protein (Figure 3.10I). Thus, the GSNO-dependent rigidification of the STIM1 24-57 segment endows the full STIM1 luminal domain with enhanced thermodynamic stability in both the Ca²⁺-loaded and -depleted states. Further, this thermodynamic stabilization occurs in a Cys49 and Cys56-specific manner.

Table 3.2 Thermodynamic stability parameters for STIM1 23-213 wildtype and Cys49Ser/Cys56Ser double mutant protein under Ca²⁺-loaded and -depleted conditions.

STIM1 23-213 protein	Treatment Condition	ΔG_{H_2O} (25 °C) (cal mol ⁻¹)	<i>m</i> -value (cal mol ⁻¹ M ⁻¹)	C_{mid} (M)
WT Ca²⁺ loaded	1 mM DTT (n=4)	5905 ± 32	1913 ± 65	3.087 ± 0.017
	1 mM GSNO (n=4)	7866 ± 150***	2391 ± 62	3.290 ± 0.063*
WT Ca²⁺ depleted	1 mM DTT (n=3)	1727 ± 9	1297 ± 37	1.331 ± 0.007
	1 mM GSNO (n=4)	3229 ± 58***	1833 ± 63	1.762 ± 0.032***
Cys49Ser/ Cys56Ser Ca²⁺ depleted	1 mM DTT (n=3)	1746 ± 31	1553 ± 108	1.124 ± 0.020
	1 mM GSNO (n=3)	1450 ± 64*	1275 ± 66	1.145 ± 0.054

ΔG_{H_2O} was calculated for using a globally fitted *m*-value for n=3-4 per group. Statistical analysis was performed using Student's unpaired t-test. **p* < 0.05 and ****p* < 0.0001 vs. DTT control.

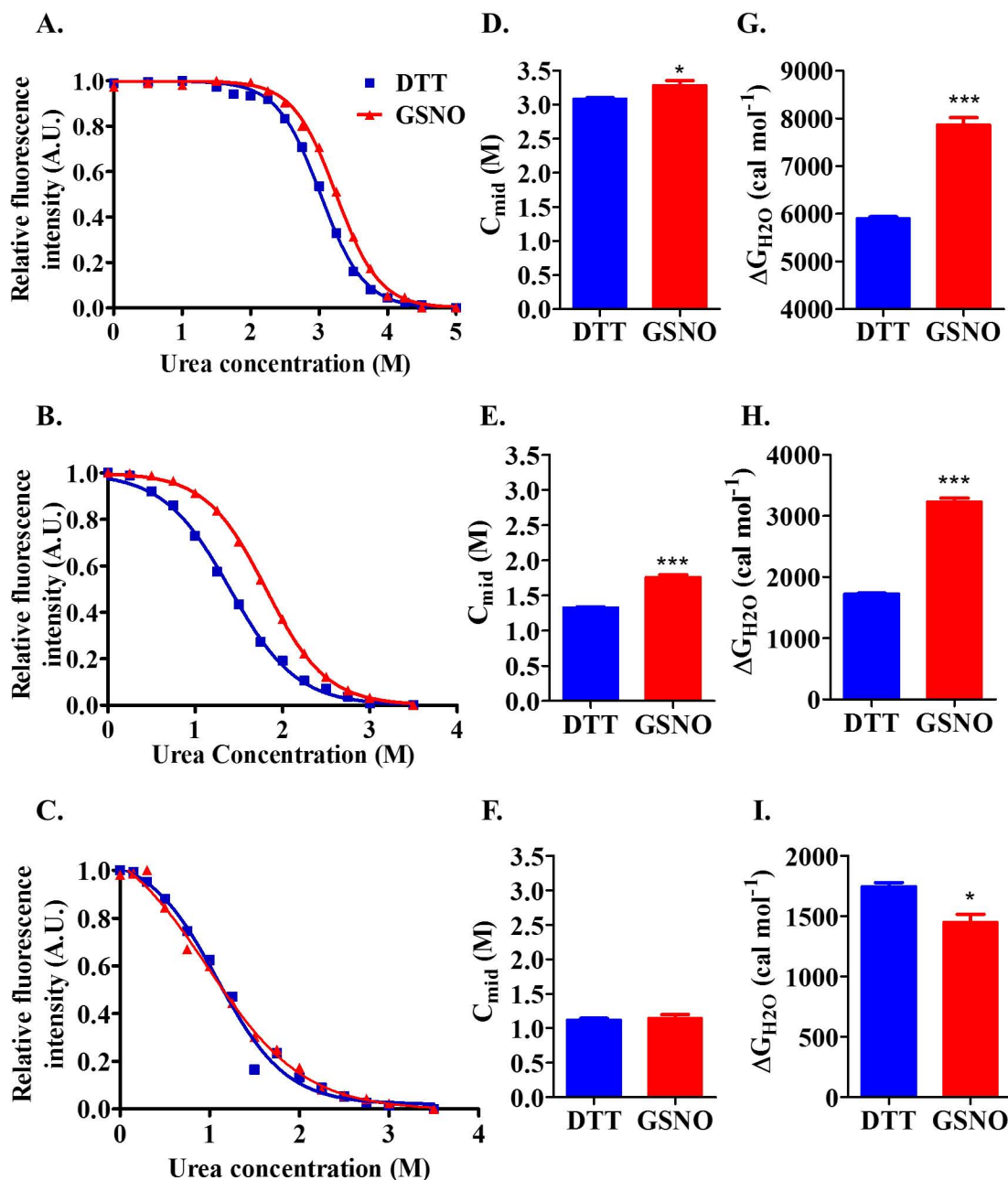


Figure 3.10. S-Nitrosylation-induced thermodynamic stabilization of STIM1 23-213. Representative urea denaturation curves of wildtype STIM1 23-213, Ca²⁺ loaded (A), Ca²⁺ depleted (B) and Cys49Ser/Cys56Ser double mutant, Ca²⁺ depleted (C) samples. The midpoint of chemical denaturation (C_{mid}) for wildtype Ca²⁺ loaded (D), Ca²⁺ depleted (E) and Cys49Ser/Cys56Ser double mutant Ca²⁺ depleted (F) samples, which is calculated by dividing a globally fitted m -value from ΔG_{H_2O} in G., H. and I. respectively. Data are presented as mean \pm standard error of the mean (SEM) of at least $n=3$ separate experiments, and statistical analysis is performed using unpaired t-test (* $p < 0.05$ and *** $p < 0.0001$ vs. DTT control).

3.8 STIM1 24-57 peptide transiently interacts with STIM1 58-201 (EF-SAM core) at residues Trp121 and Lys122.

The atomic-resolution structure of the full STIM1 23-213 region which includes the Cys49 and Cys56 has not been elucidated. Thus, to probe where the STIM1 24-57 may interact with the core EF-SAM domain and ascertain how enhanced rigidification of 24-57 may increase the thermodynamic stability of the entire luminal domain in the presence of GSNO, I applied a PRE solution NMR spectroscopy approach. An ^1H - ^{15}N -HSQC EF-SAM spectrum was acquired using a 600 μL sample containing 107 μM Cys49 and Cys56 nitroxide spin-labelled STIM1 24-57 peptide and 46 μM ^{15}N single-labelled EF-SAM protein. When the protein mixture was in the NMR buffer containing 20 mM TRIS, 50 mM NaCl and 5 mM CaCl_2 (pH 7.4), the region near Trp121N ϵ 1 [side chain indole N(H)] and Lys122 (backbone amide) on the HSQC spectrum reproducibly showed significantly lower intensities compared to the HSQC obtained following the addition of 15 mM DTT where the nitroxide spin label was removed from the Cys residues (Figure 3.11, 3.12A and 3.12B). The average intensity ratio (i.e. absence/presence of DTT) of all N(H) crosspeaks for the protein mixture was near 1, whereas the broadening effect caused by the nitroxide spin labels on the peptide resulted in a significantly lower intensity ratio near residues Trp121 and Lys122 in the EF-SAM protein (Figure 3.12C). Mapping these residue positions on the 3D solution structure of the Ca^{2+} -loaded STIM1 EF-SAM core, revealed these two residues are in the EF-hand domain, spatially near the N-terminal end of EF-SAM where the unresolved STIM1 24-57 region extends (Figure 3.13). Therefore, these PRE experiments suggested that the 24-57 region interacts with the EF-SAM core in the EF-hand domain near the Trp121 and Lys122 residues. The 3D solution structure of EF-SAM core was generated using PYMOL Molecular Graphics System, Schrödinger, LLC.

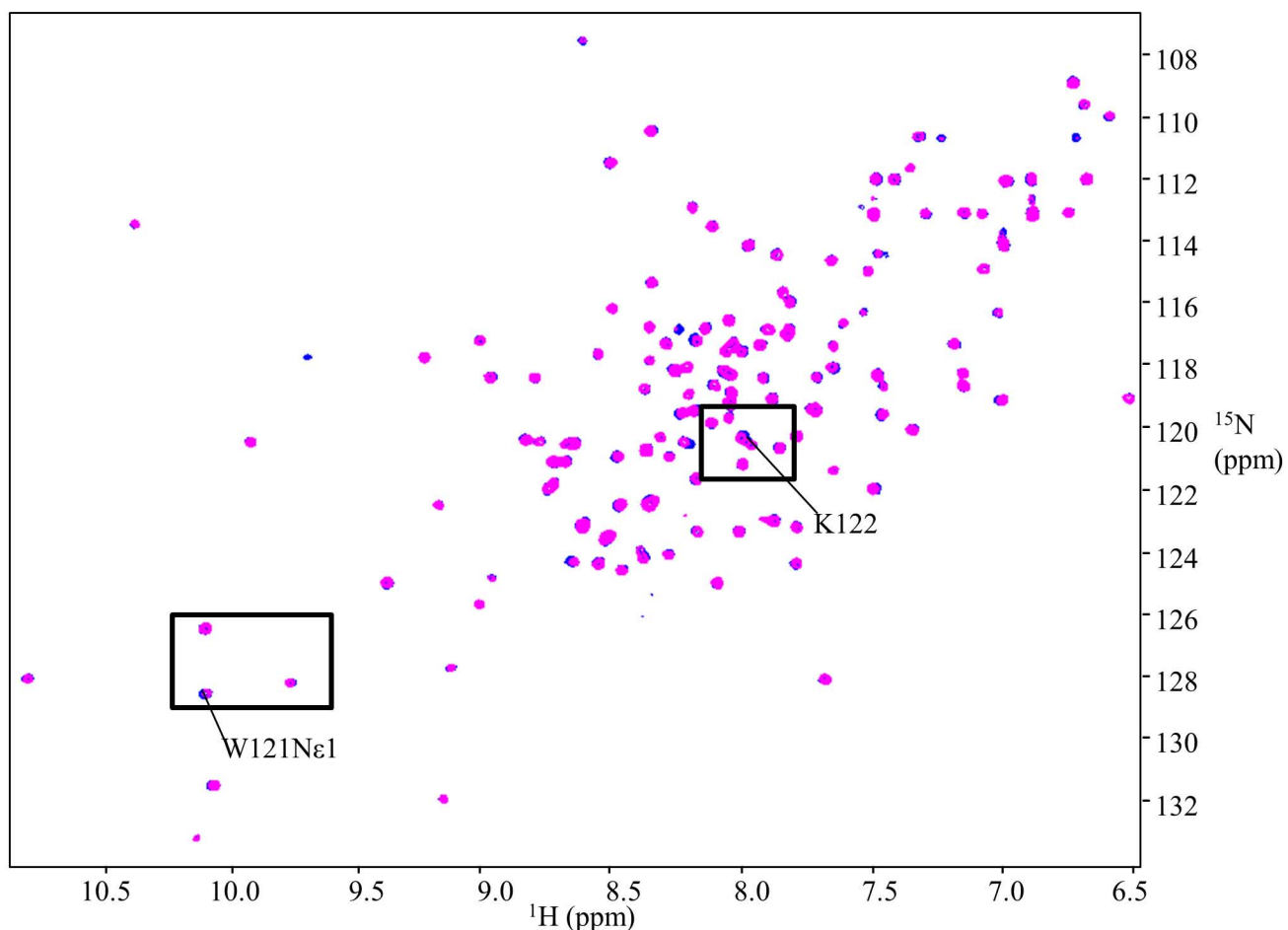


Figure 3.11. ^1H - ^{15}N -HSQC spectrum of STIM1 58-201 (EF-SAM) mixed with nitroxide spin-labelled STIM1 24-57. The protein mixture was solubilized in 150 mM NaCl, 20 mM TRIS-HCl (pH 8) and 5 mM CaCl_2 buffer at 15 °C before (magenta) and after (blue) the addition of 15 mM DTT. Nitroxide spin-labelled STIM1 24-57 (i.e. PRE-tagged STIM1 24-57) was added to ^{15}N -labelled STIM1 58-201 (EF-SAM) which resulted in residue specific decreases in crosspeak intensity localized near W121N ϵ 1 (side chain amide) and K122 (backbone amide). Data is representative of three separate experiments.

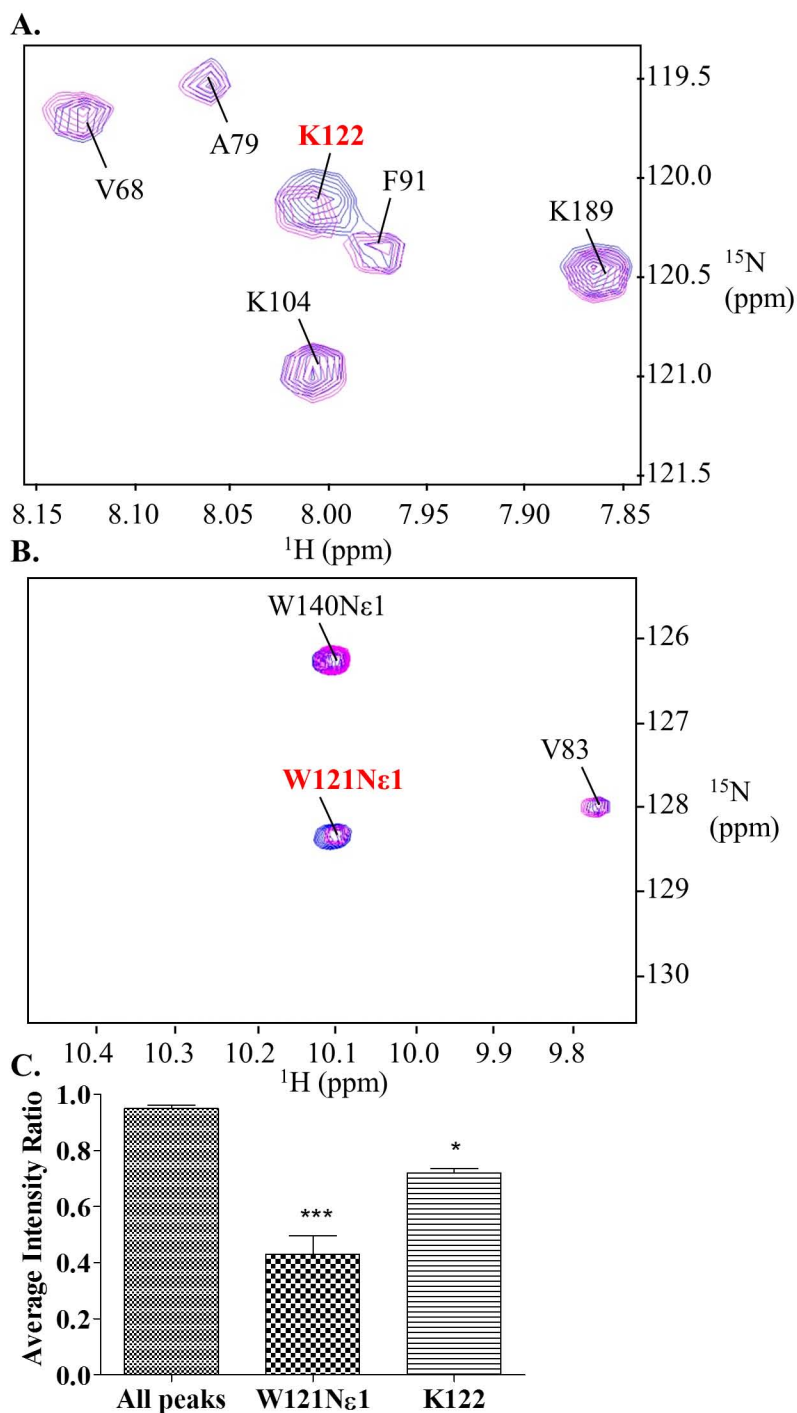


Figure 3.12. Transient binding between STIM1 24-57 and STIM1 58-201 (EF-SAM). The transient interaction was identified near the **A.** K122 N(H) and **B.** W121N ϵ 1 atoms. **C.** Average intensity ratio of the protein mixture (mean \pm SEM of three separate experiments). Statistical analysis was performed using one-way ANOVA followed by Tukey's test. (* $p < 0.05$ and *** $p = 0.0003$, $n = 3$).

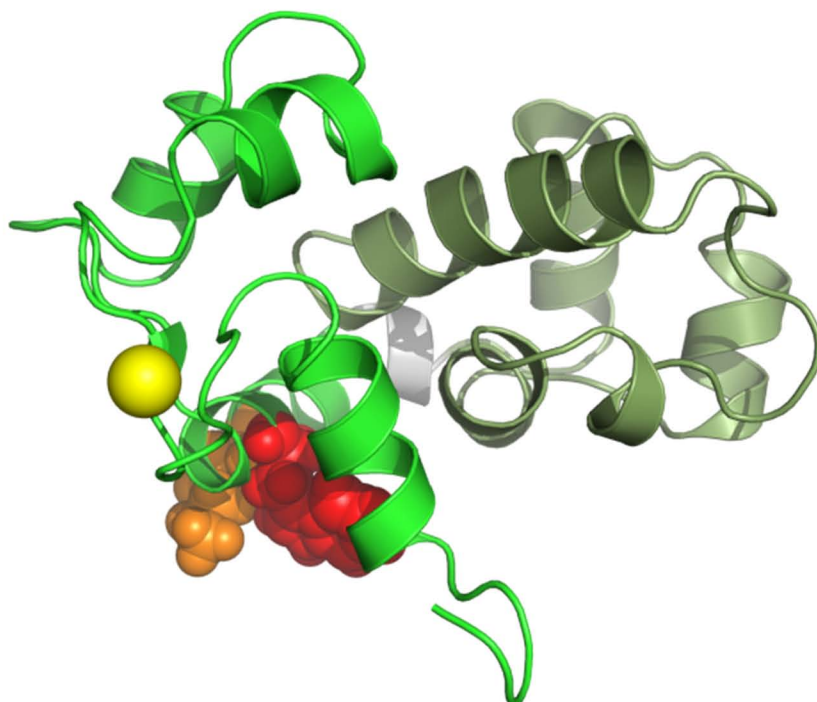


Figure 3.13. Structure of the EF-SAM domain under Ca²⁺ loaded condition (2K60.pdb). The EF-hand (light green) and SAM domain (dark green) are connected by a short linker region (grey). The Ca²⁺ atom is shown as a yellow sphere. The transient interaction site between STIM1 24-57 peptide and the EF-hand domain is localized near the W121Nε1 (red) and K122 (orange) residues. The image was generated using PYMOL Molecular Graphics System, Schrödinger, LLC.

3.9 STIM1 23-213 Trp121Glu/Lys122Glu double mutant does not de-oligomerize following GSNO treatment.

S-Nitrosyl groups add an electronegative surface potential to the modification sites (Okamoto et al., 2014). Thus, to validate that the interaction site determined by PRE was mechanistically relevant to the NO donor-mediated suppressed oligomerization, a STIM1 23-213 Trp121Glu/Lys122Glu double mutant was engineered and assessed by DLS in the presence and absence of GSNO. I rationalized that the negative charges introduced by the Trp121Glu/Lys122Glu double mutant would clash with the electronegative surface potential of the *S*-nitrosothiol groups and abrogate de-oligomerization by blocking any increased folding and stability. The oligomerization state of Ca²⁺-depleted STIM1 23-213 Trp121Glu/Lys122Glu double mutant protein in a buffer that contains 20 mM TRIS, 150 mM NaCl and, 1 mM DTT or 1 mM GSNO (pH 7.4) was assessed via DLS using a quartz MicroCuvette. At 37 °C, under the presence of the NO donor GSNO and propensity for *S*-nitrosylation of both Cys49 and Cys56 sites, the wildtype protein de-oligomerized compared to the DTT sample, as observed previously (Figure 3.6A). However, the Trp121Glu/Lys122Glu double mutant protein did not de-oligomerize even with the GSNO treatment (Figure 3.14). Indeed, this double mutation revealed the importance of the Trp121 and Lys122 residues in creating an electropositive environment conducive for complementary charge interactions with the *S*-nitrosylation sites and reinforced the notion that these residues were likely the sites where STIM1 24-57 transiently interacted with EF-SAM.

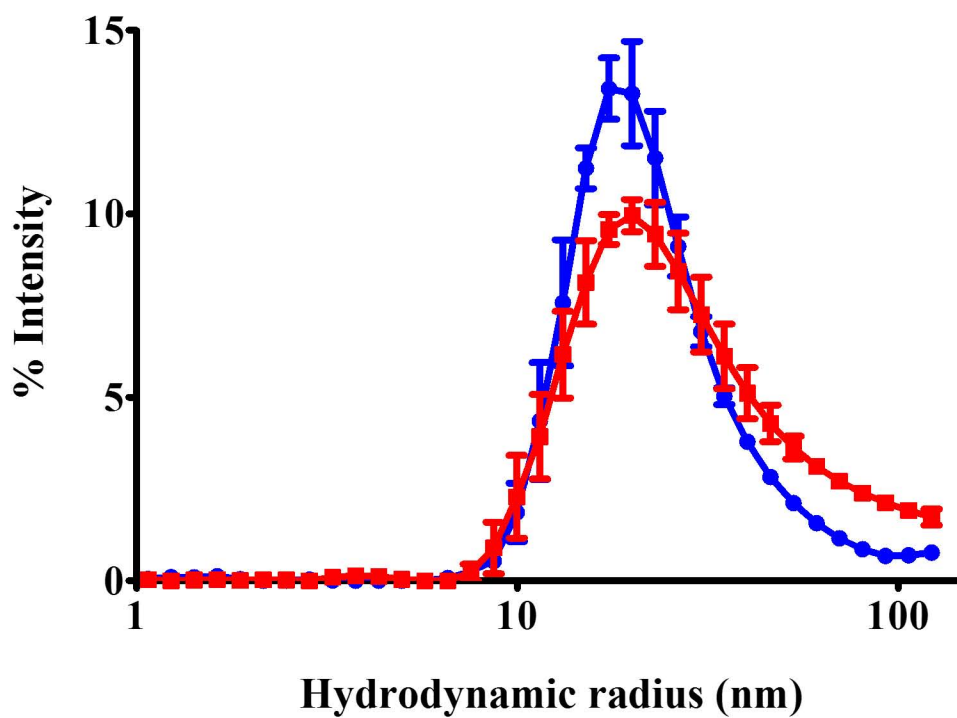


Figure 3.14. Dynamic light scattering (DLS) of STIM1 23-213 Trp121Glu/Lys122Glu double mutant protein. The contribution of the deconvoluted particle size distributions to the light scattering intensity of Ca^{2+} depleted STIM1 23-213 Trp121Glu/Lys122Glu double mutant protein (0.46 mg ml^{-1} , $n = 3$) in 20 mM TRIS-HCl (pH 7.4), 150 mM NaCl, and 1 mM DTT (blue) or 1 mM GSNO (red).

3.10 STIM1 siRNA and BTP2 blockade of Orai1 channel activity decreased PE-induced hypertrophy

The Feng laboratory has recently demonstrated that treatment of HEK293 cells co-expressing YFP-Orai1 and mCherry-STIM1 with the NO donor (GSNO) inhibited STIM1 puncta formation and CRAC current but not in cells co-expressing YFP-Orai1 and the Cys49Ser/Cys56Ser STIM1 double mutant (Gui et al., 2017). To further extend this work and to complement my *in vitro* data using the isolated STIM1 luminal domain fragments, I assessed the cell size of cultured neonatal rat cardiomyocytes treated with 50 μ M PE to induce the hypertrophic phenotype with and without STIM1 siRNA or BTP2 as SOCE inhibitors. As expected, PE treated cells showed significantly enlarged size compared to untreated controls (Figure 3.15A and 3.15B). However, when the ventricular cardiomyocytes were transfected with 10 nM STIM1 siRNA 24 h prior to PE treatment or when 5 μ M BTP2 was added concurrently with PE, essentially inhibiting the STIM1 and Orai1 proteins from the SOCE pathway, respectively, no hypertrophic phenotype was observed (Figure 3.15A and 3.15B). In the absence of PE treatment, neither the siRNA nor the BTP2 affected cardiomyocyte size. Thus, these primary culture experiments demonstrated that SOCE plays a significant role in the development of PE-induced cardiomyocyte hypertrophy.

3.11 GSNO and adenoviral nNOS inhibits PE-induced hypertrophy

To test how NO affects cardiomyocyte hypertrophy, I applied a similar cardiomyocyte size assessment to neonatal rat cardiomyocytes incubated with 100 μ M exogenous GSNO during the administration of PE or cells infected with adenoviral nNOS (moi = 10) 24 h to enhance NO production prior to PE treatment. The exogenous NO donor GSNO (Figure 3.16A and 3.16B) or ectopic adenoviral nNOS expression (Figure 3.17A and 3.17B) were both able to inhibit PE-induced neonatal rat cardiomyocyte hypertrophy

(Figure 3.16 and 3.17). In the absence of PE treatment, neither the GSNO incubation nor the adenoviral nNOS significantly affected cardiomyocyte size. Taken together, the previous work from the Feng laboratory and the present cellular cardiomyocyte experiments demonstrates that NO suppresses cardiomyocyte hypertrophy *via* a STIM1 and SOCE-dependent manner which involves Cys49 and Cys56 of STIM1.

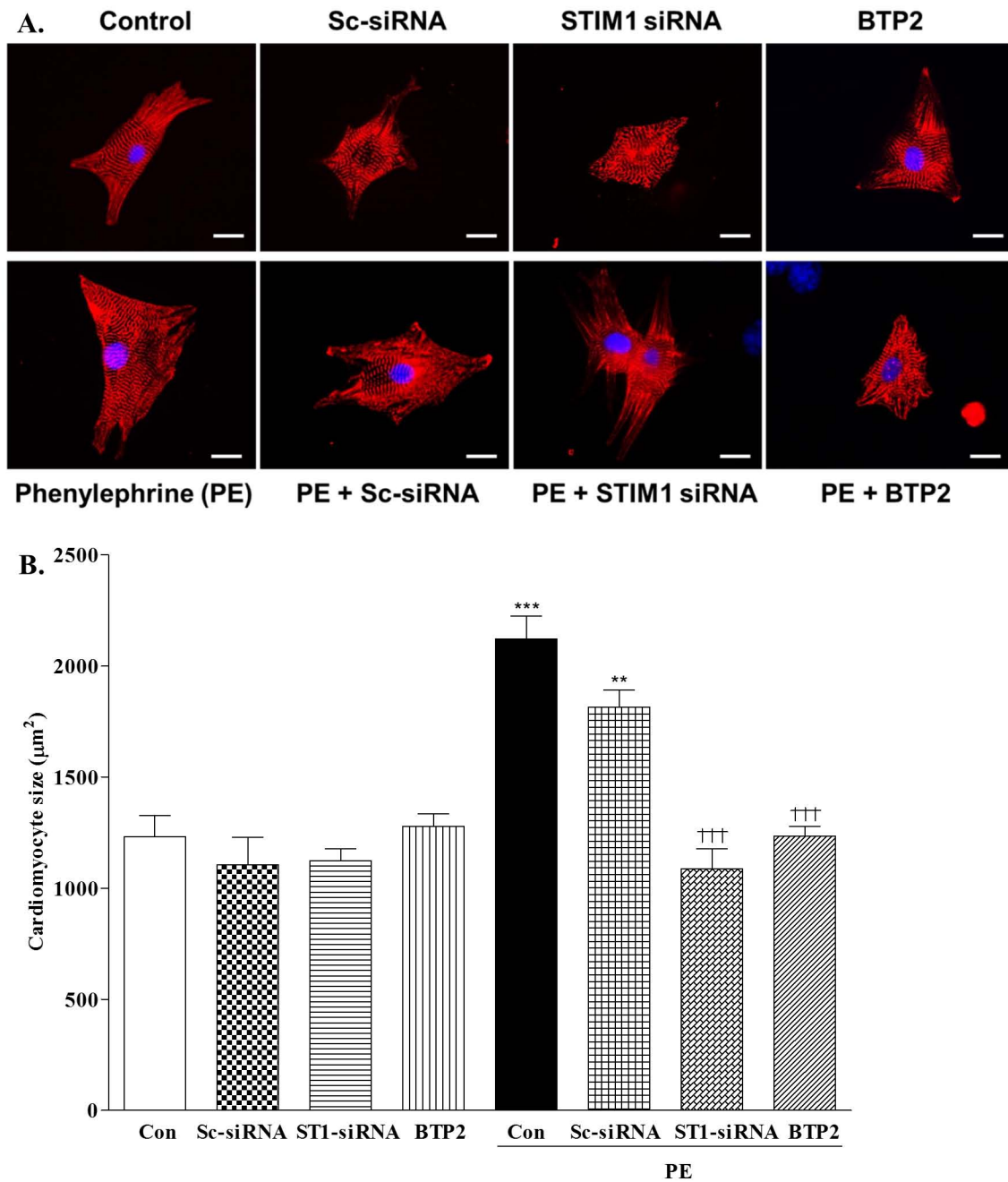


Figure 3.15. Effect of STIM1 siRNA and BTP2 on cardiomyocyte size. A. Representative fluorescent images of Sprague Dawley neonatal rat cardiomyocytes that were stained for α -actinin (red) and Hoechst stained (blue) to identify the nucleus. Scale bar (white) = 10 μm . **B.** Neonatal rat cardiomyocyte size is shown as mean \pm SEM. STIM1 and Orai1 inhibition by STIM1 siRNA and BTP2, respectively, prevents PE-induced cardiomyocyte hypertrophy. Data are \sim 100 cells per group and $n = 3-6$ separate experiments; *** $p < 0.0001$ and ** $p < 0.01$ vs. control, ††† $p < 0.0001$ vs. PE using ANOVA followed by Tukey's test.

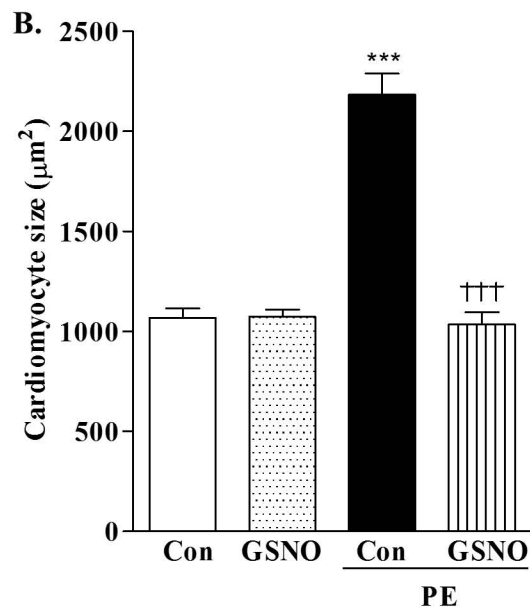
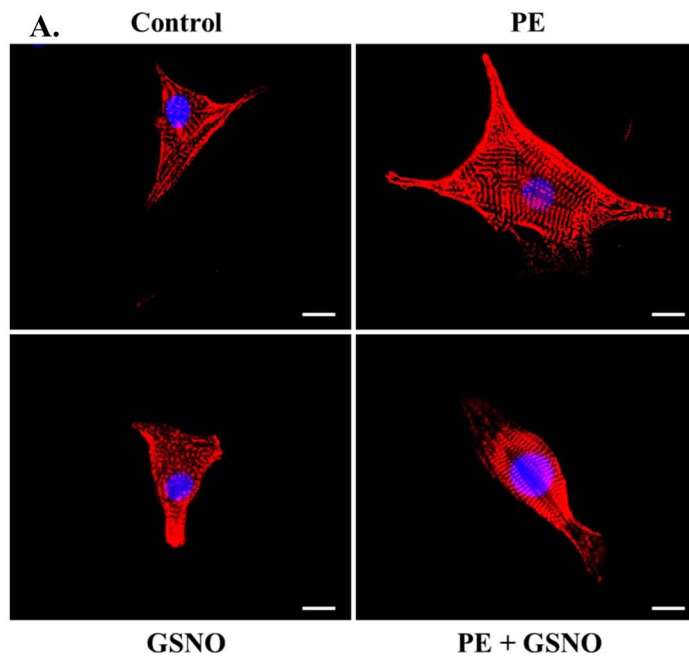


Figure 3.16. Effect of GSNO treatment on cardiomyocyte size. **A.** Representative fluorescent images of Sprague Dawley neonatal rat cardiomyocytes that were stained for α -actinin (red) and Hoechst stained (blue) to identify the nucleus. Scale bar (white) = 10 μ m. **B.** Neonatal rat cardiomyocyte size is shown as mean \pm SEM. Treatment with GSNO inhibits PE-induced cardiomyocyte hypertrophy which is consistent with the *S*-nitrosylation-mediated inhibition of STIM1 activation proposed in the *in vitro* studies. Data are \sim 100 cells per group in $n = 4$ separate experiments; *** $p < 0.0001$ vs. control, ††† $p < 0.0001$ vs. PE using ANOVA followed by Tukey's test.

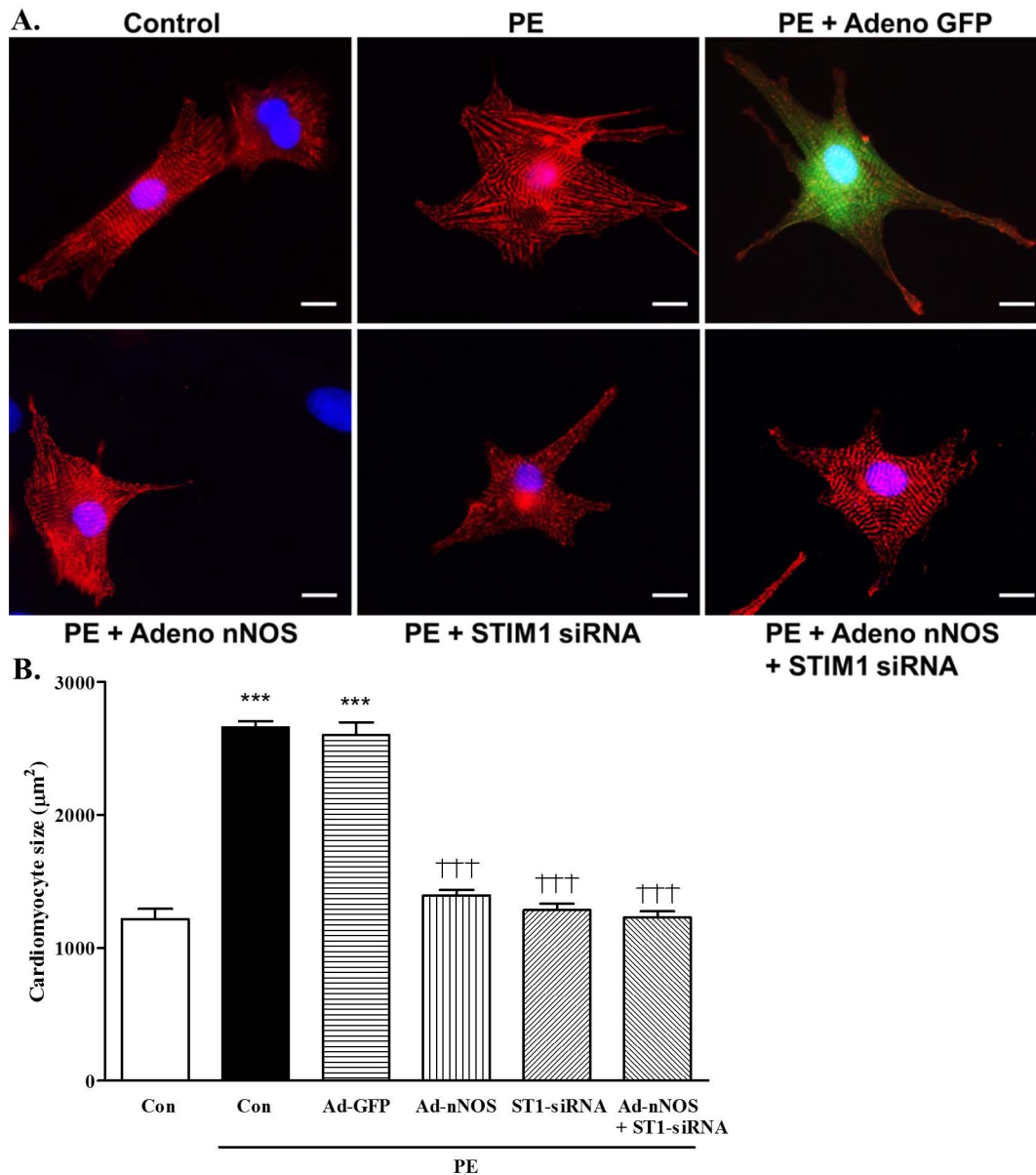


Figure 3.17. Effect of ectopic Adeno nNOS expression on cardiomyocyte size.

A. Representative fluorescent images of Sprague Dawley neonatal rat cardiomyocytes that were stained for α -actinin (red) and Hoechst stained (blue) to identify the nucleus. Scale bar (white) = 10 μm . **B.** Neonatal rat cardiomyocyte size is shown as mean \pm SEM. Treatment with ectopic Adeno nNOS prevents PE-induced cardiomyocyte hypertrophy which is consistent with the *S*-nitrosylation-mediated inhibition of STIM1 activation proposed in the *in vitro* studies. Data are \sim 100 cells per group in $n = 4$ separate experiments; *** $p < 0.0001$ vs. control, +++ $p < 0.0001$ vs. PE using ANOVA followed by Tukey's test.

Chapter 4 Discussion

4.1 Summary

It has long been known that NO plays a critical role in cardiomyocyte contractility, excitation-contraction coupling and development of the hypertrophic phenotype (Kelly et al., 1996). Over-activation of the STIM1-mediated SOCE pathway is often the precursor for pathological cardiac hypertrophy (Luo et al., 2012). Previous studies have found that *S*-glutathionylation of STIM1 at Cys56 decreases its Ca²⁺ binding affinity and promotes STIM1 oligomerization, which leads to CRAC channel formation and activation of the SOCE pathway, independent of the level of ER Ca²⁺ stores (Hawkins et al., 2010). The constitutive CRAC channel activation causes sustained Ca²⁺ level increases and can even lead to mitochondrial Ca²⁺ overload mediated apoptosis (Giorgi et al., 2012). This *S*-glutathionylation effect is opposite to the effect of *S*-nitrosylation based on my data described herein. Specifically, my results showed that *S*-nitrosylation of STIM1 luminal domain by excess NO donors like GSNO stabilized the domain via a mechanism that involves rigidification of the non-conserved N-terminal domain and enhanced folding and stability likely mediated by interactions with the EF-hand domain. These structural and dynamic changes suppressed both surface exposed hydrophobicity and oligomerization, biophysical properties that drive homomeric protein-protein interactions and STIM1-mediated initiation of SOCE. This work was extended into primary cell culture, where I demonstrated that cardiomyocytes incubated with GSNO or ectopic nNOS expression attenuated PE-induced cardiomyocyte hypertrophy. Consistently, knockdown of STIM1 or pharmacologically blocking Orai1 channel activity, also attenuated PE-induced cardiomyocyte hypertrophy. Collectively, my work suggests that NO can attenuate STIM1-mediated SOCE, by modification of the N-terminal Cys49 and Cys56 residues which suppresses the biophysical properties which promote destabilization-coupled oligomerization of the luminal domain.

4.2 *S*-Nitrosylation

S-Nitrosylation is a readily reversible post-translational modification which adds NO groups onto reduced Cys residues and forms *S*-nitrosocysteines in different proteins (Figure 1.3). The *S*-nitrosylated proteins can subsequently affect the structure and function of target proteins, thereby amplifying any regulatory effects (Gould et al., 2013; Haldar and Stamler, 2013; Hess and Stamler, 2012). For instance, a recent study showed that *S*-nitrosylation affects the function of Ca²⁺ handling proteins including cardiac troponin C, phospholamban and RyR (Irie et al., 2015). This group found that following β -AR stimulation by an agonist such as isoproterenol, the extent of Ca²⁺ handling protein *S*-nitrosylation is dependent on GSNOR levels, which ultimately regulates cardiomyocyte function (Irie et al., 2015). In another study, *S*-nitrosylation of GAPDH at Cys247 was found to inhibit its ability to appropriately function as a chaperone protein, which led to the ubiquitination and degradation of ribosomal protein L13a (Jia et al., 2012).

Dysregulated *S*-nitrosylation or denitrosylation can result in serious pathological conditions. For instance, the metabolic enzyme GSNOR can selectively reduce the *S*-nitrosothiol group from GSNO or cellular proteins and is tightly regulated in order to maintain physiological homeostasis and resist nitrosative stress-induced damage. Dysregulation of arginine metabolic pathways and lack of NO production can also lead to many pathological conditions including allergic asthmas and sepsis (Carraway et al., 1998; Maarsingh et al., 2006).

In my investigation, we applied an approach of excess NO donor treatment to promote *S*-nitrosylation of STIM1 residues Cys49 and Cys56, as has been applied previously with other proteins (Bocedi et al., 2004; Feng et al., 2011; Hao et al., 2004; Liu et al., 2002). Specific modification at Cys49 and Cys56 by GSNO was confirmed via solution NMR spectroscopy after assigning the chemical shifts of the short non-conserved luminal peptide in STIM1 upstream of the EF-SAM domain (i.e. STIM1 24-57). These short, non-conserved N-terminal regions of STIM1 have been previously shown to influence EF-SAM stability and affect the activation kinetics of Orai1 channels (Stathopoulos et al., 2009; Zhou et al., 2009). After the sequential backbone assignments were made, the

maximal chemical shift perturbations caused by GSNO treatment for the C α and C β carbons as well as the amide hydrogen and nitrogen were centered at the Cys49 and Cys56. There was also a rigidification around Cys49 following GSNO induced S-nitrosylation (Figure 3.9) based on the higher order parameter (S^2) predicted from the RCI (Berjanskii and Wishart, 2005).

Several lines of evidence suggest that S-nitrosylation of Cys49 and Cys56 is the main modification in my excess GSNO treatment strategy. First, other studies have successfully S-nitrosylated proteins using this strategy (Bocedi et al., 2004; Feng et al., 2011; Hao et al., 2004; Liu et al., 2002). Second, Cys49-Cys56 disulfide formation has been demonstrated to enhance STIM1 activation and SOCE (Prins et al., 2011). Third, S-glutathionylation, a possible modification with the use of GSNO, destabilizes the STIM1 luminal domain and promotes STIM1-mediated activation of SOCE (Stathopoulos laboratory, unpublished data; Hawkins et al., 2010). Fourth, weak NO donors such as SNAP have no effect on STIM1 23-213 stability (Stathopoulos laboratory, unpublished data). Similarly, I observed a concentration-dependent response in my SNP experiments, where lower concentrations (i.e. 1 mM) caused less stabilization of STIM1 23-213 than higher concentrations (i.e. 2 mM). Finally, the Feng laboratory has demonstrated GSNO-dependent S-nitrosylation of STIM1 using a biotin switch assay (Forrester et al., 2009; Gui et al., 2017).

4.3 S-Nitrosylation of luminal STIM1 region increases protein stability.

The SR Ca²⁺ sensing luminal region of STIM1 (i.e. STIM1 23-213) becomes activated under Ca²⁺ depletion conditions and adopts a destabilized conformation that triggers the activation of downstream processes in the SOCE pathway (Marshall et al., 2015; Stathopoulos and Ikura, 2010, 2013; Stathopoulos et al., 2006; Stathopoulos et al., 2013; Stathopoulos et al., 2009; Stathopoulos et al., 2008). Therefore, STIM1 stability inversely correlates with its ability to become activated, where STIM1 stabilization inhibits its ability to initiate SOCE.

My work showed that the luminal region of STIM1 has an α -helical structure (Figure 3.1); the level of α -helix is reduced upon Ca^{2+} depletion. This partial loss in α -helicity is evident by the reduction in negative ellipticity and is in-line with previous observations which show a loss in α -helical structure associated with STIM1 activation (Stathopoulos et al., 2006; Stathopoulos et al., 2009; Stathopoulos et al., 2008; Zheng et al., 2008). Consistent with this loss in α -helical structure, my thermal stability assessment revealed T_m values which were markedly reduced in the Ca^{2+} -depleted state for STIM1 23-213. Remarkably, however, I found that *S*-nitrosylation by GSNO or SNP under both the Ca^{2+} loaded and depleted conditions significantly increased the apparent T_m values compared to the Cys-reduced states (Figure 3.2A-D). This elevation in apparent T_m is more pronounced under Ca^{2+} depletion conditions, which is the state where STIM1 becomes activated. In order to ensure that this stabilization effect under the presence of NO donors GSNO and SNP is indeed due to *S*-nitrosylation of Cys49 and Cys56 residues in STIM1 luminal region, the STIM1 23-213 Cys49Ser/Cys56Ser double mutant protein was utilized. Although the double mutation caused an overall destabilization of the protein compared to WT, the T_m for the double mutant protein was not statistically different with and without the NO donors (Figure 3.3A and 3.3B), suggesting that the NO induced stabilization of luminal STIM1 is Cys specific.

Surprisingly, no stabilization was detectable for either Cys49Ser or Cys56Ser single mutants in the presence of GSNO. This could be due to several reasons. The stabilization effect by *S*-nitrosylation on the single mutants could be too small to be detectable in thermal denaturation experiments. The NO-stabilization effect may also be insufficient to overcome the single Cys mutation-induced destabilization. Moreover, based on my results from section 3.8 and 3.9, the interaction between STIM1 24-57 peptide and residues Trp121 and Lys122 from the EF-hand domain was necessary for *S*-nitrosylation to exert an effect. Perhaps this interaction also requires both *S*-nitrosylation sites to be present. It should be noted that our laboratory previously demonstrated that the single Cys49Ser or Cys56Ser mutants significantly decrease SOCE in HEK-293 cells incubated with GSNO (Gui et al., 2017); thus, the lack of detection of an effect *in vitro* in my experiments may have been due to insensitivity of the assays.

My chemical denaturation experiments enabled the extraction of the thermodynamic stability parameters, Gibbs free energy of unfolding in water (ΔG_{H_2O}) and cooperativity of unfolding (m -value). *S*-Nitrosylation of STIM1 23-213 wildtype protein using GSNO increased the urea concentration at which half of the macromolecules become unfolded (C_{mid}) as well as the ΔG_{H_2O} value under both the Ca^{2+} loaded and depleted conditions (Figure 3.10 A and 3.10B), consistent with my thermal stability observations. Moreover, without the presence of the *S*-nitrosylation sites, the STIM1 23-213 Cys49Ser/Cys56Ser double mutant protein did not exhibit pronounced changes in thermodynamic parameters (Figure 3.10C and 3.10I).

Since studies have qualitatively suggested both protein stabilizing (Cai et al., 2015; Kohr et al., 2014; Li et al., 2007; Renganathan et al., 2002; Takahashi et al., 2007) and destabilizing consequences (Albertos et al., 2015; Kumar et al., 2017; Qu et al., 2007) of *S*-nitrosylation, the role of this post-translational modification in folding and stability appears to be protein specific. Nevertheless, my study is the first to quantify the thermodynamic stability changes (i.e. ΔG_{H_2O}) associated with *S*-nitrosylation and may provide a starting point for understanding how the folded to unfolded equilibrium of proteins can be regulated by NO.

4.4 *S*-Nitrosylation of luminal STIM1 suppresses Ca^{2+} -dependent conformational changes and oligomerization.

The SR Ca^{2+} sensor STIM1 becomes activated upon Ca^{2+} depletion (Zhao et al., 2015). Therefore, the ability for STIM1 to change into an active conformation in response to changes in luminal Ca^{2+} concentration is critical for its function. The Ca^{2+} dissociation constant (K_d) of the wildtype STIM1 23-213 in 1 mM DTT control is 0.30 ± 0.04 mM (mean \pm SEM, $n=3$). My binding affinity estimate for the STIM1 23-213 protein is in the same range as determined for the core STIM1 EF-SAM domain previously (Stathopoulos et al., 2006; Zheng et al., 2008). This K_d fits well with the estimated magnitude of depletion in ER Ca^{2+} levels (Luik et al., 2008; Luik et al., 2006).

Quantitatively, my Ca^{2+} binding experiments suggested that GSNO-treated STIM1 23-

213 has a tighter binding affinity compared to DTT; however, the structural change associated with Ca^{2+} binding in the presence of GSNO was only $\sim 1.6\%$ compared to the Ca^{2+} free state. Thus, the K_d value in the presence of treatment with GSNO was not as reliably determined as the DTT sample which showed $\sim 20\%$ change in fluorescence intensity (Figure 3.4). Since the difference in the relative change in fluorescence intensity is an indicator of the magnitude of structural change associated with the binding, these binding experiments suggest that the GSNO treated WT protein undergoes a much smaller structural change upon Ca^{2+} binding compared to the DTT sample.

The extrinsic fluorescent dye, ANS, was used in my study to characterize these structural changes further in the presence of DTT or GSNO. ANS acts as a hydrophobic probe and has frequently been used to measure the exposed surface hydrophobicity of proteins including ubiquitin C-terminal hydrolase-1 (UCHL1) that is essential in the development of Parkinson's disease (Kumar et al., 2017), C-reactive protein (CRP) that is found at inflammatory sites (Singh et al., 2012) and folate binding protein (FBP) which affects cell growth and division via its regulation of folic acid (Holm et al., 2012), to name a few. Specifically, *S*-nitrosylation of the ubiquitin carboxyl-terminal hydrolase L1 (UCHL1) enzyme at residues Cys90, Cys152 and Cys220 was found to decrease its structural stability, promote aggregation and catalyze the oligomerization of α -synuclein which forms Lewy bodies in Parkinson's patients (Kumar et al., 2017). Under the presence of excess GSNO, the resultant high ANS fluorescence signal indicates an increase in UCHL1 exposed hydrophobicity following *S*-nitrosylation (Kumar et al., 2017). In my investigation, the ANS fluorescence in the presence of STIM1 23-213 wildtype protein plus GSNO was much lower compared to the DTT control sample, and the decrease in fluorescence intensity following the addition of 5 mM CaCl_2 was also attenuated for the GSNO experimental sample compared to the DTT control (Figure 3.5A and 3.5B). On the other hand, the STIM1 23-213 Cys49Ser/Cys56Ser double mutant protein in GSNO buffer had a much higher ANS fluorescence intensity and change in fluorescence after CaCl_2 treatment compared to the wildtype protein sample (Figure 3.5B and 3.5D). Consistent with my intrinsic fluorescence Ca^{2+} binding experiments, these ANS data show that in the presence of GSNO, STIM1 23-213 undergoes a smaller structural change than observed with DTT. However, these ANS data also reveal that the

exposed hydrophobicity in the presence and absence of Ca^{2+} is reduced in the presence of GSNO in a Cys-specific manner.

Studies have shown that oligomerization is one of the key mechanisms that activates or inhibits protein function by influencing their ability to initiate downstream processes depending on the structure of that particular protein. For instance, oligomerization of AMP-activated protein kinase (AMPK) heterotrimers leads to its autoinhibition because the active sites become hidden inside the large inert oligomers following AMPK aggregation (Scholz et al., 2009). On the other hand, oligomerization of procaspase-9, caspase-2, caspase-10 or murine caspase-11 can lead to their activation which result in inflammation and the initiation of apoptosis (Chang et al., 2003). Moreover, *S*-nitrosylation of surfactant protein (SP)-D promotes the formation of trimers instead of dodecamers or higher order multimers and induces calreticulin/CD91 and p38 MAPK activation to trigger the pro-inflammatory response (Guo et al., 2008). In this case, SOCE is initiated upon STIM1 homo-oligomerization in response to SR Ca^{2+} depletion (Luik et al., 2008; Stathopoulos et al., 2006; Stathopoulos et al., 2008). Therefore, the oligomerization state of STIM1 directly influences the SOCE pathway. Results from my DLS experiments indicate that STIM1 23-213 wildtype protein de-oligomerizes following *S*-nitrosylation by exchanging the protein into a buffer that contains excess amount of the NO donor GSNO (Figure 3.6A). As a negative control, without the *S*-nitrosylation sites, STIM1 23-213 Cys49Ser/Cys56Ser double mutant protein does not undergo this de-oligomerization event and has the same apparent particle size distribution in the presence of both DTT and GSNO (Figure 3.6B). This oligomerization assessment is consistent with the smaller structural change associated with Ca^{2+} binding and decreased exposed hydrophobicity.

4.5 STIM1 24-57 peptide interacts with STIM1 58-201 (EF-SAM domain) at residues Trp121 and Lys122 to mediate *S*-nitrosylation-induced stabilization of STIM1.

It has been previously shown that *S*-nitrosylation of methionine adenosyltransferase at

Cys121 inactivates this protein (Perez-Mato et al., 1999). However, the ability for *S*-nitrosylation to occur was greatly reduced by replacing the surrounding charged amino acids (i.e. acidic Asp355 or basic Arg357 and Arg363) with Ser (Perez-Mato et al., 1999). Interestingly, it was also found that removal of the NO donor from the isolated rat hepatocyte incubation medium quickly led to denitrosylation and reactivation of this protein, demonstrating the reversible nature of this modification (Perez-Mato et al., 1999). In a more recent study, *S*-nitrosylation of the cytoplasmic rhodanese domain from the *E. coli* membrane-bound sulfurtransferase protein (YgaP) at Cys63 has been found to enhance the stability of this protein (Eichmann et al., 2016). The structural changes were examined using NMR, and *S*-nitrosylation of rhodanese caused the C-terminal helix $\alpha 5$ to move away from the active site loop (i.e. Cys63-Thr69) due to the reduced charge interaction between this C-terminal helix and the active site, thus, disrupting the formation of an unstable conformation of the $\alpha 5$ helix (Eichmann et al., 2016). In my investigation, I applied a PRE approach to reveal the structural basis for the increased stability, decreased structural sensitivity to Ca^{2+} binding, reduction in exposed hydrophobicity and suppressed oligomerization. My PRE experiments revealed that STIM1 24-57 peptide transiently interacts with the EF-SAM domain core at residues Trp121 and Lys122 (Figure 3.11, 3.12 and 3.13). Further, when I introduced a STIM1 23-213 Trp121Glu/Lys122Glu double mutant designed based on the PRE observation, the de-oligomerization following GSNO treatment did not occur (Figure 3.14). Thus, Trp121 and Lys122 may provide a complementary electrostatic environment conducive to interactions with *S*-nitrosylated Cys49 and Cys56 residues and suggests an *S*-nitrosylation-mediated regulatory effect whereby *S*-nitrosylation of Cys49 and Cys56 lead to increased interactions between the 24-57 region and the EF-SAM core, increasing stability, suppressing hydrophobicity and inhibiting oligomerization, the key initiation event of SOCE.

4.6 Inhibition of the SOCE pathway prevents the development of PE-induced cardiomyocyte hypertrophy.

Pathological cardiac hypertrophy can develop in patients that experience chronic stress

on the heart due to hypertension, MI or genetic sarcomeric protein mutations (Levy et al., 1988; Seidman and Seidman, 2001). This deleterious hypertrophic condition is characterized by an enlargement of the heart muscle as a result of increased cardiomyocyte size (Soonpaa et al., 1996). One of the main signaling mechanisms that mediate the development of the hypertrophic phenotype is the calcineurin/NFAT pathway that can become activated in response to sustained elevation of cytosolic Ca^{2+} levels (Luo et al., 2012). Following the initial event of PE binding to the PM GPCR (α_1 -AR), IP_3 is produced by PLC and activates SR IP_3R to enable the release of Ca^{2+} store from the SR. This Ca^{2+} depletion in the SR results in STIM1 activation and translocation to the SR-PM junction as well as Orai1 recruitment and activation into forming CRAC channels. The entry of Ca^{2+} from the extracellular space via the CRAC channels maintains cytosolic Ca^{2+} elevation, initiates the calcineurin/NFAT pathway and results in the upregulation of pro-hypertrophic gene signalling (Hogan et al., 2003; Musaro et al., 1999). In my studies, when the SR Ca^{2+} sensor STIM1 or CRAC channel subunit Orai1 from the SOCE pathway is inhibited by STIM1 siRNA or BTP2, respectively, the hypertrophic phenotype does not develop in primary cultured ventricular cardiomyocytes even in the presence of the α_1 -AR agonist PE (Figure 3.15).

In my investigation, primary cultured ventricular cardiomyocytes from neonatal Sprague Dawley rats were also treated using the exogenous NO donor GSNO along with PE or adenoviral nNOS prior to the addition of PE. *S*-Nitrosylation of the Ca^{2+} sensor STIM1 by GSNO or NO that is produced by nNOS (Gui et al., 2017, in revision) attenuated the ability of STIM1 to become activated following SR Ca^{2+} depletion and inhibited the progression of the SOCE pathway, ultimately preventing the development of PE-induced cardiomyocyte hypertrophy (Figures 3.16 and 3.17).

Results from previous work in our lab indicate that nNOS deficiency or vinyl-L-N-5-(1-imino-3-butenyl)-L-ornithine (L-VNIO) treatment that selectively inhibits nNOS enhances SOCE and CRAC currents in cardiomyocytes, whereas GSNO inhibits CRAC currents in nNOS^{-/-} cardiomyocytes (Gui et al., 2017, in revision). These data are fully consistent with my observations that GSNO or adenoviral nNOS mediated *S*-nitrosylation of STIM1 inhibits its activation and prevents the development of the hypertrophic phenotype in

cardiomyocytes. This is also consistent with my data where STIM1 and Orai1 inhibition by STIM1 siRNA and BTP2, respectively, prevents PE-induced cardiomyocyte hypertrophy.

4.7 Future directions and limitations

Solution NMR spectroscopy experiments using STIM1 24-57 peptide in a buffer that contains either GSNO or DTT revealed residue specific chemical shift changes clustering near Cys49 and Cys56 as well as rigidification near Cys49 following *S*-nitrosylation. Although the structure of the STIM1 24-57 peptide that contains the *S*-nitrosylation sites was characterized in the present study, structures of the *S*-nitrosylated and de-nitrosylated STIM1 23-213 states which encompass both the short luminal peptide and EF-SAM domain will provide further insights into structural perturbations and changes associated with Cys49 and Cys56 *S*-nitrosylation in the full luminal domain context.

There are two human STIM homologues, STIM1 and STIM2, which are highly similar in sequence and domain architecture (Figure 1.2) (Hooper et al., 2013). Human STIM1 is a SR Ca^{2+} sensor that becomes activated following Ca^{2+} depletion and mediates the activation of Orai1 into forming functional CRAC channels in the SOCE pathway, whereas the homologous STIM2 functions as a main regulator of basal Ca^{2+} homeostasis (Brandman et al., 2007). Although STIM2 activation is also dependent on stored Ca^{2+} levels, it has a weaker Ca^{2+} binding affinity and becomes activated when the stores are near full (Gruszczynska-Biegala et al., 2011; Stathopoulos et al., 2013; Zheng et al., 2008; Zheng et al., 2011). STIM2 also has the two Cys residues in the luminal region available to be *S*-nitrosylated, so understanding how *S*-nitrosylation affects the biophysical properties, structure and function of STIM2 will provide valuable information on the mechanisms of basal Ca^{2+} homeostasis. Further, the N-terminal region (other than the Cys49 and Cys56) is dissimilar between STIM2 and STIM1, and so precisely how or if these differences are involved in the mechanisms of *S*-nitrosylation regulation remain to be determined.

Thus far, the effects of *S*-nitrosylation on PE-induced hypertrophy have only been investigated using neonatal Sprague-Dawley rat primary cell cultures. Moreover, *S*-nitrosylation of STIM1 was induced by treating the cells in selective wells with GSNO or adenoviral nNOS. Therefore, *in vivo* studies using STIM1 Cys49Ser/Cys56Ser transgenic mice would enable us to evaluate the effect of Cys49- and Cys56-specific *S*-nitrosylation in the larger scale physiological context.

There are limitations associated with the present study. First, aside from residues Cys49 and Cys56 in the luminal region of STIM1 under investigation, there are other Cys residues that may be *S*-nitrosylated, including Cys227 in the TM domain and Cys437 in the cytosolic CAD region. Moreover, all of my experiments were performed under the presence of excess NO donors GSNO or SNP due to the labile nature of the protein modification by *S*-nitrosylation which limited the types of investigations conducted. For instance, Ca²⁺ binding experiments were not performed using CD spectroscopy due to the pronounced elevation in high tension associated with the GSNO and SNP buffers. Direct measurement of *S*-nitrosylation by mass spectroscopy was unsuccessful due to the labile nature of this modification. The unstable modification also made it challenging to estimate the level of *S*-nitrosylated protein in ventricular cardiomyocytes. *In vitro*, the level of *S*-nitrosylated protein could not be estimated which prevented the assessment of whether both Cys49 and Cys56 residues were similarly susceptible to this modification.

4.8 Conclusions

Protein post-translational modifications including *S*-nitrosylation, phosphorylation, ubiquitination, acetylation, palmitoylation, sumoylation and redox modifications, to name a few, have been recognized as critical modulators of cell signaling, regulating the biophysical, biochemical and structural properties of myriad cellular proteins (Hess and Stamler, 2012). The modification under investigation, *S*-nitrosylation, is a reversible Cys modification that adds NO groups onto the SH sidechain of reduced Cys residues (Figure 1.3) which ultimately affects the structure and function of the *S*-nitrosylated target

protein. Understanding the thermodynamic consequences of *S*-nitrosylation and mechanisms by which *S*-nitrosylation of the SR Ca^{2+} sensor STIM1 contributes to Ca^{2+} signaling enhances our comprehension of CRAC channel mediated SOCE. Collectively, my data revealed that *S*-nitrosylation of residues Cys49 and Cys56 in the luminal domain stabilizes and inhibits STIM1 activation by promoting a more compact protein conformation with less exposed hydrophobicity and less propensity for oligomerization (Table 4.1). Moreover, my thermodynamic data quantifies the energetic effects of Cys49 and Cys56 *S*-nitrosylation on the luminal domain of STIM1.

In the full-length STIM1 context, my data suggests that *S*-nitrosylation of STIM1 prevents the Ca^{2+} -depletion dependent oligomerization and translocation of STIM1. This inhibition would preclude the recruitment and activation of Orai1 into forming functional CRAC channels at the ER-PM junctions. Ultimately, the lack of sustained cytosolic Ca^{2+} elevation mediated by CRAC would prevent calcineurin/NFAT pathway signaling and the development of the hypertrophic phenotype (Figure 4.1). Consistent with my model of STIM1 regulation by NO (Figure 4.1) SOCE inhibition at the level of STIM1 or Orai1 using STIM1 siRNA and BTP2 respectively, as well as inhibition of STIM1 activation by *S*-nitrosylation using GSNO or adenoviral nNOS prevents the development of PE-induced cardiomyocyte hypertrophy. NO has long been known to confer cardiovascular benefits by relaxing narrowed blood vessels, increasing oxygen and blood flow (Forstermann et al., 1994). However, my research demonstrates that NO may also play a role in preventing cardiac hypertrophy by inhibiting STIM1 activation.

Table 4.1. Summary of the effect of *S*-nitrosylation on various properties associated with STIM1 activation.

	-S-H ^a	-S-N=O ^a
Thermal stability^b	↓	↑

Structural change following Ca²⁺ binding^b	↑	↓
Exposed hydrophobicity^b	↑	↓
Oligomerization^b	↑	↓
Thermodynamic stability^b	↓	↑
Cardiomyocyte hypertrophy^c	↑	↓

↓ relatively lower ↑ relatively higher

^aproperties of unmodified (-S-H) relative to S-nitrosylated (-S-N=O) STIM1

^bexperiments performed using recombinant human STIM1 23-213 protein

^cexperiments performed using neonatal rat cardiomyocytes with endogenous STIM1

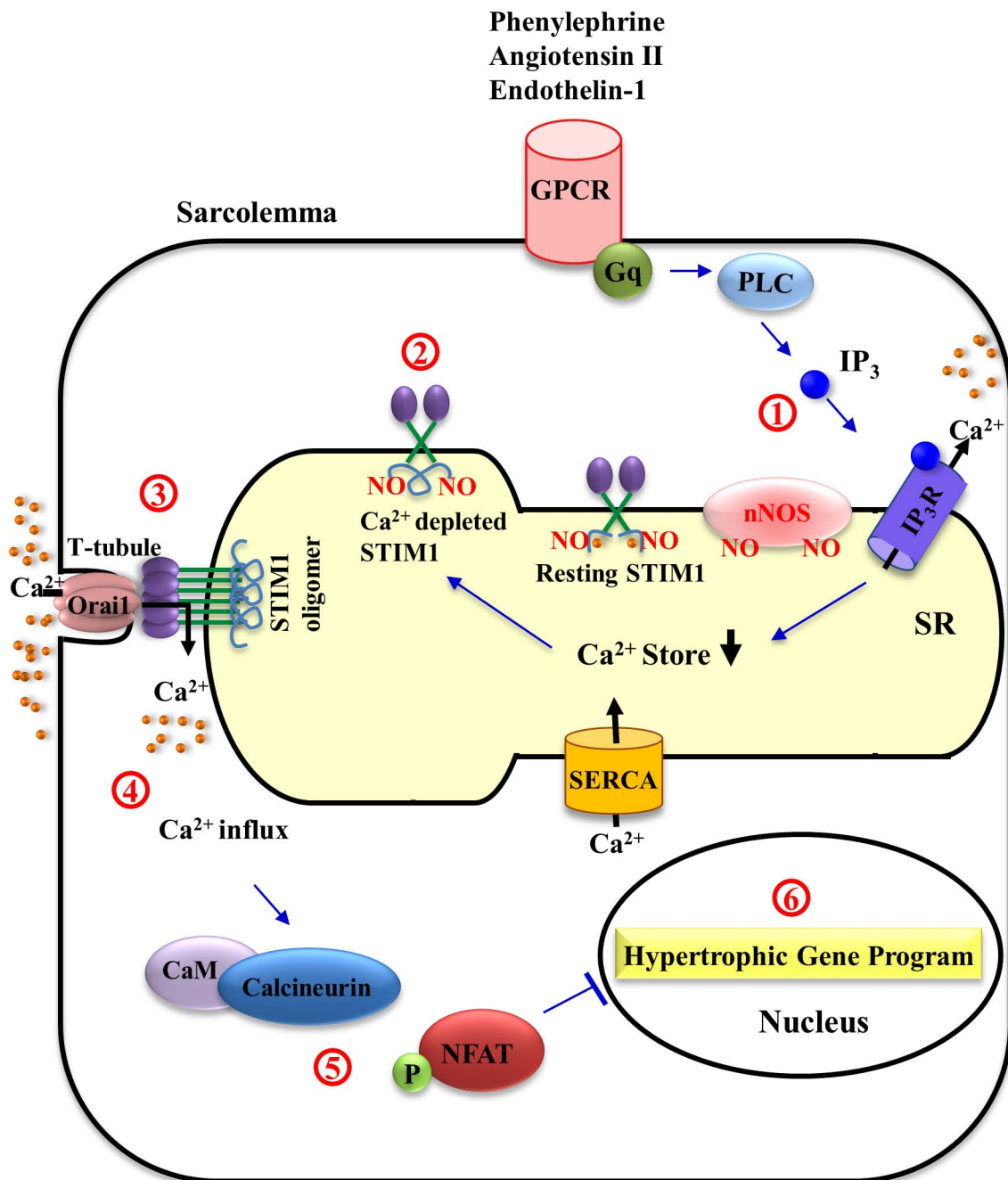


Figure 4.1. Proposed model of S-nitrosylation mediated suppression of STIM1 activity and cardiomyocyte hypertrophy. 1. NO is produced by nNOS and released into the SR lumen. 2. STIM1 is inhibited by S-nitrosylation. 3. Orail activation and CRAC channel formation are attenuated. 4. Lower Ca²⁺ influx. 5. Inhibition of calcineurin-NFAT activation. 6. Inhibition of hypertrophic gene expression.

References

- Ahern, G.P., Hsu, S.F., Klyachko, V.A., and Jackson, M.B. (2000). Induction of persistent sodium current by exogenous and endogenous nitric oxide. *J Biol Chem* 275, 28810-28815.
- Akhter, S.A., Luttrell, L.M., Rockman, H.A., Iaccarino, G., Lefkowitz, R.J., and Koch, W.J. (1998). Targeting the receptor-Gq interface to inhibit in vivo pressure overload myocardial hypertrophy. *Science (New York, NY)* 280, 574-577.
- Albertos, P., Romero-Puertas, M.C., Tatematsu, K., Mateos, I., Sánchez-Vicente, I., Nambara, E., and Lorenzo, O. (2015). S-nitrosylation triggers ABI5 degradation to promote seed germination and seedling growth. *Nat Commun* 6, 8669.
- Allard, M.F., Schonekess, B.O., Henning, S.L., English, D.R., and Lopaschuk, G.D. (1994). Contribution of oxidative metabolism and glycolysis to ATP production in hypertrophied hearts. *Am J Physiol* 267, H742-750.
- Alonso, M.T., Villalobos, C., Chamero, P., Alvarez, J., and Garcia-Sancho, J. (2006). Calcium microdomains in mitochondria and nucleus. *Cell Calcium* 40, 513-525.
- Ambily, A., Kaiser, W.J., Pierro, C., Chamberlain, E.V., Li, Z., Jones, C.I., Kassouf, N., Gibbins, J.M., and Authi, K.S. (2014). The role of plasma membrane STIM1 and Ca(2+) entry in platelet aggregation. STIM1 binds to novel proteins in human platelets. *Cellular Signalling* 26, 502-511.
- Araki, K., and Nagata, K. (2011). Protein folding and quality control in the ER. *Cold Spring Harb Perspect Biol* 3, a007526.
- Arnaiz-Cot, J.J., Damon, B.J., Zhang, X.H., Cleemann, L., Yamaguchi, N., Meissner, G., and Morad, M. (2013). Cardiac calcium signalling pathologies associated with defective calmodulin regulation of type 2 ryanodine receptor. *J Physiol* 591, 4287-4299.
- Ashby, M.C., and Tepikin, A.V. (2001). ER calcium and the functions of intracellular organelles. *Semin Cell Dev Biol* 12, 11-17.
- Baba, Y., Hayashi, K., Fujii, Y., Mizushima, A., Watarai, H., Wakamori, M., Numaga, T., Mori, Y., Iino, M., Hikida, M., *et al.* (2006). Coupling of STIM1 to store-operated Ca²⁺ entry through its constitutive and inducible movement in the endoplasmic reticulum. *Proceedings of the National Academy of Sciences of the United States of America* 103, 16704-16709.
- Barouch, L.A., Cappola, T.P., Harrison, R.W., Crone, J.K., Rodriguez, E.R., Burnett, A.L., and Hare, J.M. (2003). Combined loss of neuronal and endothelial nitric oxide synthase causes premature mortality and age-related hypertrophic cardiac remodeling in mice. *J Mol Cell Cardiol* 35, 637-644.
- Barouch, L.A., Harrison, R.W., Skaf, M.W., Rosas, G.O., Cappola, T.P., Kobeissi, Z.A.,

- Hobai, I.A., Lemmon, C.A., Burnett, A.L., O'Rourke, B., *et al.* (2002). Nitric oxide regulates the heart by spatial confinement of nitric oxide synthase isoforms. *Nature* *416*, 337-339.
- Barr, V.A., Bernot, K.M., Shaffer, M.H., Burkhardt, J.K., and Samelson, L.E. (2009). Formation of STIM and Orai complexes: puncta and distal caps. *Immunol Rev* *231*, 148-159.
- Bartels, C., Xia, T.H., Billeter, M., Guntert, P., and Wuthrich, K. (1995). The program XEASY for computer-supported NMR spectral analysis of biological macromolecules. *J Biomol NMR* *6*, 1-10.
- Bauer, M.C., O'Connell, D., Cahill, D.J., and Linse, S. (2008). Calmodulin binding to the polybasic C-termini of STIM proteins involved in store-operated calcium entry. *Biochemistry* *47*, 6089-6091.
- Berchtold, M.W., Brinkmeier, H., and Müntener, M. (2000). Calcium ion in skeletal muscle: its crucial role for muscle function, plasticity, and disease. *Physiological Reviews* *80*, 1215-1265.
- Berjanskii, M.V., and Wishart, D.S. (2005). A Simple Method To Predict Protein Flexibility Using Secondary Chemical Shifts. *ResearchGate* *127*, 14970-14971.
- Berridge, M.J., Bootman, M.D., and Roderick, H.L. (2003). Calcium signalling: dynamics, homeostasis and remodelling. *Nature Reviews Molecular Cell Biology* *4*, 517-529.
- Bers, D.M. (2002). Cardiac excitation-contraction coupling. *Nature* *415*, 198-205.
- Bocedi, A., Gradoni, L., Menegatti, E., and Ascenzi, P. (2004). Kinetics of parasite cysteine proteinase inactivation by NO-donors. *Biochem Biophys Res Commun* *315*, 710-718.
- Boyman, L., Williams, G.S., Khananshvil, D., Sekler, I., and Lederer, W.J. (2013). NCLX: the mitochondrial sodium calcium exchanger. *J Mol Cell Cardiol* *59*, 205-213.
- Braakman, I., and Hebert, D.N. (2013). Protein folding in the endoplasmic reticulum. *Cold Spring Harb Perspect Biol* *5*, a013201.
- Brandman, O., Liou, J., Park, W.S., and Meyer, T. (2007). STIM2 is a feedback regulator that stabilizes basal cytosolic and endoplasmic reticulum Ca²⁺ levels. *Cell* *131*, 1327-1339.
- Brinckmann, R., Schnurr, K., Heydeck, D., Rosenbach, T., Kolde, G., and Kühn, H. (1998). Membrane translocation of 15-lipoxygenase in hematopoietic cells is calcium-dependent and activates the oxygenase activity of the enzyme. *Blood* *91*, 64-74.
- Broniowska, K.A., Diers, A.R., and Hogg, N. (2013). S-nitrosoglutathione. *Biochim*

Biophys Acta 1830, 3173-3181.

Burger, D.E., Lu, X., Lei, M., Xiang, F.-L., Hammoud, L., Jiang, M., Wang, H., Jones, D.L., Sims, S.M., and Feng, Q. (2009). Neuronal nitric oxide synthase protects against myocardial infarction-induced ventricular arrhythmia and mortality in mice. *Circulation* 120, 1345-1354.

Cahalan, M.D. (2009). STIMulating store-operated Ca(2+) entry. *Nat Cell Biol* 11, 669-677.

Cai, X. (2007). Molecular evolution and functional divergence of the Ca(2+) sensor protein in store-operated Ca(2+) entry: stromal interaction molecule. *PloS One* 2, e609.

Cai, Z., Lu, Q., Ding, Y., Wang, Q., Xiao, L., Song, P., and Zou, M.H. (2015). Endothelial Nitric Oxide Synthase-Derived Nitric Oxide Prevents Dihydrofolate Reductase Degradation via Promoting S-Nitrosylation. *Arterioscler Thromb Vasc Biol* 35, 2366-2373.

Calloway, N., Owens, T., Corwith, K., Rodgers, W., Holowka, D., and Baird, B. (2011). Stimulated association of STIM1 and Orai1 is regulated by the balance of PtdIns(4,5)P₂ between distinct membrane pools. *Journal of Cell Science* 124, 2602-2610.

Cantrell, D.A. (2002). T-cell antigen receptor signal transduction. *Immunology* 105, 369-374.

Carraway, M.S., Piantadosi, C.A., Jenkinson, C.P., and Huang, Y.C. (1998). Differential expression of arginase and iNOS in the lung in sepsis. *Experimental Lung Research* 24, 253-268.

Chang, D.W., Ditsworth, D., Liu, H., Srinivasula, S.M., Alnemri, E.S., and Yang, X. (2003). Oligomerization is a general mechanism for the activation of apoptosis initiator and inflammatory procaspases. *J Biol Chem* 278, 16466-16469.

Chang, K.C., Bayer, J.D., and Trayanova, N.A. (2014). Disrupted calcium release as a mechanism for atrial alternans associated with human atrial fibrillation. *PLoS computational biology* 10, e1004011.

Christe, M.E., and Rodgers, R.L. (1994). Altered glucose and fatty acid oxidation in hearts of the spontaneously hypertensive rat. *J Mol Cell Cardiol* 26, 1371-1375.

Collins, H.E., Zhu-Mauldin, X., Marchase, R.B., and Chatham, J.C. (2013). STIM1/Orai1-mediated SOCE: current perspectives and potential roles in cardiac function and pathology. *American Journal of Physiology Heart and Circulatory Physiology* 305, H446-458.

Covington, E.D., Wu, M.M., and Lewis, R.S. (2010). Essential role for the CRAC activation domain in store-dependent oligomerization of STIM1. *Molecular Biology of the Cell* 21, 1897-1907.

- Cui, X., Song, L., Bai, Y., Wang, Y., Wang, B., and Wang, W. (2017). Stromal interaction molecule 1 (STIM1) regulates growth, cell cycle and apoptosis of human tongue squamous carcinoma cells. *Bioscience Reports*.
- D'Angelo, D.D., Sakata, Y., Lorenz, J.N., Boivin, G.P., Walsh, R.A., Liggett, S.B., and Dorn, G.W. (1997). Transgenic Galphaq overexpression induces cardiac contractile failure in mice. *Proceedings of the National Academy of Sciences of the United States of America* *94*, 8121-8126.
- Darbellay, B., Arnaudeau, S., Ceroni, D., Bader, C.R., Konig, S., and Bernheim, L. (2010). Human muscle economy myoblast differentiation and excitation-contraction coupling use the same molecular partners, STIM1 and STIM2. *The Journal of Biological Chemistry* *285*, 22437-22447.
- Davila-Roman, V.G., Vedala, G., Herrero, P., de las Fuentes, L., Rogers, J.G., Kelly, D.P., and Gropler, R.J. (2002). Altered myocardial fatty acid and glucose metabolism in idiopathic dilated cardiomyopathy. *J Am Coll Cardiol* *40*, 271-277.
- DeHaven, W.I., Smyth, J.T., Boyles, R.R., and Putney, J.W. (2007). Calcium inhibition and calcium potentiation of Orai1, Orai2, and Orai3 calcium release-activated calcium channels. *The Journal of Biological Chemistry* *282*, 17548-17556.
- Delaglio, F., Grzesiek, S., Vuister, G.W., Zhu, G., Pfeifer, J., and Bax, A. (1995). NMRPipe: a multidimensional spectral processing system based on UNIX pipes. *J Biomol NMR* *6*, 277-293.
- Demuro, A., Penna, A., Safrina, O., Yeromin, A.V., Amcheslavsky, A., Cahalan, M.D., and Parker, I. (2011). Subunit stoichiometry of human Orai1 and Orai3 channels in closed and open states. *Proceedings of the National Academy of Sciences of the United States of America* *108*, 17832-17837.
- Derler, I., Fahrner, M., Muik, M., Lackner, B., Schindl, R., Groschner, K., and Romanin, C. (2009). A Ca²⁺(+)release-activated Ca²⁺(+) (CRAC) modulatory domain (CMD) within STIM1 mediates fast Ca²⁺(+)-dependent inactivation of ORAI1 channels. *The Journal of Biological Chemistry* *284*, 24933-24938.
- Dobrev, D., and Wehrens, X.H. (2014). Role of RyR2 phosphorylation in heart failure and arrhythmias: Controversies around ryanodine receptor phosphorylation in cardiac disease. *Circ Res* *114*, 1311-1319; discussion 1319.
- Dráber, P., and Dráberová, L. (2005). Lifting the fog in store-operated Ca²⁺ entry. *Trends in Immunology* *26*, 621-624.
- Eichmann, C., Tzitzilonis, C., Nakamura, T., Kwiatkowski, W., Maslennikov, I., Choe, S., Lipton, S.A., and Riek, R. (2016). S-Nitrosylation Induces Structural and Dynamical Changes in a Rhodanese Family Protein. *J Mol Biol* *428*, 3737-3751.
- Erickson, J.R., Nichols, C.B., Uchinoumi, H., Stein, M.L., Bossuyt, J., and Bers, D.M.

(2015). S-Nitrosylation Induces Both Autonomous Activation and Inhibition of Calcium/Calmodulin-dependent Protein Kinase II delta. *J Biol Chem* *290*, 25646-25656.

Esposito, G., Prasad, S.V., Rapacciuolo, A., Mao, L., Koch, W.J., and Rockman, H.A. (2001). Cardiac overexpression of a G(q) inhibitor blocks induction of extracellular signal-regulated kinase and c-Jun NH(2)-terminal kinase activity in in vivo pressure overload. *Circulation* *103*, 1453-1458.

Fagard, R.H. (1997). Impact of different sports and training on cardiac structure and function. *Cardiology Clinics* *15*, 397-412.

Farrow, N.A., Muhandiram, R., Singer, A.U., Pascal, S.M., Kay, C.M., Gish, G., Shoelson, S.E., Pawson, T., Forman-Kay, J.D., and Kay, L.E. (1994). Backbone dynamics of a free and phosphopeptide-complexed Src homology 2 domain studied by ¹⁵N NMR relaxation. *Biochemistry* *33*, 5984-6003.

Feng, J.H., Jing, F.B., Fang, H., Gu, L.C., and Xu, W.F. (2011). Expression, purification, and S-nitrosylation of recombinant histone deacetylase 8 in *Escherichia coli*. *Biosci Trends* *5*, 17-22.

Feng, Q., Lu, X., Jones, D.L., Shen, J., and Arnold, J.M. (2001). Increased inducible nitric oxide synthase expression contributes to myocardial dysfunction and higher mortality after myocardial infarction in mice. *Circulation* *104*, 700-704.

Feng, Q., Song, W., Lu, X., Hamilton, J.A., Lei, M., Peng, T., and Yee, S.P. (2002). Development of heart failure and congenital septal defects in mice lacking endothelial nitric oxide synthase. *Circulation* *106*, 873-879.

Ferrantini, C., Coppini, R., Scellini, B., Ferrara, C., Pioner, J.M., Mazzoni, L., Priori, S., Cerbai, E., Tesi, C., and Poggesi, C. (2016). R4496C RyR2 mutation impairs atrial and ventricular contractility. *J Gen Physiol* *147*, 39-52.

Feske, S. (2007). Calcium signalling in lymphocyte activation and disease. *Nature Reviews Immunology* *7*, 690-702.

Feske, S. (2009). ORAI1 and STIM1 deficiency in human and mice: roles of store-operated Ca²⁺ entry in the immune system and beyond. *Immunol Rev* *231*, 189-209.

Feske, S., Gwack, Y., Prakriya, M., Srikanth, S., Puppel, S.-H., Tanasa, B., Hogan, P.G., Lewis, R.S., Daly, M., and Rao, A. (2006). A mutation in Orail causes immune deficiency by abrogating CRAC channel function. *Nature* *441*, 179-185.

Flaugh, S.L., and Lumb, K.J. (2001). Effects of macromolecular crowding on the intrinsically disordered proteins c-Fos and p27(Kip1). *Biomacromolecules* *2*, 538-540.

Forrester, M.T., Foster, M.W., Benhar, M., and Stamler, J.S. (2009). Detection of protein S-nitrosylation with the biotin-switch technique. *Free Radic Biol Med* *46*, 119-126.

- Forstermann, U., Closs, E.I., Pollock, J.S., Nakane, M., Schwarz, P., Gath, I., and Kleinert, H. (1994). Nitric oxide synthase isozymes. Characterization, purification, molecular cloning, and functions. *Hypertension* 23, 1121-1131.
- Freichel, M., Almering, J., and Tsvilovskyy, V. (2012). The Role of TRP Proteins in Mast Cells. *Front Immunol* 3, 150.
- Frischauf, I., Muik, M., Derler, I., Bergsmann, J., Fahrner, M., Schindl, R., Groschner, K., and Romanin, C. (2009). Molecular determinants of the coupling between STIM1 and Orai channels: differential activation of Orai1-3 channels by a STIM1 coiled-coil mutant. *The Journal of Biological Chemistry* 284, 21696-21706.
- Gaudin, C., Ishikawa, Y., Wight, D.C., Mahdavi, V., Nadal-Ginard, B., Wagner, T.E., Vatner, D.E., and Homcy, C.J. (1995). Overexpression of Gs alpha protein in the hearts of transgenic mice. *The Journal of Clinical Investigation* 95, 1676-1683.
- Gertz, E.W., Wisneski, J.A., Stanley, W.C., and Neese, R.A. (1988). Myocardial substrate utilization during exercise in humans. Dual carbon-labeled carbohydrate isotope experiments. *J Clin Invest* 82, 2017-2025.
- Giorgi, C., Baldassari, F., Bononi, A., Bonora, M., De Marchi, E., Marchi, S., Missiroli, S., Patergnani, S., Rimessi, A., Suski, J.M., *et al.* (2012). Mitochondrial Ca(2+) and apoptosis. *Cell Calcium* 52, 36-43.
- Gonzalez, D.R., Beigi, F., Treuer, A.V., and Hare, J.M. (2007). Deficient ryanodine receptor S-nitrosylation increases sarcoplasmic reticulum calcium leak and arrhythmogenesis in cardiomyocytes. *Proc Natl Acad Sci U S A* 104, 20612-20617.
- Gould, N., Doulias, P.-T., Tenopoulou, M., Raju, K., and Ischiropoulos, H. (2013). Regulation of protein function and signaling by reversible cysteine S-nitrosylation. *The Journal of Biological Chemistry* 288, 26473-26479.
- Gruszczynska-Biegala, J., Pomorski, P., Wisniewska, M.B., and Kuznicki, J. (2011). Differential roles for STIM1 and STIM2 in store-operated calcium entry in rat neurons. *PloS One* 6, e19285.
- Grzesiek, S., and Bax, A. (1993). Amino acid type determination in the sequential assignment procedure of uniformly ¹³C/¹⁵N-enriched proteins. *J Biomol NMR* 3, 185-204.
- Gui, L., Zhu, J.H., Lu, X.R., Sims, S.M., Lu, W.Y., Stathopoulos, P.B., and Feng, Q.P. (2017). S-Nitrosylation of stromal interaction molecule-1 by neuronal nitric oxide synthase inhibits store-operated calcium entry. *Cell Rep*.
- Guo, C.J., Atochina-Vasserman, E.N., Abramova, E., Foley, J.P., Zaman, A., Crouch, E., Beers, M.F., Savani, R.C., and Gow, A.J. (2008). S-nitrosylation of surfactant protein-D controls inflammatory function. *PLoS Biol* 6, e266.

Hafsa, N.E., Arndt, D., and Wishart, D.S. (2015). CSI 3.0: a web server for identifying secondary and super-secondary structure in proteins using NMR chemical shifts. *Nucleic Acids Research* *43*, W370-W377.

Hakamata, Y., Nakai, J., Takeshima, H., and Imoto, K. (1992). Primary structure and distribution of a novel ryanodine receptor/calcium release channel from rabbit brain. *FEBS Lett* *312*, 229-235.

Haldar, S.M., and Stamler, J.S. (2013). S-nitrosylation: integrator of cardiovascular performance and oxygen delivery. *J Clin Invest* *123*, 101-110.

Hao, G., Xie, L., and Gross, S.S. (2004). Argininosuccinate synthetase is reversibly inactivated by S-nitrosylation in vitro and in vivo. *J Biol Chem* *279*, 36192-36200.

Hawe, A., Sutter, M., and Jiskoot, W. (2008). Extrinsic fluorescent dyes as tools for protein characterization. *Pharm Res* *25*, 1487-1499.

Hawkins, B.J., Irrinki, K.M., Mallilankaraman, K., Lien, Y.-C., Wang, Y., Bhanumathy, C.D., Subbiah, R., Ritchie, M.F., Soboloff, J., Baba, Y., *et al.* (2010). S-glutathionylation activates STIM1 and alters mitochondrial homeostasis. *The Journal of Cell Biology* *190*, 391-405.

Hein, L., Stevens, M.E., Barsh, G.S., Pratt, R.E., Kobilka, B.K., and Dzau, V.J. (1997). Overexpression of angiotensin AT1 receptor transgene in the mouse myocardium produces a lethal phenotype associated with myocyte hyperplasia and heart block. *Proceedings of the National Academy of Sciences of the United States of America* *94*, 6391-6396.

Hess, D.T., and Stamler, J.S. (2012). Regulation by S-nitrosylation of protein post-translational modification. *J Biol Chem* *287*, 4411-4418.

Hofer, A.M., and Brown, E.M. (2003). Extracellular calcium sensing and signalling. *Nat Rev Mol Cell Biol* *4*, 530-538.

Hogan, P.G., Chen, L., Nardone, J., and Rao, A. (2003). Transcriptional regulation by calcium, calcineurin, and NFAT. *Genes & Development* *17*, 2205-2232.

Holm, J., Lawaetz, A.J., and Hansen, S.I. (2012). Ligand binding induces a sharp decrease in hydrophobicity of folate binding protein assessed by 1-anilinonaphthalene-8-sulphonate which suppresses self-association of the hydrophobic apo-protein. *Biochem Biophys Res Commun* *425*, 19-24.

Hooper, R., Samakai, E., Kedra, J., and Soboloff, J. (2013). Multifaceted roles of STIM proteins. *Pflugers Archiv: European Journal of Physiology* *465*, 1383-1396.

Hou, X., Pedi, L., Diver, M.M., and Long, S.B. (2012). Crystal structure of the calcium release-activated calcium channel Orai. *Science (New York, NY)* *338*, 1308-1313.

Hu, H., Chiamvimonvat, N., Yamagishi, T., and Marban, E. (1997). Direct inhibition of expressed cardiac L-type Ca²⁺ channels by S-nitrosothiol nitric oxide donors. *Circ Res* 81, 742-752.

Hulot, J.-S., Fauconnier, J., Ramanujam, D., Chaanine, A., Aubart, F., Sassi, Y., Merkle, S., Cazorla, O., Ouillé, A., Dupuis, M., *et al.* (2011). Critical role for stromal interaction molecule 1 in cardiac hypertrophy. *Circulation* 124, 796-805.

Hund, T.J., Ziman, A.P., Lederer, W.J., and Mohler, P.J. (2008). The cardiac IP3 receptor: uncovering the role of "the other" calcium-release channel. *J Mol Cell Cardiol* 45, 159-161.

Hunton, D.L., Lucchesi, P.A., Pang, Y., Cheng, X., Dell'Italia, L.J., and Marchase, R.B. (2002). Capacitative calcium entry contributes to nuclear factor of activated T-cells nuclear translocation and hypertrophy in cardiomyocytes. *The Journal of Biological Chemistry* 277, 14266-14273.

Irie, T., Sips, P.Y., Kai, S., Kida, K., Ikeda, K., Hirai, S., Moazzami, K., Jiramongkolchai, P., Bloch, D.B., Doulias, P.-T., *et al.* (2015). S-Nitrosylation of Calcium-Handling Proteins in Cardiac Adrenergic Signaling and Hypertrophy. *Circulation Research* 117, 793-803.

Iwase, M., Bishop, S.P., Uechi, M., Vatner, D.E., Shannon, R.P., Kudej, R.K., Wight, D.C., Wagner, T.E., Ishikawa, Y., Homcy, C.J., *et al.* (1996). Adverse effects of chronic endogenous sympathetic drive induced by cardiac GS alpha overexpression. *Circulation Research* 78, 517-524.

Ji, Y., Akerboom, T.P., Sies, H., and Thomas, J.A. (1999). S-nitrosylation and S-glutathiolation of protein sulfhydryls by S-nitroso glutathione. *Archives of Biochemistry and Biophysics* 362, 67-78.

Jia, J., Arif, A., Stuehr, D.J., Hazen, S.L., and Fox, P.L. (2012). Protection of Extraribosomal RPL13a by GAPDH and Dysregulation by S-Nitrosylation. *Molecular cell* 47, 656-663.

Jiang, D., Xiao, B., Yang, D., Wang, R., Choi, P., Zhang, L., Cheng, H., and Chen, S.R. (2004). RyR2 mutations linked to ventricular tachycardia and sudden death reduce the threshold for store-overload-induced Ca²⁺ release (SOICR). *Proc Natl Acad Sci U S A* 101, 13062-13067.

Kaleka, K.S., Petersen, A.N., Florence, M.A., and Gerges, N.Z. (2012). Pull-down of calmodulin-binding proteins. *Journal of Visualized Experiments: JoVE*.

Kanai, A.J., Pearce, L.L., Clemens, P.R., Birder, L.A., VanBibber, M.M., Choi, S.Y., de Groat, W.C., and Peterson, J. (2001). Identification of a neuronal nitric oxide synthase in isolated cardiac mitochondria using electrochemical detection. *Proc Natl Acad Sci U S A* 98, 14126-14131.

- Kar, R., Ikeno, Y., Masters, B., and Roman, L. (2014). Oxidative stress reduces the expression of neuronal NOS in cardiac tissue and cell (545.3). *The FASEB Journal* 28, 545.543.
- Kawasaki, T., Lange, I., and Feske, S. (2009). A minimal regulatory domain in the C terminus of STIM1 binds to and activates ORAI1 CRAC channels. *Biochemical and Biophysical Research Communications* 385, 49-54.
- Kay, L.E., Keifer, P., and Saarinen, T. (1992). Pure absorption gradient enhanced heteronuclear single quantum correlation spectroscopy with improved sensitivity. *J Am Chem Soc* 114, 10663-10665.
- Kelly, R.A., Balligand, J.-L., and Smith, T.W. (1996). Nitric Oxide and Cardiac Function. *Circulation Research* 79, 363-380.
- Knowlton, K.U., Michel, M.C., Itani, M., Shubeita, H.E., Ishihara, K., Brown, J.H., and Chien, K.R. (1993). The alpha 1A-adrenergic receptor subtype mediates biochemical, molecular, and morphologic features of cultured myocardial cell hypertrophy. *The Journal of Biological Chemistry* 268, 15374-15380.
- Kohr, M.J., Evangelista, A.M., Ferlito, M., Steenbergen, C., and Murphy, E. (2014). S-nitrosylation of TRIM72 at cysteine 144 is critical for protection against oxidation-induced protein degradation and cell death. *J Mol Cell Cardiol* 69, 67-74.
- Kolwicz, S.C., Jr., and Tian, R. (2011). Glucose metabolism and cardiac hypertrophy. *Cardiovasc Res* 90, 194-201.
- Korzeniowski, M.K., Popovic, M.A., Szentpetery, Z., Varnai, P., Stojilkovic, S.S., and Balla, T. (2009). Dependence of STIM1/Orai1-mediated calcium entry on plasma membrane phosphoinositides. *The Journal of Biological Chemistry* 284, 21027-21035.
- Kumar, R., Jangir, D.K., Verma, G., Shekhar, S., Hanpude, P., Kumar, S., Kumari, R., Singh, N., Sarovar Bhavesh, N., Ranjan Jana, N., *et al.* (2017). S-nitrosylation of UCHL1 induces its structural instability and promotes alpha-synuclein aggregation. *Sci Rep* 7, 44558.
- Le Gall, S., Neuhof, A., and Rapoport, T. (2004). The endoplasmic reticulum membrane is permeable to small molecules. *Mol Biol Cell* 15, 447-455.
- Lee, K.P., Yuan, J.P., Zeng, W., So, I., Worley, P.F., and Muallem, S. (2009). Molecular determinants of fast Ca²⁺-dependent inactivation and gating of the Orai channels. *Proceedings of the National Academy of Sciences of the United States of America* 106, 14687-14692.
- Levy, D., Anderson, K.M., Savage, D.D., Kannel, W.B., Christiansen, J.C., and Castelli, W.P. (1988). Echocardiographically detected left ventricular hypertrophy: prevalence and risk factors. The Framingham Heart Study. *Annals of Internal Medicine* 108, 7-13.

Li, F., Sonveaux, P., Rabbani, Z.N., Liu, S., Yan, B., Huang, Q., Vujaskovic, Z., Dewhirst, M.W., and Li, C.Y. (2007). Regulation of HIF-1 α stability through S-nitrosylation. *Mol Cell* 26, 63-74.

Li, Y., Lubchenko, V., and Vekilov, P.G. (2011). The use of dynamic light scattering and brownian microscopy to characterize protein aggregation. *Rev Sci Instrum* 82, 053106.

Liou, J., Fivaz, M., Inoue, T., and Meyer, T. (2007). Live-cell imaging reveals sequential oligomerization and local plasma membrane targeting of stromal interaction molecule 1 after Ca²⁺ store depletion. *Proc Natl Acad Sci U S A* 104, 9301-9306.

Liou, J., Kim, M.L., Heo, W.D., Jones, J.T., Myers, J.W., Ferrell, J.E., and Meyer, T. (2005). STIM is a Ca²⁺ sensor essential for Ca²⁺-store-depletion-triggered Ca²⁺ influx. *Current biology: CB* 15, 1235-1241.

Lipskaia, L., Chemaly, E.R., Hadri, L., Lompre, A.M., and Hajjar, R.J. (2010). Sarcoplasmic reticulum Ca(2+) ATPase as a therapeutic target for heart failure. *Expert Opin Biol Ther* 10, 29-41.

Lis, A., Peinelt, C., Beck, A., Parvez, S., Monteilh-Zoller, M., Fleig, A., and Penner, R. (2007). CRACM1, CRACM2, and CRACM3 are store-operated Ca²⁺ channels with distinct functional properties. *Current biology: CB* 17, 794-800.

Liu, L., Enright, E., Sun, P., Tsai, S.Y., Mehta, P., Beckman, D.L., and Terrian, D.M. (2002). Inactivation of annexin II tetramer by S-nitrosoglutathione. *Eur J Biochem* 269, 4277-4286.

Liu, L., Yan, Y., Zeng, M., Zhang, J., Hanes, M.A., Ahearn, G., McMahon, T.J., Dickfeld, T., Marshall, H.E., Que, L.G., *et al.* (2004). Essential Roles of S-Nitrosothiols in Vascular Homeostasis and Endotoxic Shock. *Cell* 116, 617-628.

Liu, Y., Lu, X., Xiang, F.-L., Lu, M., and Feng, Q. (2013). Nitric oxide synthase-3 promotes embryonic development of atrioventricular valves. *PloS One* 8, e77611.

Liu, Y., Lu, X., Xiang, F.-L., Poelmann, R.E., Gittenberger-de Groot, A.C., Robbins, J., and Feng, Q. (2014). Nitric oxide synthase-3 deficiency results in hypoplastic coronary arteries and postnatal myocardial infarction. *European Heart Journal* 35, 920-931.

Liu, Y.H., Carretero, O.A., Cingolani, O.H., Liao, T.D., Sun, Y., Xu, J., Li, L.Y., Pagano, P.J., Yang, J.J., and Yang, X.P. (2005). Role of inducible nitric oxide synthase in cardiac function and remodeling in mice with heart failure due to myocardial infarction. *Am J Physiol Heart Circ Physiol* 289, H2616-2623.

Loyer, X., Gomez, A.M., Milliez, P., Fernandez-Velasco, M., Vangheluwe, P., Vinet, L., Charue, D., Vaudin, E., Zhang, W., Sainte-Marie, Y., *et al.* (2008). Cardiomyocyte overexpression of neuronal nitric oxide synthase delays transition toward heart failure in response to pressure overload by preserving calcium cycling. *Circulation* 117, 3187-3198.

- Luik, R.M., Wang, B., Prakriya, M., Wu, M.M., and Lewis, R.S. (2008). Oligomerization of STIM1 couples ER calcium depletion to CRAC channel activation. *Nature* *454*, 538-542.
- Luik, R.M., Wu, M.M., Buchanan, J., and Lewis, R.S. (2006). The elementary unit of store-operated Ca^{2+} entry: local activation of CRAC channels by STIM1 at ER-plasma membrane junctions. *J Cell Biol* *174*, 815-825.
- Luo, X., Hojayeve, B., Jiang, N., Wang, Z.V., Tandan, S., Rakalin, A., Rothermel, B.A., Gillette, T.G., and Hill, J.A. (2012). STIM1-dependent store-operated Ca^{2+} entry is required for pathological cardiac hypertrophy. *Journal of Molecular and Cellular Cardiology* *52*, 136-147.
- Luttrell, L.M. (2006). Transmembrane signaling by G protein-coupled receptors. *Methods Mol Biol* *332*, 3-49.
- Maarsingh, H., Leusink, J., Bos, I.S.T., Zaagsma, J., and Meurs, H. (2006). Arginase strongly impairs neuronal nitric oxide-mediated airway smooth muscle relaxation in allergic asthma. *Respiratory Research* *7*, 6.
- Marshall, C.B., Nishikawa, T., Osawa, M., Stathopoulos, P.B., and Ikura, M. (2015). Calmodulin and STIM proteins: Two major calcium sensors in the cytoplasm and endoplasmic reticulum. *Biochem Biophys Res Commun* *460*, 5-21.
- Maruyama, Y., Ogura, T., Mio, K., Kato, K., Kaneko, T., Kiyonaka, S., Mori, Y., and Sato, C. (2009). Tetrameric Orai1 is a teardrop-shaped molecule with a long, tapered cytoplasmic domain. *J Biol Chem* *284*, 13676-13685.
- McHugh, M.L. (2011). Multiple comparison analysis testing in ANOVA. *Biochem Med (Zagreb)* *21*, 203-209.
- Mercer, J.C., Dehaven, W.I., Smyth, J.T., Wedel, B., Boyles, R.R., Bird, G.S., and Putney, J.W. (2006). Large store-operated calcium selective currents due to co-expression of Orai1 or Orai2 with the intracellular calcium sensor, Stim1. *The Journal of Biological Chemistry* *281*, 24979-24990.
- Mickelson, J.R., and Louis, C.F. (1996). Malignant hyperthermia: excitation-contraction coupling, Ca^{2+} release channel, and cell Ca^{2+} regulation defects. *Physiological Reviews* *76*, 537-592.
- Mignen, O., Thompson, J.L., and Shuttleworth, T.J. (2008). Orai1 subunit stoichiometry of the mammalian CRAC channel pore. *The Journal of Physiology* *586*, 419-425.
- Molnar, T., Barabas, P., Birnbaumer, L., Punzo, C., Kefalov, V., and Krizaj, D. (2012). Store-operated channels regulate intracellular calcium in mammalian rods. *J Physiol* *590*, 3465-3481.
- Morris, C.R., Gladwin, M.T., and Kato, G.J. (2008). Nitric oxide and arginine

dysregulation: a novel pathway to pulmonary hypertension in hemolytic disorders. *Curr Mol Med* 8, 620-632.

Muik, M., Fahrner, M., Derler, I., Schindl, R., Bergsmann, J., Frischauf, I., Groschner, K., and Romanin, C. (2009). A Cytosolic Homomerization and a Modulatory Domain within STIM1 C Terminus Determine Coupling to ORAI1 Channels. *The Journal of Biological Chemistry* 284, 8421-8426.

Muik, M., Frischauf, I., Derler, I., Fahrner, M., Bergsmann, J., Eder, P., Schindl, R., Hesch, C., Polzinger, B., Fritsch, R., *et al.* (2008). Dynamic coupling of the putative coiled-coil domain of ORAI1 with STIM1 mediates ORAI1 channel activation. *The Journal of Biological Chemistry* 283, 8014-8022.

Muik, M., Schindl, R., Fahrner, M., and Romanin, C. (2012). Ca(2+) release-activated Ca(2+) (CRAC) current, structure, and function. *Cell Mol Life Sci* 69, 4163-4176.

Mukherjee, S., and Brooks, W.H. (2014). Stromal interaction molecules as important therapeutic targets in diseases with dysregulated calcium flux. *Biochimica Et Biophysica Acta* 1843, 2307-2314.

Mullins, F.M., Park, C.Y., Dolmetsch, R.E., and Lewis, R.S. (2009). STIM1 and calmodulin interact with Orail to induce Ca²⁺-dependent inactivation of CRAC channels. *Proceedings of the National Academy of Sciences of the United States of America* 106, 15495-15500.

Mungai, P.T., Waypa, G.B., Jairaman, A., Prakriya, M., Dokic, D., Ball, M.K., and Schumacker, P.T. (2011). Hypoxia triggers AMPK activation through reactive oxygen species-mediated activation of calcium release-activated calcium channels. *Molecular and Cellular Biology* 31, 3531-3545.

Musaro, A., McCullagh, K.J., Naya, F.J., Olson, E.N., and Rosenthal, N. (1999). IGF-1 induces skeletal myocyte hypertrophy through calcineurin in association with GATA-2 and NF-ATc1. *Nature* 400, 581-585.

Nathan, C.F., and Hibbs, J.B., Jr. (1991). Role of nitric oxide synthesis in macrophage antimicrobial activity. *Curr Opin Immunol* 3, 65-70.

Neubauer, S. (2007). The failing heart--an engine out of fuel. *N Engl J Med* 356, 1140-1151.

Nicholls, D.G. (2005). Mitochondria and calcium signaling. *Cell Calcium* 38, 311-317.

Nyegaard, M., Overgaard, M.T., Sondergaard, M.T., Vranas, M., Behr, E.R., Hildebrandt, L.L., Lund, J., Hedley, P.L., Camm, A.J., Wettrell, G., *et al.* (2012). Mutations in calmodulin cause ventricular tachycardia and sudden cardiac death. *Am J Hum Genet* 91, 703-712.

Okamoto, S., Nakamura, T., Cieplak, P., Chan, S.F., Kalashnikova, E., Liao, L., Saleem,

- S., Han, X., Clemente, A., Nutter, A., *et al.* (2014). S-nitrosylation-mediated redox transcriptional switch modulates neurogenesis and neuronal cell death. *Cell Rep* 8, 217-228.
- Orrenius, S., Gogvadze, V., and Zhivotovsky, B. (2015). Calcium and mitochondria in the regulation of cell death. *Biochemical and Biophysical Research Communications* 460, 72-81.
- Pace, C.N. (1986). Determination and analysis of urea and guanidine hydrochloride denaturation curves. *Methods Enzymol* 131, 266-280.
- Parekh, A.B., and Penner, R. (1997). Store depletion and calcium influx. *Physiological Reviews* 77, 901-930.
- Parekh, A.B., and Putney, J.W. (2005). Store-operated calcium channels. *Physiological Reviews* 85, 757-810.
- Park, C.Y., Hoover, P.J., Mullins, F.M., Bachhawat, P., Covington, E.D., Raunser, S., Walz, T., Garcia, K.C., Dolmetsch, R.E., and Lewis, R.S. (2009). STIM1 clusters and activates CRAC channels via direct binding of a cytosolic domain to Orai1. *Cell* 136, 876-890.
- Park, W.J., and Oh, J.G. (2013). SERCA2a: a prime target for modulation of cardiac contractility during heart failure. *BMB Rep* 46, 237-243.
- Paternostro, G., Pagano, D., Gneccchi-Ruscione, T., Bonser, R.S., and Camici, P.G. (1999). Insulin resistance in patients with cardiac hypertrophy. *Cardiovasc Res* 42, 246-253.
- Penna, A., Demuro, A., Yeromin, A.V., Zhang, S.L., Safrina, O., Parker, I., and Cahalan, M.D. (2008). The CRAC channel consists of a tetramer formed by Stim-induced dimerization of Orai dimers. *Nature* 456, 116-120.
- Perez-Mato, I., Castro, C., Ruiz, F.A., Corrales, F.J., and Mato, J.M. (1999). Methionine adenosyltransferase S-nitrosylation is regulated by the basic and acidic amino acids surrounding the target thiol. *J Biol Chem* 274, 17075-17079.
- Periasamy, M., and Janssen, P.M. (2008). Molecular basis of diastolic dysfunction. *Heart Fail Clin* 4, 13-21.
- Pinton, P., Giorgi, C., Siviero, R., Zecchini, E., and Rizzuto, R. (2008). Calcium and apoptosis: ER-mitochondria Ca²⁺ transfer in the control of apoptosis. *Oncogene* 27, 6407-6418.
- Pinton, P., Pozzan, T., and Rizzuto, R. (1998). The Golgi apparatus is an inositol 1,4,5-trisphosphate-sensitive Ca²⁺ store, with functional properties distinct from those of the endoplasmic reticulum. *The EMBO Journal* 17, 5298-5308.
- Pluim, B.M., Zwinderman, A.H., Laarse, A.v.d., and Wall, E.E.v.d. (2000). The Athlete's

Heart. *Circulation* *101*, 336-344.

Prakriya, M., Feske, S., Gwack, Y., Srikanth, S., Rao, A., and Hogan, P.G. (2006). Orail is an essential pore subunit of the CRAC channel. *Nature* *443*, 230-233.

Prins, D., Groenendyk, J., Touret, N., and Michalak, M. (2011). Modulation of STIM1 and capacitative Ca²⁺ entry by the endoplasmic reticulum luminal oxidoreductase ERp57. *EMBO Rep* *12*, 1182-1188.

Putney, J.W. (1986). A model for receptor-regulated calcium entry. *Cell Calcium* *7*, 1-12.

Qu, J., Liu, G.H., Wu, K., Han, P., Wang, P., Li, J., Zhang, X., and Chen, C. (2007). Nitric oxide destabilizes Pias3 and regulates sumoylation. *PLoS One* *2*, e1085.

Randriamampita, C., and Trautmann, A. (2004). Ca²⁺ signals and T lymphocytes; "New mechanisms and functions in Ca²⁺ signalling". *Biology of the Cell* *96*, 69-78.

Razzell, W., Evans, I.R., Martin, P., and Wood, W. (2013). Calcium flashes orchestrate the wound inflammatory response through DUOX activation and hydrogen peroxide release. *Curr Biol* *23*, 424-429.

Redondo, P.C., Harper, M.T., Rosado, J.A., and Sage, S.O. (2006). A role for cofilin in the activation of store-operated calcium entry by de novo conformational coupling in human platelets. *Blood* *107*, 973-979.

Renganathan, M., Cummins, T.R., and Waxman, S.G. (2002). Nitric oxide blocks fast, slow, and persistent Na⁺ channels in C-type DRG neurons by S-nitrosylation. *J Neurophysiol* *87*, 761-775.

Ringer, S. (1883). A further Contribution regarding the influence of the different Constituents of the Blood on the Contraction of the Heart. *The Journal of Physiology* *4*, 29-42.23.

Roberts-Thomson, S.J., Peters, A.A., Grice, D.M., and Monteith, G.R. (2010). ORAI-mediated calcium entry: mechanism and roles, diseases and pharmacology. *Pharmacology & Therapeutics* *127*, 121-130.

Roos, J., DiGregorio, P.J., Yeromin, A.V., Ohlsen, K., Lioudyno, M., Zhang, S., Safrina, O., Kozak, J.A., Wagner, S.L., Cahalan, M.D., *et al.* (2005). STIM1, an essential and conserved component of store-operated Ca²⁺ channel function. *The Journal of Cell Biology* *169*, 435-445.

Salazar, N.C., Chen, J., and Rockman, H.A. (2007). Cardiac GPCRs: GPCR Signaling in Healthy and Failing Hearts. *Biochimica et biophysica acta* *1768*, 1006-1018.

Sandoo, A., van Zanten, J.J., Metsios, G.S., Carroll, D., and Kitas, G.D. (2010). The endothelium and its role in regulating vascular tone. *Open Cardiovasc Med J* *4*, 302-312.

Santella, L., Lim, D., and Moccia, F. (2004). Calcium and fertilization: the beginning of life. *Trends Biochem Sci* 29, 400-408.

Schlessinger, J. (2000). Cell Signaling by Receptor Tyrosine Kinases. *Cell* 103, 211-225.

Scholz, R., Suter, M., Weimann, T., Polge, C., Konarev, P.V., Thali, R.F., Tuerk, R.D., Viollet, B., Wallimann, T., Schlattner, U., *et al.* (2009). Homo-oligomerization and activation of AMP-activated protein kinase are mediated by the kinase domain alpha-helix. *J Biol Chem* 284, 27425-27437.

Sears, C.E., Bryant, S.M., Ashley, E.A., Lygate, C.A., Rakovic, S., Wallis, H.L., Neubauer, S., Terrar, D.A., and Casadei, B. (2003). Cardiac Neuronal Nitric Oxide Synthase Isoform Regulates Myocardial Contraction and Calcium Handling. *Circulation Research* 92, e52-e59.

Seidman, J.G., and Seidman, C. (2001). The genetic basis for cardiomyopathy: from mutation identification to mechanistic paradigms. *Cell* 104, 557-567.

Shimizu, I., and Minamino, T. (2016). Physiological and pathological cardiac hypertrophy. *J Mol Cell Cardiol* 97, 245-262.

Singh, S.K., Thirumalai, A., Hammond, D.J., Jr., Pangburn, M.K., Mishra, V.K., Johnson, D.A., Rusinol, A.E., and Agrawal, A. (2012). Exposing a hidden functional site of C-reactive protein by site-directed mutagenesis. *J Biol Chem* 287, 3550-3558.

Soboloff, J., Spassova, M.A., Tang, X.D., Hewavitharana, T., Xu, W., and Gill, D.L. (2006). Orai1 and STIM reconstitute store-operated calcium channel function. *J Biol Chem* 281, 20661-20665.

Song, X., Kusakari, Y., Xiao, C.-Y., Kinsella, S.D., Rosenberg, M.A., Scherrer-Crosbie, M., Hara, K., Rosenzweig, A., and Matsui, T. (2010). mTOR attenuates the inflammatory response in cardiomyocytes and prevents cardiac dysfunction in pathological hypertrophy. *American Journal of Physiology Cell Physiology* 299, C1256-1266.

Soonpaa, M.H., Kim, K.K., Pajak, L., Franklin, M., and Field, L.J. (1996). Cardiomyocyte DNA synthesis and binucleation during murine development. *The American Journal of Physiology* 271, H2183-2189.

Spassova, M.A., Soboloff, J., He, L.-P., Xu, W., Dziadek, M.A., and Gill, D.L. (2006). STIM1 has a plasma membrane role in the activation of store-operated Ca(2+) channels. *Proceedings of the National Academy of Sciences of the United States of America* 103, 4040-4045.

Spirito, P., Bellone, P., Harris, K.M., Bernabo, P., Bruzzi, P., and Maron, B.J. (2000). Magnitude of left ventricular hypertrophy and risk of sudden death in hypertrophic cardiomyopathy. *The New England Journal of Medicine* 342, 1778-1785.

Spirito, P., Pelliccia, A., Proschan, M.A., Granata, M., Spataro, A., Bellone, P., Caselli,

- G., Biffi, A., Vecchio, C., and Maron, B.J. (1994). Morphology of the "athlete's heart" assessed by echocardiography in 947 elite athletes representing 27 sports. *The American Journal of Cardiology* 74, 802-806.
- Stathopoulos, P.B., and Ikura, M. (2010). Partial unfolding and oligomerization of stromal interaction molecules as an initiation mechanism of store operated calcium entry. *Biochem Cell Biol* 88, 175-183.
- Stathopoulos, P.B., and Ikura, M. (2013). Structure and function of endoplasmic reticulum STIM calcium sensors. *Curr Top Membr* 71, 59-93.
- Stathopoulos, P.B., Li, G.-Y., Plevin, M.J., Ames, J.B., and Ikura, M. (2006). Stored Ca^{2+} depletion-induced oligomerization of stromal interaction molecule 1 (STIM1) via the EF-SAM region: An initiation mechanism for capacitive Ca^{2+} entry. *J Biol Chem* 281, 35855-35862.
- Stathopoulos, P.B., Schindl, R., Fahrner, M., Zheng, L., Gasmi-Seabrook, G.M., Muik, M., Romanin, C., and Ikura, M. (2013). STIM1/Orai1 coiled-coil interplay in the regulation of store-operated calcium entry. *Nature Communications* 4, 2963.
- Stathopoulos, P.B., Zheng, L., and Ikura, M. (2009). Stromal interaction molecule (STIM) 1 and STIM2 calcium sensing regions exhibit distinct unfolding and oligomerization kinetics. *J Biol Chem* 284, 728-732.
- Stathopoulos, P.B., Zheng, L., Li, G.-Y., Plevin, M.J., and Ikura, M. (2008). Structural and mechanistic insights into STIM1-mediated initiation of store-operated calcium entry. *Cell* 135, 110-122.
- Stewart, T.A., Yapa, K.T.D.S., and Monteith, G.R. (2015). Altered calcium signaling in cancer cells. *Biochimica Et Biophysica Acta* 1848, 2502-2511.
- Straub, V., and Campbell, K.P. (1997). Muscular dystrophies and the dystrophin-glycoprotein complex. *Current Opinion in Neurology* 10, 168-175.
- Stryer, L. (1965). The interaction of a naphthalene dye with apomyoglobin and apohemoglobin. A fluorescent probe of non-polar binding sites. *J Mol Biol* 13, 482-495.
- Stuehr, D.J. (1997). Structure-function aspects in the nitric oxide synthases. *Annual Review of Pharmacology and Toxicology* 37, 339-359.
- Südhof, T.C. (2012). Calcium Control of Neurotransmitter Release. *Cold Spring Harbor Perspectives in Biology* 4.
- Sugden, P.H. (1999). Signaling in myocardial hypertrophy: life after calcineurin? *Circulation Research* 84, 633-646.
- Sun, Y., Carretero, O.A., Xu, J., Rhaleb, N.E., Yang, J.J., Pagano, P.J., and Yang, X.P. (2009). Deletion of inducible nitric oxide synthase provides cardioprotection in mice with

2-kidney, 1-clip hypertension. *Hypertension* 53, 49-56.

Takahashi, H., Shin, Y., Cho, S.J., Zago, W.M., Nakamura, T., Gu, Z., Ma, Y., Furukawa, H., Liddington, R., Zhang, D., *et al.* (2007). Hypoxia enhances S-nitrosylation-mediated NMDA receptor inhibition via a thiol oxygen sensor motif. *Neuron* 53, 53-64.

Tang, C.-M., and Insel, P.A. (2004). GPCR expression in the heart; "new" receptors in myocytes and fibroblasts. *Trends in Cardiovascular Medicine* 14, 94-99.

Tardiff, J.C. (2006). Cardiac hypertrophy: stressing out the heart. *J Clin Invest* 116, 1467-1470.

Taur, Y., and Frishman, W.H. (2005). The cardiac ryanodine receptor (RyR2) and its role in heart disease. *Cardiol Rev* 13, 142-146.

Thompson, J.L., and Shuttleworth, T.J. (2013). How many Orai's does it take to make a CRAC channel? *Scientific Reports* 3, 1961.

Tojyo, Y., Morita, T., Nezu, A., and Tanimura, A. (2014). Key components of store-operated Ca²⁺ entry in non-excitabile cells. *Journal of Pharmacological Sciences* 125, 340-346.

Tokuriki, N., Kinjo, M., Negi, S., Hoshino, M., Goto, Y., Urabe, I., and Yomo, T. (2004). Protein folding by the effects of macromolecular crowding. *Protein Sci* 13, 125-133.

Umar, S., van der Valk, E.J., Schaliij, M.J., van der Wall, E.E., Atsma, D.E., and van der Laarse, A. (2009). Integrin stimulation-induced hypertrophy in neonatal rat cardiomyocytes is NO-dependent. *Mol Cell Biochem* 320, 75-84.

van Bilsen, M., van Nieuwenhoven, F.A., and van der Vusse, G.J. (2009). Metabolic remodelling of the failing heart: beneficial or detrimental? *Cardiovasc Res* 81, 420-428.

van der Loo, E.M., Cnossen, J., and Meijer, C.J. (1981). Morphological aspects of T cell subpopulations in human blood: characterization of the cerebriform mononuclear cells in healthy individuals. *Clin Exp Immunol* 43, 506-516.

Varga-Szabo, D., Braun, A., and Nieswandt, B. (2009). Calcium signaling in platelets. *Journal of thrombosis and haemostasis: JTH* 7, 1057-1066.

Vig, M., Beck, A., Billingsley, J.M., Lis, A., Parvez, S., Peinelt, C., Koomoa, D.L., Soboloff, J., Gill, D.L., Fleig, A., *et al.* (2006a). CRACM1 multimers form the ion-selective pore of the CRAC channel. *Curr Biol* 16, 2073-2079.

Vig, M., DeHaven, W.I., Bird, G.S., Billingsley, J.M., Wang, H., Rao, P.E., Hutchings, A.B., Jouvin, M.H., Putney, J.W., and Kinet, J.P. (2008). Defective mast cell effector functions in mice lacking the CRACM1 pore subunit of store-operated calcium release-activated calcium channels. *Nat Immunol* 9, 89-96.

- Vig, M., Peinelt, C., Beck, A., Koomoa, D.L., Rabah, D., Koblan-Huberson, M., Kraft, S., Turner, H., Fleig, A., Penner, R., *et al.* (2006b). CRACM1 is a plasma membrane protein essential for store-operated Ca²⁺ entry. *Science* *312*, 1220-1223.
- Voelkers, M., Salz, M., Herzog, N., Frank, D., Dolatabadi, N., Frey, N., Gude, N., Friedrich, O., Koch, W.J., Katus, H.A., *et al.* (2010). Orai1 and Stim1 regulate normal and hypertrophic growth in cardiomyocytes. *Journal of Molecular and Cellular Cardiology* *48*, 1329-1334.
- Walsh, C.M., Chvanov, M., Haynes, L.P., Petersen, O.H., Tepikin, A.V., and Burgoyne, R.D. (2009). Role of phosphoinositides in STIM1 dynamics and store-operated calcium entry. *The Biochemical Journal* *425*, 159-168.
- Wang, A.C., Lodi, P.J., Qin, J., Vuister, G.W., Gronenborn, A.M., and Clore, G.M. (1994). An efficient triple-resonance experiment for proton-directed sequential backbone assignment of medium-sized proteins. *J Magn Reson B* *105*, 196-198.
- Wang, Y., Wang, H., Li, L., Li, J., Pan, T., Zhang, D., and Yang, H. (2016). Elevated expression of STIM1 is involved in lung tumorigenesis. *Oncotarget* *7*, 86584-86593.
- Wang, Y.G., Dedkova, E.N., Ji, X., Blatter, L.A., and Lipsius, S.L. (2005). Phenylephrine acts via IP₃-dependent intracellular NO release to stimulate L-type Ca²⁺ current in cat atrial myocytes. *The Journal of Physiology* *567*, 143-157.
- Werry, T.D., Wilkinson, G.F., and Willars, G.B. (2003). Mechanisms of cross-talk between G-protein-coupled receptors resulting in enhanced release of intracellular Ca²⁺. *Biochemical Journal* *374*, 281-296.
- Wink, D.A., Kasprzak, K.S., Maragos, C.M., Elespuru, R.K., Misra, M., Dunams, T.M., Cebula, T.A., Koch, W.H., Andrews, A.W., Allen, J.S., *et al.* (1991). DNA deaminating ability and genotoxicity of nitric oxide and its progenitors. *Science* *254*, 1001-1003.
- Wu, Y., Lu, X., Xiang, F.-L., Lui, E.M.K., and Feng, Q. (2011). North American ginseng protects the heart from ischemia and reperfusion injury via upregulation of endothelial nitric oxide synthase. *Pharmacological Research* *64*, 195-202.
- Xu, K.Y., Huso, D.L., Dawson, T.M., Bredt, D.S., and Becker, L.C. (1999). Nitric Oxide Synthase in Cardiac Sarcoplasmic Reticulum. *ResearchGate* *96*, 657-662.
- Yano, M., Ikeda, Y., and Matsuzaki, M. (2005). Altered intracellular Ca²⁺ handling in heart failure. *J Clin Invest* *115*, 556-564.
- Yao, J., Dyson, H.J., and Wright, P.E. (1997). Chemical shift dispersion and secondary structure prediction in unfolded and partly folded proteins. *FEBS Lett* *419*, 285-289.
- Yeromin, A.V., Roos, J., Stauderman, K.A., and Cahalan, M.D. (2004). A store-operated calcium channel in *Drosophila* S2 cells. *J Gen Physiol* *123*, 167-182.

- Yeromin, A.V., Zhang, S.L., Jiang, W., Yu, Y., Safrina, O., and Cahalan, M.D. (2006). Molecular identification of the CRAC channel by altered ion selectivity in a mutant of Orai. *Nature* *443*, 226-229.
- Yoshida, Y., and Imai, S. (1997). Structure and function of inositol 1,4,5-trisphosphate receptor. *Japanese Journal of Pharmacology* *74*, 125-137.
- Yuan, J.P., Zeng, W., Dorwart, M.R., Choi, Y.-J., Worley, P.F., and Muallem, S. (2009). SOAR and the polybasic STIM1 domains gate and regulate Orai channels. *Nature Cell Biology* *11*, 337-343.
- Zhang, S.L., Yeromin, A.V., Hu, J., Amcheslavsky, A., Zheng, H., and Cahalan, M.D. (2011). Mutations in Orai1 transmembrane segment 1 cause STIM1-independent activation of Orai1 channels at glycine 98 and channel closure at arginine 91. *Proceedings of the National Academy of Sciences of the United States of America* *108*, 17838-17843.
- Zhang, S.L., Yu, Y., Roos, J., Kozak, J.A., Deerinck, T.J., Ellisman, M.H., Stauderman, K.A., and Cahalan, M.D. (2005). STIM1 is a Ca²⁺ sensor that activates CRAC channels and migrates from the Ca²⁺ store to the plasma membrane. *Nature* *437*, 902-905.
- Zhao, G., Li, T., Brochet, D.X.P., Rosenberg, P.B., and Lederer, W.J. (2015). STIM1 enhances SR Ca²⁺ content through binding phospholamban in rat ventricular myocytes. *Proceedings of the National Academy of Sciences of the United States of America* *112*, E4792-4801.
- Zheng, H., Zhou, M.-H., Hu, C., Kuo, E., Peng, X., Hu, J., Kuo, L., and Zhang, S.L. (2013). Differential roles of the C and N termini of Orai1 protein in interacting with stromal interaction molecule 1 (STIM1) for Ca²⁺ release-activated Ca²⁺ (CRAC) channel activation. *The Journal of Biological Chemistry* *288*, 11263-11272.
- Zheng, L., Stathopoulos, P.B., Li, G.Y., and Ikura, M. (2008). Biophysical characterization of the EF-hand and SAM domain containing Ca²⁺ sensory region of STIM1 and STIM2. *Biochem Biophys Res Commun* *369*, 240-246.
- Zheng, L., Stathopoulos, P.B., Schindl, R., Li, G.Y., Romanin, C., and Ikura, M. (2011). Auto-inhibitory role of the EF-SAM domain of STIM proteins in store-operated calcium entry. *Proc Natl Acad Sci U S A* *108*, 1337-1342.
- Zhou, L., and Zhu, D.Y. (2009). Neuronal nitric oxide synthase: structure, subcellular localization, regulation, and clinical implications. *Nitric Oxide* *20*, 223-230.
- Zhou, M.-H., Zheng, H., Si, H., Jin, Y., Peng, J.M., He, L., Zhou, Y., Muñoz-Garay, C., Zawieja, D.C., Kuo, L., *et al.* (2014). Stromal interaction molecule 1 (STIM1) and Orai1 mediate histamine-evoked calcium entry and nuclear factor of activated T-cells (NFAT) signaling in human umbilical vein endothelial cells. *The Journal of Biological Chemistry* *289*, 29446-29456.

Zhou, Y., Mancarella, S., Wang, Y., Yue, C., Ritchie, M., Gill, D.L., and Soboloff, J. (2009). The short N-terminal domains of STIM1 and STIM2 control the activation kinetics of Orai1 channels. *The Journal of Biological Chemistry* *284*, 19164-19168.

Zhou, Y., Meraner, P., Kwon, H.T., Machnes, D., Oh-hora, M., Zimmer, J., Huang, Y., Stura, A., Rao, A., and Hogan, P.G. (2010a). STIM1 gates the store-operated calcium channel ORAI1 in vitro. *Nature Structural & Molecular Biology* *17*, 112-116.

Zhou, Y., Ramachandran, S., Oh-Hora, M., Rao, A., and Hogan, P.G. (2010b). Pore architecture of the ORAI1 store-operated calcium channel. *Proceedings of the National Academy of Sciences of the United States of America* *107*, 4896-4901.

Zhu-Mauldin, X., Marsh, S.A., Zou, L., Marchase, R.B., and Chatham, J.C. (2012). Modification of STIM1 by O-linked N-acetylglucosamine (O-GlcNAc) attenuates store-operated calcium entry in neonatal cardiomyocytes. *The Journal of Biological Chemistry* *287*, 39094-39106.

Zorzato, F., Fujii, J., Otsu, K., Phillips, M., Green, N.M., Lai, F.A., Meissner, G., and MacLennan, D.H. (1990). Molecular cloning of cDNA encoding human and rabbit forms of the Ca²⁺ release channel (ryanodine receptor) of skeletal muscle sarcoplasmic reticulum. *J Biol Chem* *265*, 2244-2256.

Curriculum Vitae

Name: Jinhui Zhu

Post-secondary Education and Degrees: Western University
London, Ontario, Canada
Honors Specialization BMSc
2011-2015

Western University
London, Ontario, Canada
MSc in Physiology and Pharmacology
2015-2017

Honours and Awards: Western Scholarship of Excellence
2011-2012

Dean's Honor List
2011-2015

Queen Elizabeth II Aiming for the Top Scholarship
2011-2015

Western Graduate Research Scholarship
2015-2017

Related Work Experience Research Assistant
Western University
2014-2015

Teaching Assistant
Physiology 3130z
The University of Western Ontario
2015-2017

Publications:

Zhu JH, Feng QP and Stathopoulos PB (2017). STIM/Orai structures: isolated and in complex. *Store-operated calcium entry (SOCE) pathway - emerging signaling concepts in human (patho) physiology, 2nd Edition*. Springer Verlag, New York. (in press)

Choi YJ, **Zhu JH**, Chung S, Siddiqui N, Stathopoulos PB. Targeting cysteine thiols for *in vitro* site-specific glycosylation of recombinant proteins. *J Vis Exp*. (submitted/under review)

Gui L, **Zhu JH**, Lu XR, Sims SM, Stathopoulos PB, Lu WY, Feng QP. Neuronal nitric oxide synthase inhibits store-operated Ca²⁺ entry in cardiomyocytes via S-nitrosylation of stromal interaction molecule-1. *Cell Rep*. (submitted/under review)

Presentations:

The 9th Annual Department of Physiology and Pharmacology Research Day, Western University, London, ON, 2015.

Title: The effect of S-nitrosylation on the structure and function of stromal interaction molecule-1

London Health Research Day, London, ON, 2016

Title: The effect of S-nitrosylation on the structure and function of stromal interaction molecule-1 in cardiomyocytes

The 10th Annual Department of Physiology and Pharmacology Research Day, Western University, London, ON, 2016

Title: S-nitrosylation-mediated suppression of stromal interaction molecule-1 activity and cardiomyocyte hypertrophy

Collaboration of Practitioners and Researchers (CPR) Seminar Series, Western University, London, ON, 2016.

Title: S-nitrosylation-mediated suppression of stromal interaction molecule-1 activity and cardiomyocyte hypertrophy

London Health Research Day, London, ON, 2017

Title: S-nitrosylation-mediated suppression of stromal interaction molecule-1 activity and cardiomyocyte hypertrophy

Cardiovascular Journal Club, Western University, London, ON, 2017

Title: S-nitrosylation-mediated suppression of stromal interaction molecule-1 activity and cardiomyocyte hypertrophy